# Order from Disorder: Measuring Reversibility and Local Equilibration in Self-Assembly

Grant, James

*Award date:*
2012

*Awarding institution:*
University of Bath

# Order from Disorder: Measuring reversibility and local equilibration in self-assembly

submitted by

James Grant

for the degree of Doctor of Philosophy

of the

University of Bath

Department of Physics

August 2012

# Dedication

To you and you. Always remembered.

# Acknowledgements

First and foremost I would like to thank my supervisor Dr. Rob Jack for his patience and support in all aspects of teaching and research over the four years of the project, it was, is and will be greatly appreciated.

To all members past and present of 3W3.2a and b, in particular, in chronological order, Dr Matthew Mizielinski, Dr Douglas Ashton, Dr Daphne Klotsa, Mr Ryan Curtis and Mr Clement Law, thank you and good luck. I would also like to thank the University of Bath and EPSRC for accommodation and funding respectively. Also to the organiser of all events, conferences and workshops I have attended over the course of my study, in particular Dr Paddy Royall and members of his group at the University of Bristol.

More personally I would like to family and friends without whom I would not be where I am now. To Mum for your relentless support through good and bad, deserved and probably not; Laurel and William, whatever happened to you both it seems to have worked; and to Joe for looking after you all. To all my friends who have been so supportive in fun times and hard, providing a much needed boost. Finally Rachel, when things were tough I would not have made it without you. All my love.

# Contents

# List of Figures

# Declaration

No portion of the work referred to in this thesis has been submitted in support of an application for another degree or qualification of this or any other university or other institution of learning.
Where the work of others has been reproduced it is clearly stated and references provided.

# Abstract

We illustrate self-assembly with several systems which aim to harness the process of assembly to create new functional structures. The concept of kinetic trapping preventing assembly and the importance of reversibility, breaking as well as making bonds, for avoiding such traps are introduced. We aim to identify how reversible systems are, with the aim of affecting the prediction, control and design of new systems.

In four systems a lattice gas model, and three models based upon patchy particle schemes, a yield is defined and used to identify optimal assembly at a given time. Three measurements relevant to reversibility are described, applied, and compared with the results of similar studies. The first simply counts the bonding and un-bonding events, or kinks, over the whole assembly process and compares the total number of events with the net bonding events. We measure values of $100 - 1000$kinks per bond in crystal systems, and $60 - 200$ for closed structures. In analogy with a toy model the values can be related to a 'forgivingness', a ratio of bad bonding sites, to good ones.

We then turn to measurements at early times which allow for the prediction of when assembly will occur. These include rate measurements of kinks which provide an instant measure of reversibility and comparison of correlation and response functions with the equilibrium fluctuation dissipation theory. These methods examine the dynamics of the assembly process while our third approach examines the structures during assembly. We examine how each of the measurements provide information about the assembly process and how it relates to the particles, their interactions and the final structure. The possibility of using the methods in combination is shown to be relevant to the prediction of assembly and how they might be used to implement design and control schemes to improve assembly.

# Chapter 1

# What is self-assembly?

Self-assembly is the spontaneous evolution of an initially disordered system of particles into an ordered equilibrium structure[33]. Structures can be extended, such as novel crystals[18, 30, 49, 62], or closed as with viral capsids[23]. Crystals may contain typically $N_A \approx 6 \times 10^{23}$ atoms or molecules, while at the other end of the scale examples from biological systems may contain just tens of proteins[58]. In addition to the variety in numbers of particles, their size may vary from single atoms to micron-sized colloids[25].

Experimental work exploiting the properties of biological systems, particularly DNA[40, 65], has driven a growing interest in self-assembly. A contributing factor is that despite the magnificent efforts of silicon, our ability to manipulate it physically and electronically is (or at least may be) reaching its limits[41]. Even the traditional approach of top-down design and manufacture is recognised as being open to reappraisal and particularly keen on new possibilities are those who see self-assembly as the basis for a ready made alternative to current technologies[30, 65].

The potential scale and functionality of artificial self-assembled structures appears endless. If you want a 'conventional' transistor[39], an optoelectronic device [68], a laser[73] or even a quantum computer[7], self-assembly may be the answer. It all seems too good to be true: design a basic unit(s) that will assemble into your desired device and watch it make itself. And presumably it will ...

Unfortunately it doesn't and there has been much interest in understanding the processes involved in assembly[76, 36, 74, 59]. The problem is that an assembling system changes from a disordered state away from equilibrium to an ordered one which is at equilibrium. In spite of over 100 years of research, there is no general theoretic approach to non-equilibrium systems[20]. Thermodynam-

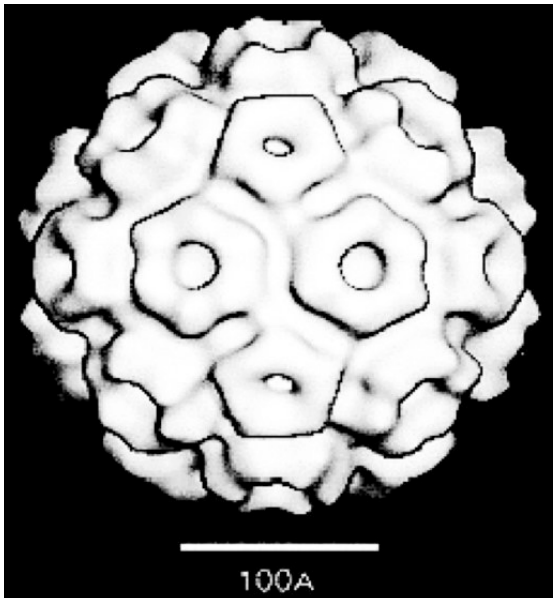


**Figure 1-1:** *Electron micrograph of the CCMV capsid[23]. Individual proteins form pentagons and hexagons which assemble into the final 'football' structure.*

ics can tell us the equilibrium properties of a system at different state points, but not how long it will take to relax into its new structure if we change its condition abruptly, for example quenching a fluid to a solid. We know that if we waited forever our system would achieve the intended structure, but that's not particularly spontaneous, or useful from a manufacturing perspective. The focus of the present work is identifying and relating general features in the dynamics of self-assembly, in order to aid the design and control of systems and predict their behaviour. Before introducing the prominent themes of the present work, it is useful to illustrate the difficulties of producing a self-assembling system by considering some experimental systems and their potential applications. First we examine a standard model of assembly, the viral capsid in detail.

## 1.1 Self-assembling systems

### 1.1.1 Viral capsids: A paradigm for self-assembly

A virus consists of two principal parts: the viral genome, containing the genetic material of the virus, and the capsid, a shell which allows the virus to move between and within hosts[1]. The capsid is an assembly of, often identical, 'coat proteins' in a shell which encloses the genome. In the case of the

cowpea chlorotic mottle virus (CCMV) 180 proteins assemble into a 28nm diameter football like structure in two stages: first individual proteins assemble into pentagonal and hexagonal capsomers; in the second stage twelve pentagons and twenty of the hexagons become the faces of the capsid[23]. Figure 1-1 shows an electron micrograph[23] of the CCMV capsid in which the individual proteins and capsomers are readily identified.

The proteins are coded by the genome[1] and when produced by the host cell they fold into a particular shape, the conformation, due to interactions between hydrophobic and hydrophilic groups along the protein and the solvent[1]. Once folded, the proteins interact with each other and the solvent through the groups that are left exposed on the surface of the conformation. Studies have shown that the proteins continue to assemble *in vitro*[23], in the absence of the viral genome, indicating that the capsid structure is the thermodynamic equilibrium state for the system[23].

Although each virus has a different coat protein, the icosahedral symmetry of the CCMV is common to many viruses. Others, for example the tobacco mosaic viral capsid, have a helical structure composed of rod like proteins[1]; while the capsid of the foot and mouth virus is composed of three different proteins[13]. Aside from the variety of structures, what is most astonishing about viral capsids is the quantity of high fidelity product: tens or hundreds of millions can be produced in a single infected cell, all identical[1].

The potential uses of artificial capsids are wide ranging involving varying degrees of variation from the naturally occurring examples. The most subtle of changes has already been mentioned, to assemble the capsid without enclosing the viral genome. When viruses enter a host it is the external surface of the capsid that the body 'sees'; this is what antibodies recognise and react to in order to attack the virus before it is able to infect a cell. If you can produce capsids empty of infectious disease then you have an ideal vaccine, identical to the original but non-infective[10].

Another proposed use of designer capsids is for drug delivery[10]. Chemotherapy is often a component in the treatment of cancers using drugs that target dividing cells, but unfortunately they attack all cells indiscriminately, including those that are not cancerous. Encapsulating the drug in an artificial capsid would offer significant benefits: the drug is chemically isolated until the capsid is broken down; the assembling protein can be designed to have surface groups that are naturally delivered to specific locations in the body; the capsid can be bro-

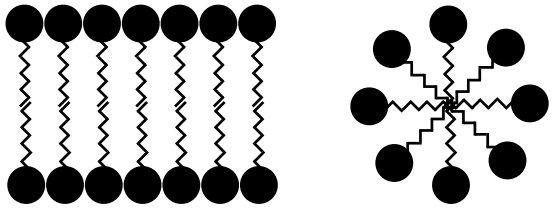

**Figure 1-2:** *Schematic illustration of surfactants forming bilayers and micelles (the latter may be spherical or cylindrical). Polar, hydrophilic, 'heads' readily dissolve in aqueous solution, while the hydrophobic tails group together.*

ken apart using laser or ultrasound further confining the treatment to the target location. In combination these features could improve treatments by allowing a larger specific dose to the cancer while reducing the total dose and greatly reducing side-effects.

Viral capsids offer a hint of what might be achievable if we can develop an experimental and theoretical understanding of the structures that may be assembled. If the proteins that form capsids can be modified without affecting their assembly, while making the resulting structures electronically or optically active then capsids may be a route to a new generation of devices. An additional benefit of self-assembly is that it may be possible to modify capsids so that they assemble into 3-dimensional systems which would offer a significant improvement over existing manufacturing techniques which are currently restricted to 2D. Although ideas for altering or designing new capsids are still in their infancy there have been many successful attempts to create viable and potential products from assembled structures some of which we consider next.

### 1.1.2 From nano-fabrication to crystallisation

Although held up as a paradigm for self-assembly capsids are far from being the only system whose natural behaviour we would like to harness, or indeed have. We briefly discuss some of the systems where our findings might be put to use. Historically surfactants were the first self-assembling systems to be harnessed to man's ends, as soaps[12]. In water, the hydrophilic 'heads' and hydrophobic 'tails' of surfactants can lead to the formation of structures including bilayer sheets and micelles[79] illustrated in Fig. 1-2. Besides a 5000 year history as soap however, surfactants are involved in many vital biological functions, such as the absorption of complicated fats, vitamins and as cell membranes[1] .

More recently DNA based subunits have been used to grow a variety of

structures[65] by harnessing DNA hybridisation that couples single DNA strands into the famous double helix. Either alone or in combination with existing technologies several remarkable experimental systems have been developed. With advanced bio-engineering of molecules the electronic properties of the resultant structures can be altered[40] by modifying the groups on the DNA to form desired structures and encapsulate optically or electronically active components. DNA is seen as one of the leading candidates upon which to base bottom-up nano-fabrication.

Chaperonins are an assembly of a small number of proteins, that are believed to play in a role in the folding other other proteins[1]. One class found in extremophiles, heat shock protein of the Archaea, has been found to have interesting assembling properties separate from any biological function. As with capsids, proteins assemble into chaperonins, composed of two rings of nine units, in a roughly spherical form and some groups again remain exposed and able to interact with other chaperonins. By making small modifications to the base protein, the chaperonins they form may assemble into 2D crystal sheets or 1D filaments[58].

The problems of nucleation and growth of high quality crystals plays an important role in modern technologies from computers to medical science and climatology. For computing applications large high quality crystals are grown using empirically developed techniques. The individual wafers that are used to manufacture chips are cut from this. In medical science the crystallisation of proteins plays a vital role in the process of determining the protein structure via diffraction studies[17]. Climatology currently receives a great deal of attention, however a full understanding of clouds, in particular the role of nucleation in cloud formation in the atmosphere is absent[69]. Until it is better understood the inclusion of the effect of clouds in climate models will be guesstimated at best.

### 1.1.3 Novel Experimental Systems

Since the present work will focus on simulations of simple models it is interesting to link with experimental systems by considering colloidal systems. Novel approaches to self-assembling systems have sought to create an interaction from scratch rather than piggybacking on DNA or other biological systems. Two examples that are currently receiving a great deal of attention are the family of Janus

particles and lock and key colloids. Having sizes on the order of $\mu m$, colloids are an ideal model system for studying self-assembly and other non-equilibrium processes: colloids are small enough that they undergo Brownian motion in suspension but big enough to be imaged with light. Furthermore advances in the manufacture of colloids and the level of control over their size and shape have led to some very interesting results. The particularly attractive aspect of colloids is that they stand as it were between simulation and experiment, realising the modellers ideal of simple shapes and interactions.

Lock and key colloids require deforming a large sphere so that it has a hollow 'lock' particle into which a smaller 'key' snugly fits[67]. If the two particles are put into suspension with some polymer particles typically an order of magnitude smaller then the locks and keys come together to form a dimer. The interaction is due to the depletion effect[48]: the smaller polymers are unable to approach within their radius of the locks and keys, leading to an excluded volume. By forming a dimer some of the excluded volume of the lock and key overlaps making the additional volume available to the polymer. This results in an effective interaction between lock and key stabilising the dimer state, becoming stronger as the density of the polymer is increased.

The depletion effect is interesting as it is a purely geometric, entropic interaction not requiring the tailoring of particle surfaces[37]. This means that once you have the ability to readily manufacture mono-disperse spheres the only challenge is to distress the surface of the locks. The remarkable techniques of colloidal scientists have been successful in growing locks with sufficient reproducibility and precision to achieve lock and key assemblies. One of the particularly interesting aspects of the lock and key system is that the product is flexible. If nano- and micro-machines are to be realised then the lock and key joint could become an important feature of devices.

Janus particles are named after the two-faced, Roman god of transitions. Janus particles were designed to act as solid surfactant-like particles having one-half hydrophobic and one half hydrophilic[14]. Originally produced to investigate their properties at liquid-liquid interfaces, they have since been found to exhibit interesting self-assembling properties. The development of manufacturing techniques has also led to the tri-block Janus or ternary particle[56] which has different interactions at the poles and the equator. These have shown two stage assembly, first clustering in small groups before crystallising into standard HCP or FCC structures. Recent simulation work has shown how a slight modification in the

design of the particles can allow selection between the two structures[64]. This is significant since normally they have similar free energies at equilibrium and have similarly likely probabilities of formation in assembly/crystallisation processes. This is of particular interest in optics since although the two polymorphs have similar free energies and so are similarly likely to form, FCC and associated structures have preferable optical characteristics[64].

### 1.1.4 Beyond Self-assembly

Self-assembly is one of many open problems in non-equilibrium physics, but can its elucidation inform other areas? Perhaps its closest relation is self-organisation, another process of which many examples are found in biological systems. Whereas self-assembly involves the evolution to an ordered equilibrium state, self-organisation describes systems where ordering occurs as a result of a perturbation which maintains the system in a non-equilibrium steady state (NESS)[33]. The perturbation may be anything which involves a flow of energy through the system. Self-organisation has a breadth applicability potentially greater even than self-assembly.

Self-organised behaviour has been identified in systems as varied as life and sand piles and from lasers to earthquakes[6]. One of the measurements studied here has previously received attention in relation to NESSs and ideas of the two approaches are closely related, with both leading to ordering of the system as it changes. It is likely that if the results here are not able to directly benefit the study of self-organisation then the advances in both areas will help direct future studies and approaches to non-equilibrium processes in general.

A further process of vital importance in biological systems is the folding of proteins. As has been mentioned in relation to viral capsids, proteins are initially formed in a disordered state by the machinery of the host cell and quickly fold into a particular conformation depending upon the cellular environment. Folding commences while the protein is still being produced[1] and typically completes on timescales of $\mu s$ to $ms$[47]. The single stable conformation is dependent upon the environment of the protein and often alters in order to interact with other proteins and biomolecules. The folding pathways are vital to life and failures resulting in denaturing of proteins can result in illnesses including eyesight loss[21] and are believed to play a crucial role in some neurological disorders[71].

## 1.2 The dynamics of self-assembly: Towards a general theoretic approach

The majority of theoretic and simulation work on self-assembly has focussed on particles and the structures they form. A number of papers have investigated the process of assembly initially qualitatively and more recently several have considered the dynamics and structures observed during the assembly process[36, 43, 28, 27, 32, 59, 77, 78]. This aim of this work is to contribute to the understanding of self-assembling systems aiding their design, their prediction, and how obstacles to assembly may be avoided or overcome.

The criterion that the system evolves to an equilibrium state is a essential feature of self-assembly. It means that in principle the tools of thermodynamics and statistical mechanics can be used to identify the favoured structure at different state points. Unfortunately despite 100 years of study into non-equilibrium systems, no general approaches exist which can tell us how long a particular system will take to relax to its equilibrium state[20]. An intriguing feature of self-assembly is that in principle we can use thermodynamics, either analytically or through numerical studies, to identify the final state of a system, but not how it gets there. Conversely the physical system appears to know how to get 'there', but not where it's going.

In particular the effects of kinetic trapping cannot be taken into account with standard equilibrium treatments. Kinetic trapping occurs when 'imperfect' bonds form, which are not present in the final structure and are unable to relax on experimental timescales. This can occur as the temperature $T/\epsilon_{\mathrm{b}}$ is lowered increasing the activation time $\exp(-\epsilon_{\mathrm{b}}/T)$ associated with breaking bonds. In the limit of $T/\epsilon_{\mathrm{b}} \to 0$, bonds never break and any defects that form will be unable to anneal.

For the present purpose, the yield of a system is defined as the proportion of particles in the assembled state, having all bonds formed in the correct orientation. In the case of simple crystallisation where a single crystal state condenses from a fluid then thermodynamics will say that highest equilibrium yield will be achieved at the lowest temperature. The consideration of kinetic trapping shows that this is not the case in evolving systems however and instead we observe an non-monotonic yield with optimal assembly occurring at a temperature, $T^*$, at the kinetic crossover where trapping is not yet significant but the equilibrium product has a good yield.

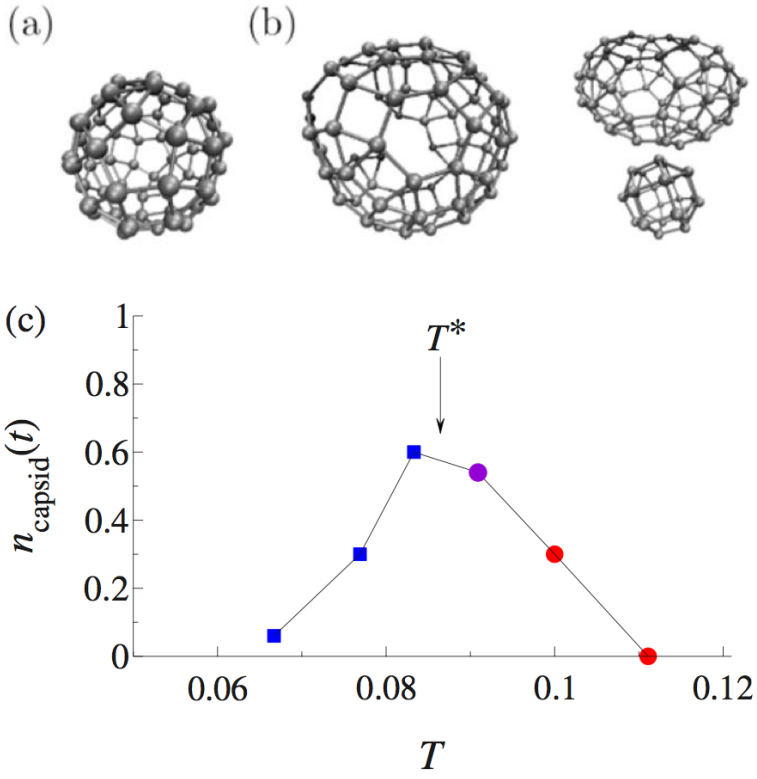


**Figure 1-3:** *a) Target structure for viral capsid model and b) examples of malformed structures at low temperature. c) Yield plot for viral capsid simulations showing non-monotonic yield in temperature.[36]*

For illustration we present plots showing the non-monotonic yield of some model systems. Fig.1-3c) reproduced from Jack *et al*[36] demonstrates the key features of yield plots in self-assembling systems. This is one of a number of model viral capsid formers where the equilibrium state at low temperature is a stable closed structure[31] (we discuss more of the detail of the model in the following chapter). At high temperature the particles exist as a gas since thermal processes break up clusters. As the temperature is reduced the system forms closed units shown in Fig.1-3a)[36] . The yield, at a fixed simulation time and temperature, measures the proportion of particles that are in complete capsids.

At low temperature as in Fig.1-3b) we observe malformed capsids where closed structures have formed but contain defects. At intermediate temperatures defects are able to relax and the majority of particles form into complete capsid structures. Once a closed structure has formed several bonds have to be broken in order to remove one particle making a very stable configuration and preventing full assembly in the kinetically trapped examples.

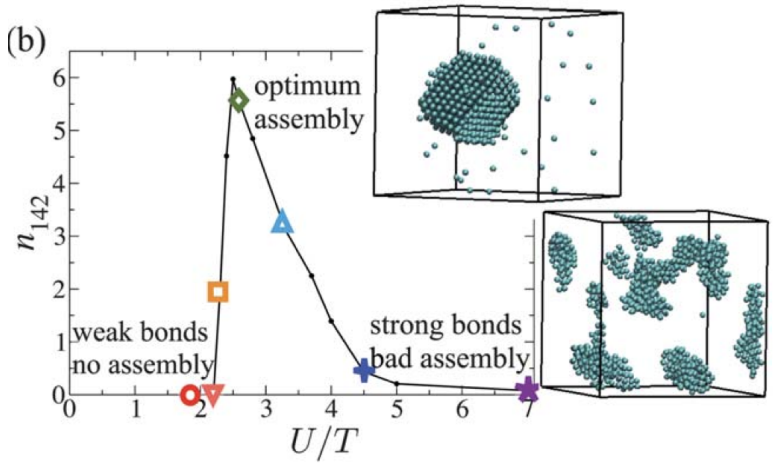


**Figure 1-4:** *Yield plot for sticky spheres showing configurational snapshots of the system at different state points.[43]*

A second example is provided by sticky spheres, shown in Fig. 1-4 reproduced from Klotsa *et al*[43] (again the model is discussed in more detail in the following section). This is a simple model of a crystal former and here the yield is a measure of the crystallinity, with only particles within particular local structures contributing. The behaviour of the yield is however consistent with that of the capsid model in spite of the great differences between the particles and final structures. At high temperature no large crystals form and the crystallinity remains zero. At low temperature long-lived fractal like structures form, preventing assembly and leading to a low yield. At intermediate temperatures the system is able to proceed quickly towards its equilibrium state.

### 1.2.1 (Ir)reversibility

Reversible processes are defined as those which can be 'exactly retraced by infinitesimal changes in control parameters'[15]. As a result a system undergoing reversible change has to do so slowly so that it remains at equilibrium throughout the process. Conversely irreversible changes abound in real systems where theoretical conditions of infinitesimal and arbitrarily slow change are just theoretical.

By definition optimal assembly occurs when the system has assembled the quickest, this means that its behaviour is irreversible, starting in a non-equilibrium state, and ending in an equilibrium one. It is then perhaps surprising and paradoxical that the importance of kinetic trapping preventing assembly at low temperatures has led to the recognition of the role played by reversibility in self-

assembling systems[76]. This qualitative statement about the dynamics of self-assembly is very persuasive: in order to assemble, bonds that aren't present in the final structure must break or anneal before the system reaches equilibrium. In order that this happens Whitesides argues that the local environment must be explored reversibly to avoid kinetic trapping.

The matter of reversibility is far from trivial however. Although on the microscopic length and timescales the system must appear reversible, on macroscopic, experimental, scales the irreversibility must come to dominate behaviour. Measuring the microscopic reversibility, the timescales over which this relaxes to irreversible behaviour, and how these measurements relate to the assembling particles and structures formed is the focus of this thesis. Quantifying the role of reversibility in different classes of assembling systems and gaining an understanding of the processes involved can only aid the design and control of assembly.

The two yield plots reproduced in the previous section are taken from papers which examined the measurement of reversibility through comparison of correlation and response functions[36, 43]. These can reveal interesting information about the reversibility of a system's dynamics by comparing the measurements with the Fluctuation Dissipation Theory (FDT) which describes their behaviour at equilibrium. The aims of this work were to identify whether measurements at early times in assembly processes could reveal the long term behaviour. Part of the findings of this work are that FDT measurements demonstrate Whitesides' idea of the importance of reversibility in self-assembly. Furthermore they can reveal information on different timescales that systems should appear reversible on short timescales and irreversible over long trajectories.

The work of Wilber *et al*[77, 78] is of interest on several counts. In the first instance they describe a systematic approach to producing closed structures based upon spherical particles designed to assemble into a Platonic solid. In the target structure particles are located at the vertices of the chosen solid and interact via patches positioned where particles touch. In doing so they describe a system which at high temperature exists as a gas of separate particles while at low temperature particles assemble into the chosen solid which then exist as a 'cluster gas'.

An important finding in their work is the role of stabilising intermediary structures in assembly pathways. Of the five solids, three, the tetrahedra, octahedra and icosahedra have triangular faces, while for the cube and dodecahedra the faces are square and pentagonal respectively. This is found to have an strong ef-

fect on the time dependency of yield: triangle faces require only three particles to come together and form a stable structure. In contrast for square faces four particles have to come together correctly to four a stable intermediary when making cubes (increasing to five for the dodecahedra). While the squares and pentagons require more particles to arrive at the stabilising structure they also allow more opportunity for forming kinetically trapped clusters which further suppress yield.

Although the idea of reversibility in terms of making and breaking bonds suggests that the dynamics of the systems should be of interest, several approaches have considered structures present in assembling systems. Rapaport[59] has studied a model system of viral capsids showing that in self-assembling systems clusters are in general more likely to undergo disassociation than growth, confirming that bond breaking and hence reversibility are important in the assembly process. The exceptions to this were stable structures where energy minimised structures had additional stability.

More recently a study by Hagan *et al*[32] has considered rates of growth and in particular the quality of clusters in more detail. This approach is rooted in the idea that it is not sufficient to grow large clusters but these must also be high quality to avoid kinetic trapping. The quality of clusters is assessed by comparing the properties of equilibrated clusters with those in an assembling steady state. Both a model viral capsid system and the Ising Lattice Gas show clearly that as temperature is reduced, the quality of growing clusters, how closely they approach their equilibrium properties, falls. This approach to quantifying the quality of clusters has been referred to as cluster equilibration, in a later chapter we use local equilibration as clusters are locally equilibrated, for a similar study.

A final point of consideration before we turn to the focus of the present work is to ensure that effects such as kinetic trapping are not artificially introduced to model systems through a poor choice of system and/or dynamics. One method for ensuring realistic dynamics is Virtual Move Monte Carlo (VMMC) due to Whitelam *et al*[74]. This details how a system's dynamics may be based upon cluster moves chosen to mimic the physical behaviour of the real system and avoid unphysical artefacts. We use a variation of their scheme, where appropriate, and explain how trapping is avoided when simpler dynamics are sufficient.

## 1.3 What we will do

Our aims in the present work are severalfold. In the first instance we need to measure the yield of systems in order to identify where self-assembly occurs. This will be done in a variety of systems that represent both closed and extended systems. Second we wish to clarify the role of reversibility in self-assembly and in particular identify methods of quantifying how (ir)reversible each system is at a range of temperatures, at optimal assembly and in poor assembly regimes. We can then use these methods to clarify the mechanism by which assembly occurs and how it relates to the equilibrium phase diagram of the systems.

Once we have measurements of reversibility we can begin to identify relationships between the different measurements and how the measurements vary across systems with different particles and target structures. This leads on to the final objectives which are to help understand how reversibility on short timescales can give way to irreversible behaviour at longer times. This should help to predict, design and control new assembling systems.

To be of use, particularly in the case of predicting where and when assembly will occur, measurements of the dynamics of assembly will primarily concentrate on times far earlier than those at which we observe significant yield. In order to be useful for experiments we would ideally make measurements at times two or more orders magnitude earlier than those that at which we observe significant yield. With this in mind, once we have established the yield of systems we concentrate on the behaviour at early times when there may be little or no yield, or indication of where high yield would be achieved at long times.

With regard to the design and control of systems, as we have already intimated, since thermodynamics allows us to identify equilibrium behaviour, assembling particles for particular target structures are relatively easy to design. Understanding how different inter-particle interactions modify assembling pathways and how readily (or not) systems assemble will assist in the design of assembling systems.The idea of controlling assembly would be to harness the knowledge developed to design assembly protocols that accelerate assembly. These schemes might vary temperature monotonically or fluctuate it in order to accelerate assembly rather than operating at a fixed temperature. While the last two long term goals are not addressed directly we will return to assess progress toward them in our concluding remarks.

In the following chapter we will introduce the chief protagonists of our story,

two model systems: the Ising lattice gas and a system of 'patchy' particles. The former, in its various forms is one of the most studied models in physics. Initially conceived as a simple model of ferromagnetism it has subsequently been found to have wider applicability. The latter has been conceived as a simple but elegant solution by Wilber *et al*[78] for the simulation of designer systems as with the capsid model discussed earlier. Their relevance to self-assembly and how their behaviour compares with other model systems are discussed. Additionally two important methods, a cluster algorithm for ensuring physically realistic motion and a 'no-field' method for measuring responses functions are presented.

In model systems, a naive approach to measuring reversibility is simply to count the making and breaking of bonds, focussing on the dynamics of the process[28, 27]. Two forms of this measurement are explored in Chapter 3, comparing integrated or cumulative and rates of traffic and flux. Traffic is the total activity, obtained from the sum of breaking and making events, while the flux is the net bond making, the difference between the two measurements. The behaviour of the measurements in different systems and the relationship to the particles and their assembly product is examined.

In Chapter 4 more subtle correlations and response functions and the relevance of fluctuation dissipation theory are considered. In particular, analysis of the relationship of the functions to each other, the system and to bond making and breaking is presented. This shows a correspondence with traffic and flux measurements in keeping with the qualitative idea of microscopic reversibility and hints at how the crossover to macroscopic irreversibility might be studied.

An alternative approach to reversibility examining how structures present in systems evolve to their equilibrium state is considered in Chapter 5. This builds on previous work which has examined the role of local equilibration a local measure of the departure from equilibrium. The chapter begins with a brief overview of classical nucleation theory (CNT) before detailing the problems with its approach in relation to self-assembly. After presenting measurements of the different systems the potential relationship with the dynamic measures of the previous chapters, in particular correlation and response functions is examined.

# Chapter 2

# Models & Techniques

Modelling is a key aspect of many areas of science, particularly in physics, where in essence, all hypotheses and theories are to one degree or another based upon models. Since Newton's discovery of the laws of motion, the idea of reality behaving as if it were a mathematical system has become ubiquitous (one could even take this back to the Greeks' supposition of the circular orbits of the stars and planets). The use of simple models that retain just sufficient detail to reconstruct experimental results is a hugely powerful tool in understanding (apparently) complex phenomena in our environment. Atomistic models of many particle systems led Boltzmann to his discoveries of statistical mechanics and allowed Einstein to evidence the atom with his analysis of the origin of Brownian motion.

With the advent of the computing age the increasing ability to perform computational experiments 'in silico' has offered the potential to greatly assist both traditional experiments and theory. While they cannot replace experiments, simulation can be used for preliminary studies of systems to confirm the principles of theory, allowing specific experiments to consider a reduced, specific set of conditions. In other cases exact analytic results are not derivable in theory and numerical approaches are the only ones open to workers.

Monte Carlo methods have a long history, originating in the work of Buffon. In order to obtain a value for $\pi$, Buffon proposed dropping a needle onto a paper ruled with a grid[55]. He had obtained an expression for $\pi$ relating the size of the grid, needle and proportion of attempts where the needle intersected the grid. Although statisticians have demonstrated the speed at which application of the estimate converged shows that later experimenters almost certainly cheated, the principle of the method has survived, finding use in many areas of science.

Monte Carlo methods rely upon the random sampling of phase space, in

Buffon's experiment this is the random dropping of the needle onto the paper, a form of numerical integration. It received its name following its use in the Manhattan project when the method was used to solve a variety of problems that were not analytically tractable. The name arose because of the correspondence to the randomness of gambling and its association with the Monte Carlo Casino in Monaco[55]. Although the methods require the generation of pseudo-random number sequences they were the quickest available. Since their introduction Monte Carlo methods have been applied to problems from condensed matter[54] to astronomy[24] and medicine[22].

In simulation, Monte Carlo methods have flourished with new algorithms under continual development[4, 2, 3, 16, 74]. The alternative method of Molecular Dynamics(MD) considers trajectories of particles[60]. A particle's coordinates and velocities are supplemented by the acceleration due to interactions with other particles, and at each time-step all particles' coordinates are updated. If one is simulating a system of particles in suspension in a solvent however, all particles must be considered explicitly, both those of interest and those of the solvent, and simulation time can be too costly. An alternative method is to use Brownian Dynamics where the solvent is effectively integrated out by modifying the particle velocity by an additional random, uncorrelated nudge at each time-step and a damping force.

In contrast Monte Carlo simulations generally begin from moving a single particle at a time. Moves are proposed sequentially and accepted with probabilities chosen to ensure that the system behaves in accordance with the laws of thermodynamics. The nature of moves may vary enormously depending upon the system and problem studied and the resources available. If the problem is to identify phase behaviour, non-local and unrealistic moves such as inserting or removing a particle from the system might be appropriate. As more complex problems have been addressed simulation schemes have been devised where many particles may be moved in a single move or particles introduced through a series of phantom stages. Provided phase space is sampled correctly and the simulation runs in a sensible time there is an opportunity to let one's creativity run wild.

In the present work these techniques are not always appropriate however. When considering a finite number of particles assembling into a cluster, and the dynamics of that process, it is necessary to carefully consider how to mimic the process in simulation. Proposing and accepting a move which takes a random distribution of the particles and puts them straight into the assembled state

clearly will not tell you anything about the assembly process. Instead local moves are employed whereby the particles move to a nearby location in a way which has a clear physical interpretation, i.e. diffusion. The current work makes use of Monte Carlo simulations of one-component systems chosen because they can reproduce typical features of real self-assembling systems.

## 2.1 Ising Model

The Ising model was first suggested as a simplified model of a ferromagnetic system by Lenz in 1920 though it derives its name from a paper by his student Ising in 1925[34]. The motivation for the model was to provide a theoretical basis for phase transitions in ferromagnets[15]. At the Curie point the susceptibility of a ferromagnet diverges and the material may be magnetised by an infinitesimal field. The divergence or discontinuity of thermodynamic properties is a general characteristic of phase transitions [79] suggesting that the underlying microscopic behaviour can not only be simplified but that the particular system under study is unimportant at the critical point. The point is to ignore the particular detail of the system and concentrate on emergent cooperative behaviour[11].
The model operates on a lattice of spins of a given dimension and the energy of the system is given most generally by

$$E = -\sum_{\langle ij \rangle} J_{ij}\sigma_i\sigma_j - \sum_i h_i\sigma_i \tag{2.1}$$

where $\langle ij \rangle$ indicates that the sum is over nearest neighbours, $\sigma_i$ is the spin taking values $\pm 1$, $J_{ij}$ is the coupling between sites, typically 1 for nearest neighbours and 0 otherwise, and $h_i$ is an applied site-dependent field. Since the system will tend to lower energy, a positive $J_{ij}$ or $h_i$ will encourage alignment with neighbours, or with the applied field.
Ising was able to show that in 1D there is no phase transition and proposed that this remained the case in higher dimension. This was however incorrect and the model does indeed exhibit a phase transition in 2D. A full solution in 2D, without an applied field and with $J$ constant was given by Onsager in 1944[57]. The model remains unsolved in higher dimensions. If the up and down spins are instead taken as empty and occupied sites the system is instead a simple model of a fluid. Instead of a coupling between spins there is a bonding between particles and at temperatures below the critical point the up and down phases are high

and low density regions, liquid and gas.

### 2.1.1 Lattice Gas

We will study the Lattice Gas in 2D of dimension $L$ containing a fixed number of particles $N \leq V = L^2$, having a nearest neighbour coupling $\epsilon_\mathrm{b}$ and where no site can have more than one particle. With no applied field the energy of the system, $E$, may be written as

$$E = -\frac{\epsilon_\mathrm{b}}{2} \sum_p n_p \tag{2.2}$$

where the sum runs over all particles $p$ and $n_p$ is the number of bonds (occupied nearest neighbours) of a particle. The yield, the amount of optimal product, is just the proportion of particles having all their nearest neighbour sites occupied, in the case of 2D this is just the proportion of particles with four neighbours. As we have in mind a dilute solution of assembling particles the number of particles is fixed at $N = 1638$ and lattice size $L = 128$ giving a density $\phi = N/L^d \approx 0.1$.

In grand canonical implementations of the Lattice Gas, particle insertions/removals are attempted at random. Under this scheme the density fluctuates allowing phase space to be sampled but the physical interpretation of appearing and disappearing particles means that the dynamics is not realistic. Instead we make use of the canonical ensemble where realistic behaviour is obtained by fixing the number of particles and attempting local moves.

In the simplest implementation Kawasaki moves[38] are proposed by picking a random particle, $p$, and a random direction in which to move a single lattice spacing. If the new site is already occupied the move is rejected because each site can only hold one particle. Otherwise the difference in the number of bonds the particle has in its initial and proposed position is used to generate a move acceptance probability. Because the number of neighbours relates directly to the system's energy change, $\Delta E = \Delta n_p \epsilon_\mathrm{b}$, a specific choice of acceptance probabilities ensures that the system behaves in accordance with the laws of thermodynamics.

The important condition is detailed balance and it ensures that at for a system at equilibrium the system is in a steady state:

$$W(\nu \leftarrow \mu)\rho_{\mathrm{eq}}(\mu) = W(\mu \leftarrow \nu)\rho_{\mathrm{eq}}(\nu) \tag{2.3}$$

where $W(\nu \leftarrow \mu)$ is the transition rate from configuration $\mu$ to $\nu$ and $\rho_{\mathrm{eq}}(\mu)$ is the probability of being in $\mu$ at equilibrium. Since this must be the case for all pairs

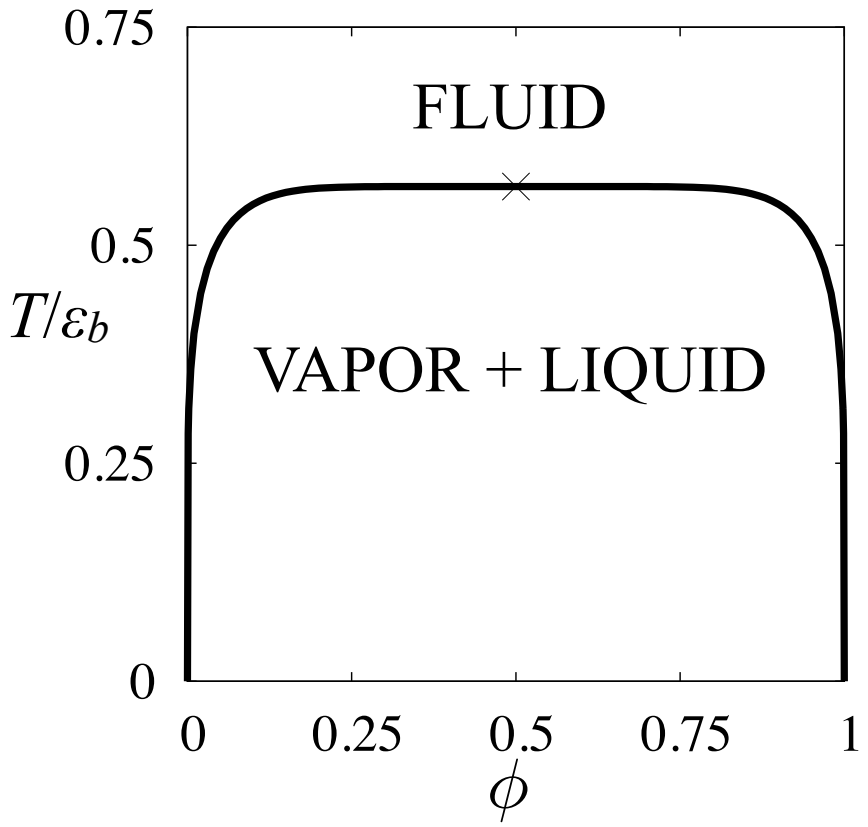


**Figure 2-1:** *Exact phase diagram for the lattice gas. At high temperature the system equilibrates in a single fluid phase while below the binodal it separates into high and low density phases.*

of configurations the probabilities must be constant at equilibrium. In order to ensure configurations are visited with appropriate frequencies in accordance with the Boltzmann factor, transition rates obey

$$\frac{W(\nu \leftarrow \mu)}{W(\mu \leftarrow \nu)} = \exp(-\beta \Delta E(\nu, \mu)) \tag{2.4}$$

where $\beta = \frac{1}{k_{\mathrm{B}}T}$ is the inverse temperature, here and throughout $k_{\mathrm{B}}$ is set to unity.

### 2.1.2 A simple model of self-assembly

At equilibrium the behaviour of the system depends only upon the ratio $T/\epsilon_{\mathrm{b}}$ and the volume fraction $\phi = L/N$ and is exactly described by $\sinh^4(\epsilon_{\mathrm{b}}/2T) > (1-(2\phi-1)^8)^{-1}$[8], illustrated in Fig. 2-1. Here and throughout $\epsilon_b = 1$ where

it is not included explicitly in expressions, also, whenever we refer to increasing temperature, we could equivalently, decrease bonding strength and vice-versa. The thick black line is the binodal which separates different phase behaviour. Above the critical temperature, $T_c$, the system exists in a single fluid phase. Below the critical temperature and outside the binodal the system is either a gas or liquid. Inside the binodal the system phase separates into gas and liquid having volume fractions of the binodal, and this is the region of interest. For $T$ and $\phi$ the relative proportion of each phase, $\sigma_g$ and $\sigma_l$ having volume fractions $\phi_g$ and $\phi_l$ is obtained by the lever rule

$$\sigma_l = \frac{\phi - \phi_g}{\phi_l - \phi_g}. \tag{2.5}$$

This is the thermodynamic behaviour of the model given that it is at equilibrium, and is exactly known analytically. As soon as a system departs from equilibrium however the situation is not as clear. If the system having a fixed number of particles is initialised in a random configuration corresponding to a high temperature fluid and quenched to $T$ within the binodal then the system must spatially separate into the two phases and no general theory exists to calculate how long the process will take. If the dense fluid phase is taken as an approximation of a crystal, then high quality is obtained by growing a single large cluster having a paucity of defects. No clustering or growing disordered clusters corresponds to poor assembly.

In what follows the Lattice Gas will be shown as a crude analogy for self-assembly in spite of its simplicity. That it turns out to be valid shows that by carefully retaining sufficient detail of the real system, particular information may be subsumed and only specific features such as dimension, shape, or interaction range are required to obtain complex behaviour. The aim is that in simple systems the reasons why features manifest in the way they do might be identified more readily.

### 2.1.3 Cluster Moves

The system described above, utilising single particle moves, has an unphysical feature which can fortunately be avoided with relatively little cost, from either computation or implementation viewpoints. The problem is the unphysical diffusion of clusters of particles. In Brownian systems clusters of $n$ particles diffuse

with a rate $D \propto 1/n$[74]. If particles are moved individually however, then in order to move, particles will have to separate from the cluster and move to their new position in turn. A naive (under)estimate of the diffusion rate, assuming each particle only needs to break a single bond, $D \propto \exp(-\beta n)$, shows moves will have an unphysical, exponential, temperature and size dependence. The solution is to use a cluster algorithm which recovers Brownian type diffusion.

The 'Cleaving Algorithm' due to Whitelam[74] achieves this for the Ising model. It involves selecting a seed particle randomly and adding neighbouring particles to the growing cluster to generate a cluster of particles to move. Each bond is tested at most once with the new particle added to the cluster with probability $1-\exp\left(-\lambda\epsilon_{\mathrm{b}}/T\right)$ (if both particles are already in the cluster the bond is not tested). $\lambda$ is a parameter that determines a fictive temperature at which the bonds are tested. For the present work $\lambda = 0.9$ for reasons that are set out below. Bonds are tested recursively until bonds to all neighbours of particles in the cluster have been interrogated. The proposition probability of a particular move is just the product $P_{\mathrm{prop}}(C,\mu) = \prod_x 1-\exp\left(-\lambda\epsilon_{\mathrm{b}}/T\right)\prod_y \exp\left(-\lambda\epsilon_{\mathrm{b}}/T\right)\frac{1}{N}$, where $x$ is the number of unbroken bonds and $y$ the number of bonds broken during the formation of the cluster, $C$, $\mu$ is a configuration and $1/N$ is the probability of selecting the seed.

In order to ensure that the model exhibits Brownian like diffusion, for each move a maximum cluster size, $n_{\max}$, always greater than unity, is generated randomly from the distribution $P(n_{\max} > n) = 1/n^2$. If the size of the proposed cluster, $n$, is greater than $n_{max}$ then the move is automatically rejected. Because clusters of size $n$ are chosen with a probability proportional to $n$, each particle is equally likely to be chosen as the seed, the choice of distribution ensures that a Brownian like dependence upon cluster size, $D \propto n \times 1/n^2 = 1/n$, should be approximated.

Next a random direction is chosen and a move of one lattice spacing in that direction attempted. Since no site can hold more than one particle, moves are rejected if they would result in particles overlapping. Finally the energy change, $\Delta E$, associated with the move can be evaluated and the move accepted in accordance with the acceptance probability, $P_{\mathrm{a}}$ given by

$$P_{\mathrm{a}}(\Delta E) = \begin{cases} 1 & \Delta E < -\delta/2 \\ \frac{2\alpha}{1+\exp([1-\lambda]\beta\Delta E)} & -\delta/2 < \Delta E < \delta/2 \\ \exp(-[1-\lambda]\beta\Delta E) & \Delta E > \delta/2 \end{cases} \tag{2.6}$$

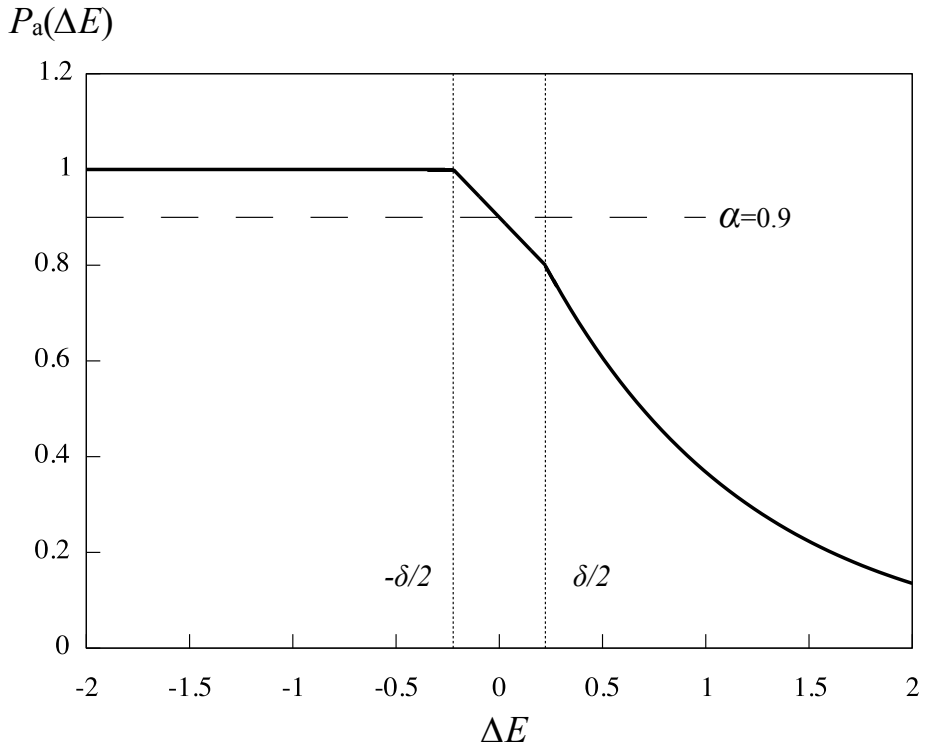


**Figure 2-2:** *Schematic plot of the acceptance probability,* $P_{\rm a}$ *as a function of energy change* $\Delta E$*. The Metropolis probability is modified by a small Glauber form about* $\Delta E = 0$*.*

where setting $\frac{\delta}{2} = \frac{-\ln(2\alpha-1)}{\beta}$ ensures that the $P_a$ is continuous at all energy changes. The full acceptance probability is illustrated in Fig.2-2 showing the three components separated by vertical dashed lines indicating the values of $\delta/2$ with a horizontal dashed line for $\alpha = 0.9$. For the purposes of the figure the factor $[1-\lambda]\beta$ is set to 1, but in practice the particular choice of $\lambda$ and the temperature will alter the acceptance probabilities.

This choice allows the implementation of a Metropolis acceptance probability for the majority of moves which approximate physically realistic behaviour: downhill energy moves are accepted with unit probability and those which increase the energy are thermally activated. The no-field method for the response, detailed below, requires the acceptance probability to be differentiable about possible energy changes[16]. With the introduction of the Glauber type part with the limits above and as long as $|\epsilon_{\rm b}| \gg |\frac{\delta}{2}| \gg |h_k|$, where $h_k$ is the strength of the perturbation, the acceptance probability is continuous, monotonic and differentiable about allowed integer changes in energy.

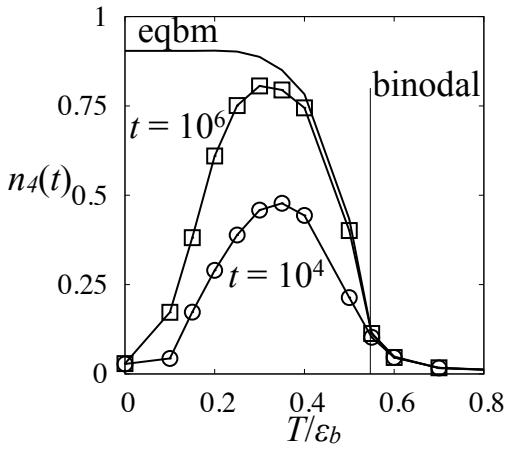


**Figure 2-3:** *Plot of yield $n_4(t)$ against reduced temperature $T/\epsilon_\mathrm{b}$, for $t = 10^4$ and $10^6$ MCS. For this range of times, the yield is maximised at $T/\epsilon_\mathrm{b} \approx 0.35$. The equilibrium yield is shown (labelled 'eqbm'): as $t \to \infty$ the yield approaches this result. The binodal at $T/\epsilon_\mathrm{b} = 0.547$ is shown as a vertical line.*

The values of $\alpha$ and $\lambda$ depend upon the the physical system we have in mind and the measurements we wish to make. In particular aside from physical considerations, the way in which the method used to obtain response functions couples to the system has a bearing on the values chosen. For our purposes the two parameters should be as close to unity as possible. In order to ensure a monotonic acceptance probability we require $\alpha > e^{-1}$ but since there is no physical barrier to diffusion, setting $\alpha = 0.9$ more closely approximates the behaviour we aim to replicate. In the case of $\lambda \to 0$ tested bonds are always broken when building a cluster and the cleaving algorithm reduces to single particle moves. Since the algorithm is implemented to specifically avoid the unrealistic diffusion of single particle dynamics we take $\lambda = 0.9$[27].

To summarise: the probability of a move $P(\nu \xleftarrow{C} \mu)$ from one configuration $\mu$ to another $\nu$ via a particular cluster $C$ of size $n_C$ is given by:

$$P(\nu \xleftarrow{C} \mu) = \delta_{n_\nu - n_\mu} P(n_\mathrm{max} > n) P_\mathrm{a}(\Delta E(\nu, \mu)) P_\mathrm{prop}(C, \mu), \tag{2.7}$$

where the delta function $\delta_{n_\nu - n_\mu}$ rejects overlapping particles, it is 1 if the number of particles in the two configurations is equal and 0 otherwise.

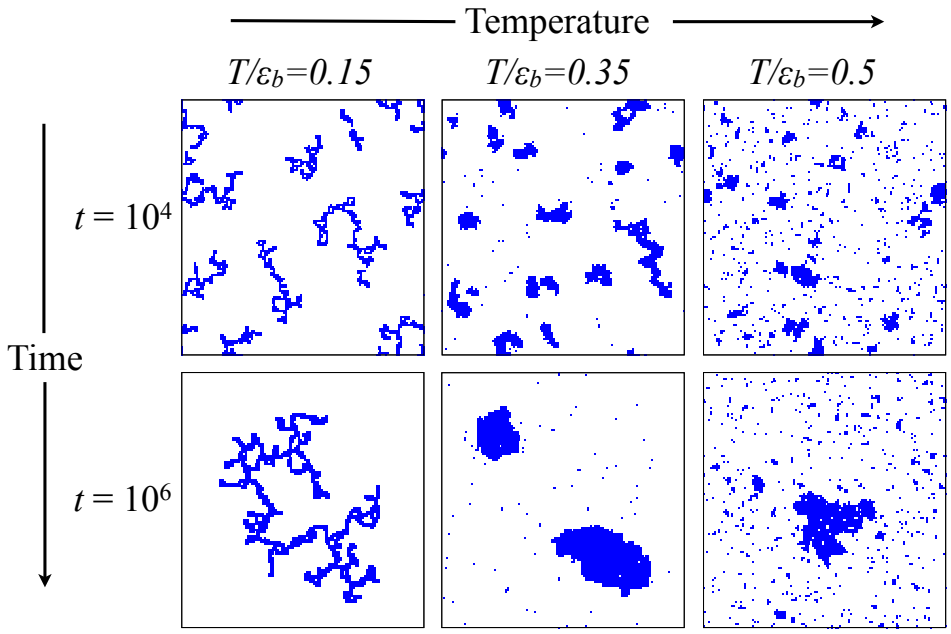


**Figure 2-4:** *Configurations are shown for three reduced temperatures* $T/\epsilon_{\mathrm{b}} = 0.15, 0.35, 0.5$*, illustrative of kinetic trapping, optimal assembly, and poor assembly at* $t = 10^4$ *and* $10^6$ *MCS.*

### 2.1.4 Yield in the Lattice Gas

Finally we are in position to examine the dynamic behaviour of the system which is illustrated in Fig.2-3. As in the previous section where we reproduced yield in a capsid and crystal model, the yield measures the quality, or amount, of product in the system at a particular time. In the 2D lattice gas we define the yield as the fraction of particles having four occupied neighbour sites. We plot the yield, $n_4(t)$, the proportion of particles which have all nearest neighbours occupied at $t = 10^4, 10^6$ after initialisation in random configurations for a range of temperatures and averaged over many trajectories. The location of the binodal at the density simulated, $\phi = 0.1$, and the equilibrium yield, $n_4(\infty)$ are also indicated. The equilibrium expectation does not reach 100% because the relatively small number of particles in the systems gives a relatively large surface where particles are not fully bonded. The yield shows the non-monotonic temperature dependence typically observed in self-assembling systems[36, 43, 28].

Above the binodal the yield quickly reaches the equilibrium expectation and by the later time, temperatures below but close to the binodal are approaching the equilibrium expectation. Optimal assembly occurs at $T^* \approx 0.35$ and shows

a broad, stable peak between the two times considered. At lower temperatures the yield falls well below the equilibrium expectation. To help illustrate why this occurs we include configurational snap shots for systems at $T/\epsilon_{\rm b} = 0.15, 0.35, 0.5$ in Fig.2-4 at the two times for which the yield is plotted.

Beginning with the righthand column at temperatures just within the binodal, small clusters at early times grow and merge to form a single large, but poor quality cluster when the system approaches equilibrium, though a large proportion of particles remain dispersed in the low density phase. At low temperature the system rapidly forms small string-like clusters which assemble into a single fractal-like structure similar to those produced in diffusion limited aggregation[53]. At optimal assembly the system assembles steadily into large clusters having few defects with few particles remaining in the dilute phase.

## 2.2 Patchy Particles

Many studies have considered simplified particles designed to assemble into specific structures while retaining varying levels of detail of the original systems. Recent examples have included capsid models[31, 59], chaperonin schemes[74, 75] and the family of Janus particles[63]. While these have taken inspiration directly from biological systems or experimental advances, other work has considered systems of patchy particles designed to assemble into the platonic solids[77, 78].

Spherical particles are positioned at the vertices of the given solid and have circular patches located about the points where edges cut the sphere and neighbouring particles touch. Particles experience a Lennard-Jones like interaction if patches on both particles are intersected by the line connecting their centres. The size of the patches and the range and angular dependence of the interaction are chosen to approximate hydrophobic interactions[77].

### 2.2.1 The Model

We take the same basic model for our system of patchy hard particles, but instead of a circle and angular-dependent Lennard-Jones-like interaction, 'patches' are points and if two patches are within a distance $\epsilon_{\rm r}$ then they interact with an energy, $-\epsilon_{\rm b}$. As with the lattice gas the system is initialised in a random configuration and undergoes translational or rotational moves of single particles. Translational moves are generated randomly within a cube of $\pm\delta_r$ and rotational

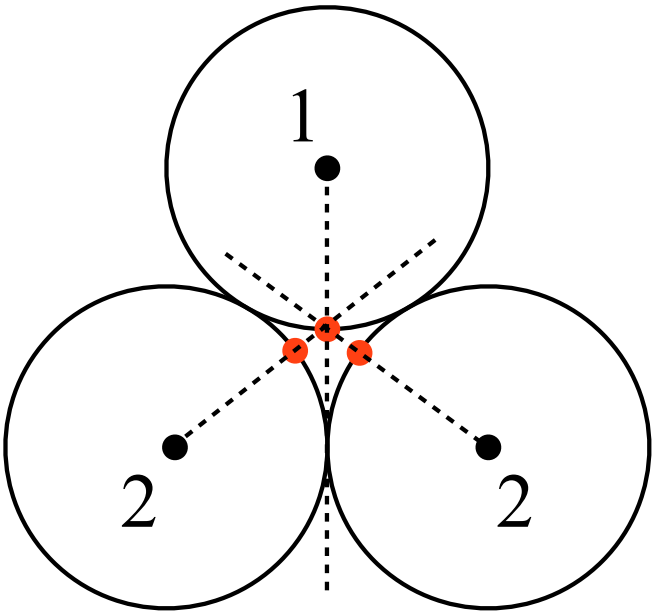


**Figure 2-5:** *Geometry for maximum range of inter-patch interactions in the patchy particle scheme. A projection of the three particles show all touching. The patch (red) on particle 1 points towards the contact point between particles 2. Patches on particles 2 are then oriented towards the patch on particle 1 giving a maximum range of* $\approx 0.1195\sigma$.

moves, about a random axis **r** by a random angle $\theta_r$ such that the maximum arc length that may be travelled at the equator equals $\delta_r$.

Proposed moves are accepted with the same modified Metropolis probability, Eq.2.6, that was used earlier for the lattice gas. However, since only single particle moves are attempted, the $[1 - \lambda]$ term does not appear and acceptance is decided just on the basis of the energy difference between the initial and proposed configurations. Finally the type of move is selected at random for each move with equal probability of translational and rotational moves. Provided the interaction range $\epsilon_\mathrm{b}$ is comparable with the maximum move size $\delta_r$ then clusters of particles are able to move without breaking bonds. This means that although single particle moves will not necessarily approximate Brownian diffusion, they do not result in the unphysical activated diffusion that is found in the lattice gas.

In order for the particles to assemble as intended, it is important to consider the limitations to the range of the interaction between 'patches'; importantly each must only be able to interact with one other 'patch'. Illustrated in Fig.2-5 the limit can be obtained by positioning three particles so that they all touch: a patch on particle (marked 1 in the figure) points towards the contact of the other two particles; the patches on the remaining particles (marked 2) point

towards the patch on the first. The interaction range is limited by the distance between the patches and is found by simple geometry to be $\epsilon_r < 0.1195\sigma$. This is independent of the type of assembling particle (and target structure) simulated here and we take $\epsilon_r = 0.1\sigma$ throughout. Checking distances between patches scales as $n_p^2$ which is a drawback of the model system. The interaction is simple to consider analytically but quite computationally costly to implement compared to that used in the work of Wilber and in the capsid simulation which scales with $n_p$.

A simple square well interaction has several useful features: particles are either bonded or not, relationships between measurements that we derive for the Lattice Gas are easily generalised to the system and bonded particles are able to diffuse without breaking the bond, and without having to implement a cluster algorithm. Additionally the design of patchy particles can easily be modified to assemble into extended structures meaning that the dynamics of the assembly of both classes of structure may be addressed within the same model system. While time constraints limit the extent to which this is investigated in the present work preliminary results with the systems are presented and compared with results obtained in the Lattice Gas.

Throughout data is presented for a system of $N = 1000$ particles and a cubic cell structure of length $L = 24\sigma$. For $\delta_r = \epsilon_r = 0.1\sigma$ typical of values used in the study this gives a volume fraction of $\rho \approx 0.038$. The energy of the system is calculated in just the same way as in the Lattice Gas model, Eq. 2.2, while the maximum number of bonds is the number of patches $n_\mathrm{p}$. In the present work we present preliminary results for systems forming tetrahedra, $n_p = 3$, icosahedra, $n_p = 5$ and close-packed extended hexagonal sheets, $n_p = 6$.

These three systems are chosen because they are all composed of triangular units. In their studies Wilber *et al*[78] found that in simulations of closed structures the tetrahedra and icosahedra with triangular faces assembled more readily than cubic or dodecahedral systems. They argued that this is because the cube, for example, having square faces required four particles to come together in stable configuration before further assembly could take place. In contrast triangular faces are almost self-stabilising, when clusters of three particles form they will naturally form triangles.

### 2.2.2 Yield in patchy particle systems

We now turn to the yield of the three systems, beginning with the two closed systems in Fig.2-6. Yield, $y(t)$ is now taken as the proportion of particles fully bonded *and* in fully formed closed structures. In the first plot, the yield in the tetrahedra is plotted first with the icosahedral yield below. For clarity, snapshots imaging the target structure are included here and, where relevant, fully bonded particles are shown in grey. We simulate both systems for $10^7$MCS at which point we use the yield to identify optimal assembly, however we also include plots of the yield at earlier times.

In the tetrahedral system optimal assembly is at $T^* = 0.95$ with a yield of $\approx 90\%$ and unlike in the lattice gas where $T^*$ remained broadly stable over several orders of magnitude, the location of optimal assembly changes substantially as the system evolves. At $t = 10^6$ the maximum in yield is at $T \approx 0.105$ so the location of optimal assembly falls as the systems age. At $t = 10^5$ there is no significant yield across the range of temperatures. This also contrasts with the lattice gas where substantial yield is observed two orders of magnitude before we stop simulations.

In the icosahedral system we observe similar general features with the yield remaining small at all temperatures at $t = 10^6$. Again the peak at the earlier time is located at $T \approx 0.13$ while by the end of simulation optimal assembly is found to be $T^* = 0.12$. Despite having to make clusters of twelve particles rather than the four in the tetrahedral system roughly 80% of particles are found in the target structure, comparable with the simpler system.

In Fig.2-6 we present similar data for the close packed sheet and include illustrative snapshots of systems at low temperature and at optimal assembly, the final time is again at $t = 10^7$. Yield is now just the proportion of particles fully bonded (shown in grey in snapshots). Optimal assembly is located at $T = 0.155$, achieving a yield of about 70% and differently from the closed systems this has increased in temperature from the earlier time. Although this is smaller than the two closed systems it should be borne in mind that crystals have a surface where particles will have free bonds and this puts an upper bound on the yield (this is also seen in the lattice gas where the equilibrium yield is about 90%).

The snapshot at optimal assembly shows the majority of particles in a single sheet spanning the periodic boundaries of the system. Two pairs of particles are highlighted in red and circled. These are all in the sheet but are not fully bonded at the time the configuration is recorded. They have undergone a spontaneous

fluctuation which has temporarily broken a bond in each pair however this would be expected to quickly relax back to the fully bonded state. In the snapshot at lower temperature the system is more disordered having disparate clusters of particles. In a larger cluster we identify two rings of particles surrounding a particle vacancy, typical of the defects found in kinetically trapped systems.

## 2.3 Chaperonin Model & Other systems

While the two systems described above have been studied by the author it is useful to compare their behaviour with other systems to ascertain the generality or limitations of the methods and measurements we will describe. The simplest of these are continuum analogies of the lattice gas in two and three dimensions, sticky disks and spheres. In these systems short-range square-well attractive interactions favour phase separation into high and low density phase as the temperature is lowered.

The assembling behaviour of the lattice gas was compared with that of the Chaperonin model in our recent paper, and some of these results are reproduced here. Whitelam's Chaperonin model[74], like the patchy particle system of Wilber, makes use of an angular dependent Lennard-Jones interaction which can be tuned to favour polar or equatorial bonding. This choice selects between the Chaperonins forming chains or sheets at low temperature/high bonding strength. Additionally the angular dependence may be adjusted to alter how specifically aligned particles must be in order to interact.

The final system we consider simulates viral capsids and was studied in a paper[36] from which the major themes of the present work continue. This is one of several classes of models designed to mimic the symmetry of the viral capsids[31]. Again particles interact through patchy particles having modified Lennard-Jones attractions and form closed structures having greater complexity than the simple Platonic solid formers described above.

## 2.4 Measuring Responses

Response functions are of interest because one approach to measuring the way in which a non-equilibrium system deviates from equilibrium is to compare response and correlation functions. A brief summary of the Fluctuation Dissipation Theory (FDT), which equates correlation and response functions at equilibrium, its

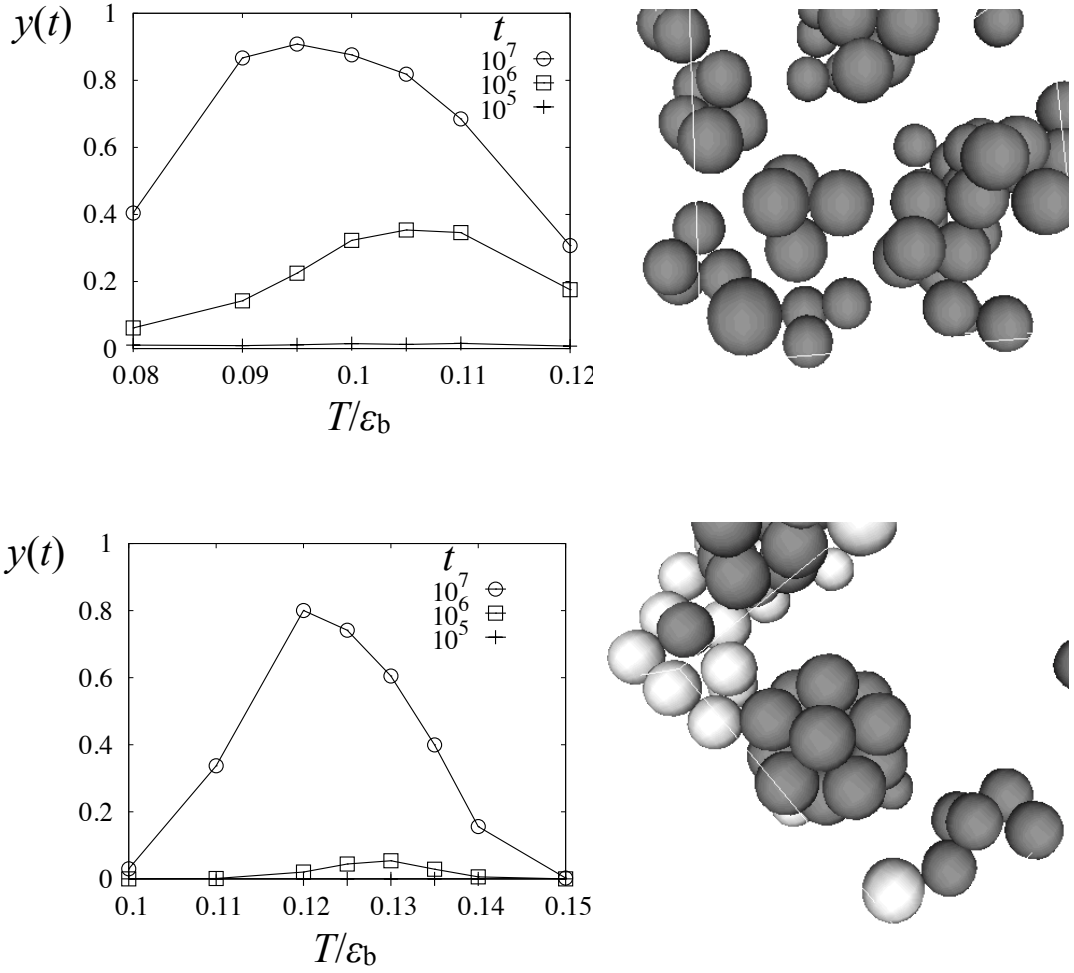


**Figure 2-6:** *Yield plots for patchy particle systems forming tetrahedra (top) and icosahedra (bottom) as a function of temperature at* $t = 10^5, 10^6$ *and* $10^7$ *MCS. At the earliest time there is no significant yield in either systems. The peak in assembly moves to lower* $T/\epsilon_b$ *reaching 80-90% during the simulation. Snapshots of the target product are shown for each system where fully bonded particles are shaded in dark grey.*

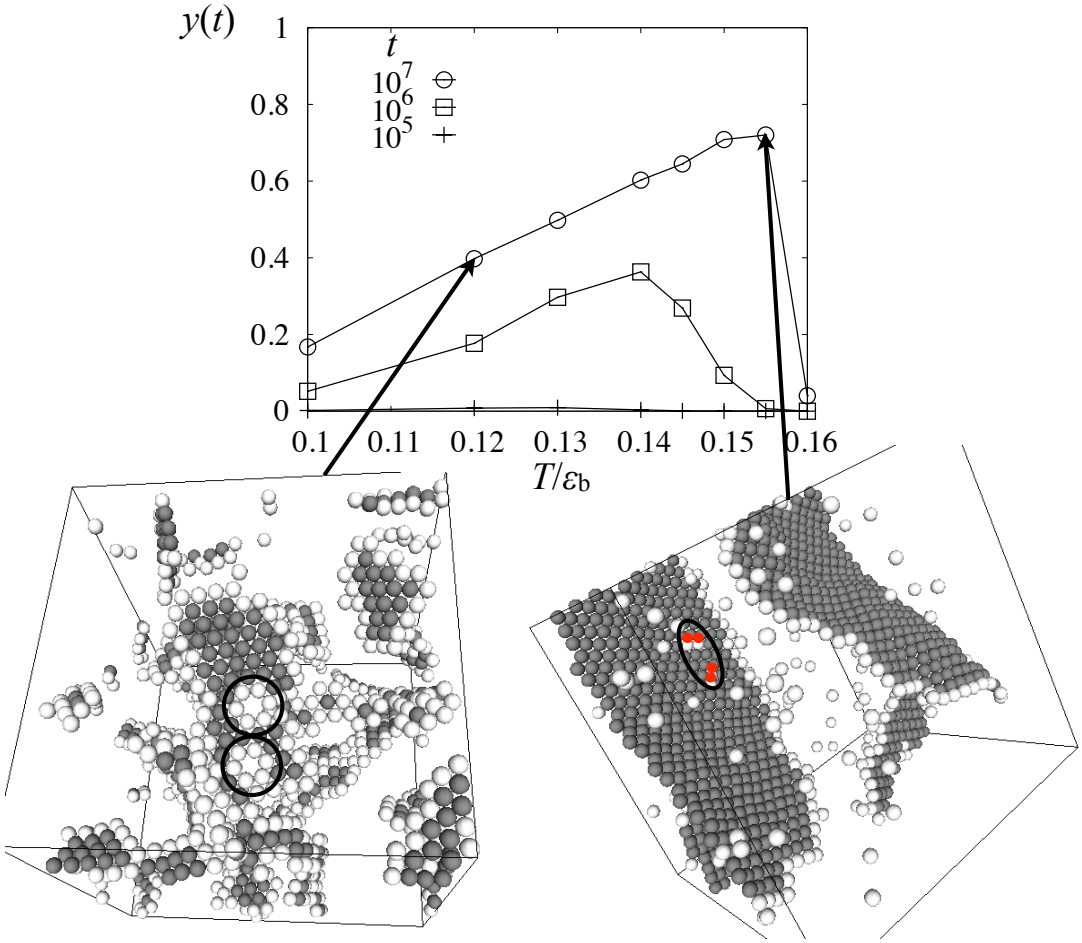


**Figure 2-7:** *Yield plots for patchy particle system forming closed packed hexagonal sheets (bottom). Yield is plotted at* $t = 10^5, 10^6$ *and* $10^7$ *MCS. At the earliest time there is no significant yield and the peak in assembly moves to higher temperatures at later times. Configurational snapshots are shown for the final time for poor and optimal assembly systems. In the former many disordered clusters make up the system, two hole defects are indicated in a large fragment. In contrast at optimal assembly a single high quality sheet dominates the system having only four (highlighted) particles within the sheet that are not fully bonded having undergone a fluctuation.*

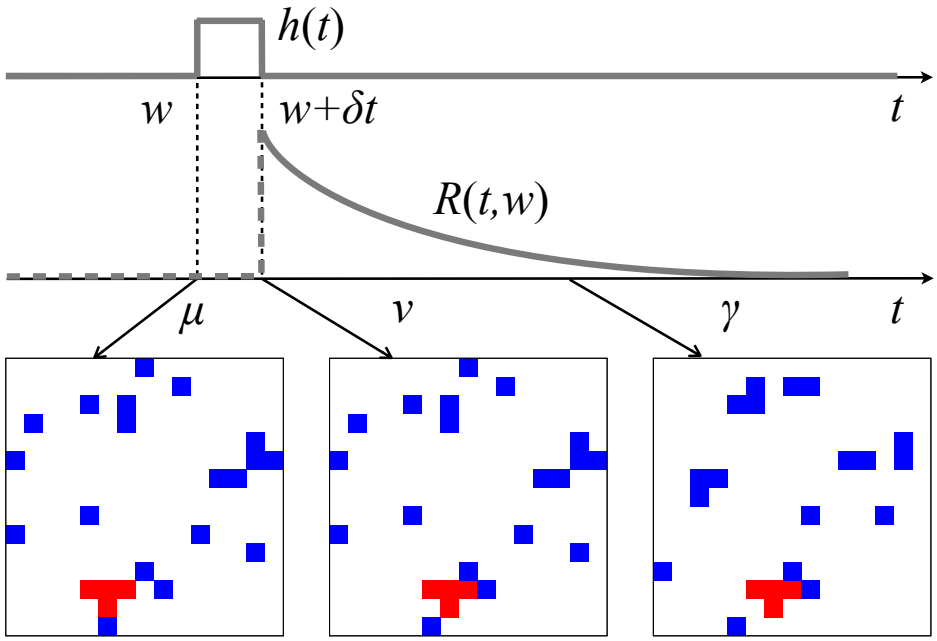


**Figure 2-8:** *Procedure for measuring the impulse response. The system is initialised in a random configuration. After a waiting time, $w$, a perturbation is applied for a single MC move during which the system attempts a move from configuration $\mu$ to $\nu$. The field is then switched off and the system allowed to evolve until time $t$, at which point its configuration is denoted by $\gamma$. The typical response of the system is indicated, together with snapshots showing how particles might move through the system. (The cluster that moves in the step while the perturbation is applied is highlighted.)*

origins and a derivation is given in Chapter 4. The method we implement for measuring responses plays an important role in the design of our model systems, with particular relevance to the parameters $\alpha$ and $\lambda$ introduced earlier. Here we introduce the idea of a response and derive the *no-field* method for measuring the response for the general case and specifically how it applies to the systems studied.

If a system for instance a ferromagnet in the earth's magnetic field, is subjected to a magnetic field, its magnetism will change. Changing the relative strength of protein-protein interactions by modifying the pH of their solvent will alter the behaviour of the proteins. In both cases the systems respond to a perturbation. In general one can write the impulse response, $R(t, w)$, of an observable,

$\langle A(t)\rangle$, as

$$R(t,w) = \frac{1}{\delta t}\frac{\partial\langle A(t)\rangle}{\beta\partial h_w}. \tag{2.8}$$

The response is a two time function depending on $w$, the time at which the field, $h_w$ is applied, and $t$ the time at which the response is measured. This is illustrated in Fig. 2-8. The impulse response is represented schematically by a step function at a time $w$, historically this is the 'waiting' time, following initialisation, at which the field is applied. The observable responds to the perturbation during its application and begins to relax once the field is turned off. In practice however, whether in experiment or simulation, it is difficult to obtain measurements of $R(t,w)$ directly, because of statistical noise in measurements.

As a result most studies have considered the integrated response[20, 66, 36] $\chi(t,w)$, to a field which is turned on at $w$ and remains applied until the later time $t$,

$$\chi(t,w) = \int_w^t R(t,t')dt', \tag{2.9}$$

which has the same affect as applying a series of impulse perturbations successively from $w$ until $t$. Although it is still necessary to average over many instances, measuring the response of a system over a finite interval means that the measurement is less susceptible to statistical noise and in some cases similar information may be obtained from it by taking the measured integrated response and differentiating numerically with respect to the time of the perturbation, $w$.

In order to differentiate one needs many measurements of $R(t,w)$ with different $w$ and simulations must be run turning the field on at each $w$. To obtain measurements at different $w$ one cannot simply use the same data set for the different measurements, as once the field is turned on the system is no longer in its original unperturbed state (different $t$ may be obtained by simply running the experiments/simulations and making measurements at successive $t$). Under this methodology responses have been measured in experiments and simulations. Even then the need to guarantee a linear response requires the consideration of different strength fields and as the strength of the perturbation is reduced so is the response relative to noise, increasing the difficulty of measurement.

Recently however studies of responses[16, 61, 26, 50, 51, 5, 70] have found that in simulation, and in particular with Monte Carlo techniques, it is possible to measure the response of the system without having to apply a field. These

build on work expressing the response as a correlation function of the form

$$R(t, w) = \langle A(t)B(w)\rangle \tag{2.10}$$

where $A(t)$ remains the observable that the field couples to and $B(w)$ is a function of the system at the time at which the field is applied.

These methods are of great benefit to those studying response functions because it means that data for many $w$ can be obtained in a single simulation, since no field is applied the system is always in an unperturbed state. Also by definition the linear response is being measured so there is no need to repeat simulations at successively weaker field strengths to check the measurements. These mean that the number of simulations required to obtain accurate data is greatly reduced allowing more detailed numerical study.

### 2.4.1 The No-Field Method

In deriving expressions for the no-field method it is useful to start from expressions of the observable $\langle A(t)\rangle$. In a system at equilibrium this may be written as

$$\langle A_{\text{eq}}\rangle = \sum_{\mu} A(\mu)\rho_{\text{eq}}(\mu) \tag{2.11}$$

where we use $\mu$ to represent a configuration and $A(\mu)$ is the value of the observable $A$ in that configuration. $\rho_{\text{eq}}(\mu)$ is the equilibrium probability of being in $\mu$ and the sum is performed over all configurations. For a system not at equilibrium the expression must be modified to

$$\langle A(t)\rangle = \sum_{\mu} A(\mu)\rho_t(\mu) \tag{2.12}$$

where $\rho_t(\mu)$ is now the time dependent probability of being in configuration $\mu$.

In order to measure the response it is necessary to represent the trajectory of the system in configuration space. After a single attempted move, taking $\delta t$, we may write the expectation value as

$$\langle A(t+\delta t)\rangle = \sum_{\gamma\mu C} A(\gamma)\delta t W^0(\gamma \xleftarrow{C} \mu)\rho_t(\mu). \tag{2.13}$$

where we have introduced the transition rate $W^0(\gamma \xleftarrow{C} \mu) = P^0(\gamma \xleftarrow{C} \mu)/\delta t$,

the superscript 0 is used to indicate that the system is not perturbed, while we have included the dependence upon the proposed cluster $C$ (since this can in principle affect the no-field method) and summation over possible cluster moves. Expanding to longer trajectories and introducing $u = t - w$ for compactness of notation, the propagator, $G_u^0(\gamma \leftarrow \mu)$ is the probability of being in configuration $\gamma$ at time $t$ given that the system was in $\mu$ at time $w$. The value of the observable at time $t$ may now be expressed in terms of the probability distribution at time $w$

$$\langle A(t) \rangle = \sum_{\gamma\mu} A(\gamma) G_u^0(\gamma \leftarrow \mu) \rho_w(\mu). \tag{2.14}$$

The sum is now over both configurations $\gamma$ and $\mu$.

If the effect of the perturbation at $w$ to the trajectory is introduced the propagator is $G_u^h(\gamma \leftarrow \mu)$, $h$ indicating the field. But if the field is applied only at $w$ for a single move attempt $\delta t$ the propagator may be separated into a perturbed part, at $w$ and an unperturbed part for the remainder of the trajectory. Using $u' = t - w - \delta t$ this gives

$$G_u^h(\gamma \leftarrow \mu) = \sum_{\nu C} G_{u'}^0(\gamma \leftarrow \nu) \delta t W^h(\nu \overset{C}{\leftarrow} \mu). \tag{2.15}$$

Figure 2-8 helps to clarify what this describes: Greek letters represent configurations, $t$ and $w$ times, while $u$ and $u'$ are intervals of time. At time $w$ the system is in configuration $\mu$; it attempts a move to configuration $\nu$ under the influence of the perturbation; after $\delta t$ the field is turned off and the system evolves to the final configuration $\gamma$ at time $t$. The transition rate $W^h(\nu \overset{C}{\leftarrow} \mu)$ is used for convenience later. The expectation value of the observable $A(t)$ under the application of a field at an earlier time is obtained by combining Eq.2.14 and Eq.2.15,

$$\langle A(t) \rangle = \sum_{\gamma\nu\mu C} A(\gamma) G_{u'}^0(\gamma \leftarrow \nu) \delta t W^h(\nu \overset{C}{\leftarrow} \mu) \rho_w(\mu). \tag{2.16}$$

The response is just the derivative of the perturbed expectation value with respect to the field. Because the field is only applied at $w$ and the only part of the trajectory that depends upon the field is the transition rate, the response is

$$\begin{aligned} R(t,w) &= \frac{1}{\delta t} \frac{\partial}{\beta \partial h_w} \langle A(t) \rangle \\ &= \frac{1}{\beta} \sum_{\gamma\nu\mu C} A(\gamma) G_{u'}^0(\gamma \leftarrow \nu) \frac{\partial}{\partial h_w} W^h(\nu \overset{C}{\leftarrow} \mu) \rho_w(\mu). \end{aligned} \tag{2.17}$$

We need to normalise by the time step $\delta t$ because of the discrete time step of the methods we implement, and this cancels with the $\delta t$ in Eq.2.16. The final step in obtaining the general result for the no-field method measurement of response is to re-write the derivative of the transition rate using $\frac{\partial X}{\partial x} = X \ln \frac{\partial X}{\partial x}$ to obtain

$$R(t,w) = \frac{1}{\beta} \sum_{\gamma\nu\mu C} A(\gamma) G^0_{u'}(\gamma \leftarrow \nu) W^0(\nu \overset{C}{\leftarrow} \mu) \frac{\partial}{\partial h_w} \ln W^h(\nu \overset{C}{\leftarrow} \mu) \rho_w(\mu) \quad (2.18)$$

and it is just left to recognise the result of the transition probability $G^0_{u'}(\gamma \leftarrow \nu) W^0(\nu \leftarrow \mu)$ is just the probability of an unperturbed trajectory starting in $\mu$ and ending in $\gamma$, of duration $u$, via $\nu$ through the cluster $C$ at $w$. This is then just a correlation function of the form of Eq. 2.10 where $B(w)$ receives the contribution

$$B(\nu \overset{C}{\leftarrow} \mu) = \frac{\partial}{\beta \partial h_w} \ln W^h(\nu \overset{C}{\leftarrow} \mu). \quad (2.19)$$

### 2.4.2 The Chatelain Field in the Lattice Gas

The last step in developing no-field methods is to decide how to measure $B(w)$. In the method due to Chatelain[16], $B(w)$ is measured by considering the effect of a perturbation on the move that happens at $w$, i.e. in the attempted move from $\mu$ to $\nu$. Other implementations have noticed that rather than the particular move that occurs at $w$, all moves that could occur can be included, $B(w) = \sum_{C,\nu} B(\nu \overset{C}{\leftarrow} \mu)$, improving the statistics of the measurement[50, 19]. In order to do this however one must be able to account for all possible moves at $w$ and whether this is practical or possible depends upon the particular dynamics employed. For the cluster algorithm and continuum models it is convenient to use Chatelain's method[27].

In order to utilise the method clearly the transition rates for moves must be differentiable, otherwise $B(w)$ cannot be evaluated. As described earlier we implement a Metropolis algorithm as this best approximates the physical systems we have in mind. For energy decreasing moves the Metropolis-like acceptance probability is always unity and so if $E(\nu) < E(\mu)$ the application of an infinitesimal field does not change the probability of the move and the contribution to the Chatelain field is $B(\nu, \mu) = 0$. Conversely, if $E(\nu) > E(\mu)$ and $\Delta E(\nu, \mu) = E(\nu) - E(\mu)$ the move is accepted with a Boltzmann probability $P_{\rm a} = \exp(-\Delta E(\nu, \mu))$.

The contribution now depends on the way in which the perturbation couples to the move probability. If the perturbation affects the coupling between particles

then the additional energy change of the move is

$$\Delta E^h(\nu,\mu) = h_p \Delta n_p(\nu,\mu), \tag{2.20}$$

where $\Delta n_p = n_p(\nu) - n_p(\mu)$ is the change in the numbers of bonds of the particle whose bonding strength is changed. In our implementation the effect of this is incorporated directly into the acceptance probability giving $P_{\rm a} = \exp(-\Delta E^0(\nu,\mu) - \Delta E^h(\nu,\mu))$. Since this is the only component of the transition rate that depends on the field we can evaluate $B(\nu \overset{C}{\leftarrow} \mu)$ by taking the natural logarithm, followed by the derivative with respect to the applied field. This gives

$$\begin{aligned} B_p(\nu \overset{C}{\leftarrow} \mu) &= \frac{\partial}{\beta \partial h_w}(-\beta \Delta E^0(\nu,\mu) - \beta \Delta E^h(\nu,\mu)) \\ &= \Delta n_p(\nu,\mu), \end{aligned} \tag{2.21}$$

where the subscript $p$ indicates that each particle receives its own Chatelain field contribution at each attempted move. This is the contribution to the individual particles 'Chatelain field' if the move would result in an increase in the system energy and accepted. What if the proposed move is instead rejected? Returning to Eq. 2.17, if a move to the $\nu$ configuration is rejected one may write

$$\begin{aligned} R(t,w) =& \frac{1}{\beta} \sum_{\gamma\nu\mu C} A(\gamma) G^0_{u'}(\gamma \leftarrow \mu) \\ & \times W^0(\mu \overset{C}{\leftarrow} \mu) \frac{\partial}{\partial h_w} \ln W^h(\mu \overset{C}{\leftarrow} \mu) \rho_t(\mu) \end{aligned} \tag{2.22}$$

where the need to consider the particular cluster is now clear, many rejected moves leave the system unchanged, and the propagator now runs from $\mu$ since the rejected move at $w$ leaves the system unchanged. But the change in the transition rate for rejecting the move is just the negative of the change observed when the move is accepted which gives

$$\begin{aligned} R(t,w) =& \frac{1}{\beta} \sum_{\gamma\nu\mu C} A(\gamma) G^0_{u'}(\gamma \leftarrow \mu) \\ & \times \left( -W^0(\nu \overset{C}{\leftarrow} \mu) \frac{\partial}{\partial h_w} \ln W^h(\nu \overset{C}{\leftarrow} \mu) \right) \rho_t(\mu). \end{aligned} \tag{2.23}$$

In order to identify the contribution to $B_p(w)$ it is necessary to combine the propagator and transition rate, but this must be for the rejected rate as in Eq.

2.22 not the accepted rate as in Eq. 2.23. This can be simply manipulated to

$$\begin{aligned} R(t,w) =& \frac{1}{\beta}\sum_{\gamma\nu\mu C} A(\gamma)G^0_{w'}(\gamma \leftarrow \mu)W^0(\mu \overset{C}{\leftarrow} \mu) \\ & \times \left(-\frac{W^0(\nu \overset{C}{\leftarrow} \mu)}{W^0(\mu \overset{C}{\leftarrow} \mu)}\frac{\partial}{\partial h_w}\ln W^h(\nu \overset{C}{\leftarrow} \mu)\right)\rho_t(\mu). \end{aligned} \tag{2.24}$$

The contribution to the Chatelain field for rejected moves, $B_p(\mu \overset{C}{\leftarrow} \mu)$ may then be extracted from this giving

$$B_p(\mu \overset{C}{\leftarrow} \mu) = -\frac{W^0(\nu \overset{C}{\leftarrow} \mu)}{W^0(\mu \overset{C}{\leftarrow} \mu)}\frac{\partial}{\partial h_w}\ln W^h(\nu \overset{C}{\leftarrow} \mu), \tag{2.25}$$

where the notation $B(\mu \overset{C}{\leftarrow} \mu)$ implies that the system stays in its initial configuration by rejecting a move of the cluster $C$. This is just the negative of the contribution from accepted moves, modified by the ratio of the probabilities of each move. Physically the origin of the negative is clear, if the perturbation makes the move more likely, it increases the probability of making the move, and decreases the chances of rejecting the move.

The contributions derived are for energy increasing and decreasing moves. As the Metropolis formula has a discontinuous gradient at $\Delta E^0 = 0$, it is not compatible with the no-field method. To see this consider a perturbation applied during a move which would otherwise leave the system energy unchanged. If under the perturbation the move would decrease the system energy, acceptance probability would remain equal to unity. Conversely if the perturbation would increase the final energy, the acceptance probability would be decreased as described above. Now since one direction has a modified probability but not the reverse a situation would result which is not consistent with detailed balance.

Previous studies have considered Glauber acceptance probabilities, in part because this gives a continuous and differentiable function for all energy changes. Earlier the parameter $\alpha = 0.9$ was used to determine the acceptance probability for moves where the energy remains unchanged. For the purposes of implementing the no-field method a Glauber form is introduced for moves where the unperturbed energy change is zero:

$$P_{\mathrm{a}}(\Delta E(\nu,\mu)) = \frac{2\alpha}{1+\Delta E(\nu,\mu)}. \tag{2.26}$$

This is now differentiable and it is simple to show that it gives a contribution to accepted moves

$$B_p(\nu \overset{C}{\leftarrow} \mu) = \frac{1}{2}\Delta n_p(\nu, \mu). \tag{2.27}$$

Rejected moves have a contribution modified by the acceptance probability divided by the rejection probability as with energy increasing moves. The appearance of the factor of a half is natural because whereas uphill-downhill pairs of moves only receive a response from the uphill move, when the move is energy neutral both directions contribute to the response. The different contributions to the Chatelain field can be summarised as $B_p(\nu, \mu) = \Theta(\Delta E^0(\nu, \mu))I\Delta n_p(\nu, \mu)$, where $\Theta$ is the step function with $\Theta(0) = \frac{1}{2}$, $I = 1$ if the move is accepted and $I = -W(\nu \overset{C}{\leftarrow} \mu)/(1 - W(\nu \overset{C}{\leftarrow} \mu))$ if the move is rejected. This formulation is valid for any system employing the acceptance probability described and having discrete energy levels allowing it to be applied directly to the patchy particle system.

### 2.4.3 Implementing No-field Methods

Now that the contributions to the response have been derived it is worthwhile fully describing the implementation. From the correlation form of the response it is clear that two measurements must be recorded: the Chatelain field contributions $B_p(w)$ and the conjugate observable $A_p(t)$, which for the perturbation considered is just the energy, or equivalently the number of bonds of the particle. These must be recorded for each particle during the simulation so that the correlation may be calculated at the end.

In practice we do not measure the impulse but the integrated response so the individual $B_p(w)$ are instead recorded in 'bins' $B_p(i)$ of width $\Delta t$, i.e. all contributions to a particle's Chatelain field in the interval $w < t' < w + \Delta t$, where $i$ is used as the index for the bins such that $i = w/\Delta t$. The response is calculated according to

$$\chi(t, w) = \sum_p n_p(t) \times \sum_{i=w/\Delta t}^{i=(t/\Delta t)-1} B_p(i). \tag{2.28}$$

The models we have described show behaviour consistent with more detailed models of assembling systems considered in previous studies. Demonstrating that systems assemble is however only the start of our story. We will now investigate

the behaviour of a series measurements in our model systems with the aim of improving our understanding of why assembly occurs where and when it does.

# Chapter 3

# Flux and Traffic

The work presented in this chapter includes material reproduced from two papers published by the author: Grant *et al* [28] and Grant and Jack[27].

Having introduced the models and techniques we are now in position to consider measurements of the dynamics of self-assembly. The importance of the role of reversibility in self-assembly is qualitatively persuasive, however in order to make use of the idea it needs to be put on a more quantitative foundation. In this chapter we will describe a measurement that 'in silico' is both intuitive and easily measured. Applied to several systems it will allow us to address two important questions, 'how reversible must a system be to assemble?' and 'how does the reversibility relate to the particles and assembled structure?'.

We begin by illustrating two versions of the measurement in the Lattice Gas together with a toy model that helps to interpret the results. This results in the introduction of complementary features of systems, 'forgivingness' and 'specificity' which will be defined and examined in the patchy particle model and compared with earlier results for the chaperonin system.

## 3.1 Kinks

A naive approach to measuring reversibility is simply to count (un)bonding events of particles, or 'kinks'. We record all events in which particles' bond numbers either increase or decrease, $K^{\pm}(t_1, t_2)$, in a given interval $t_1$ to $t_2$. If we consider a system from initialisation, $t_1 = 0$, until $t$ we can define an integrated *traffic*, or dynamic activity,

$$\mathcal{T}(t) = \frac{\langle K^{+}(t)\rangle + \langle K^{-}(t)\rangle}{N} \tag{3.1}$$

as the sum of bonding and unbonding events normalised by the number of particles. Similarly we can define the integrated *flux*,

$$\mathcal{F}(t) = \frac{\langle K^+(t)\rangle - \langle K^-(t)\rangle}{N} \tag{3.2}$$

as the net number of bonding events and we have again normalised by the number of particles[28]. The integrated flux is just the number of bonds an average particle gains during the simulation. We can consider two limiting cases for measurements of the flux and traffic: for a system initialised at equilibrium there is no net flux, $\mathcal{F}(t) = 0$ (or will plateau when a non-equilibrium system reaches equilibrium), while in the limit $T/\epsilon_{\rm b} \to 0$ unbonding events are not allowed and we have $\mathcal{F}(t) = \mathcal{T}(t)$. In general, the higher $\mathcal{T}(t)/\mathcal{F}(t)$, the more reversible a system's dynamics.

In a system which has evolved to the assembled state by $t$, $\mathcal{F}(t) \approx \mathcal{N}_{\rm max}$ is just the number of bonds that each particle has gained, where $\mathcal{N}_{\rm max}$ is the maximum number of bonds a particle can have. The integrated traffic, $\mathcal{T}(t)$ is the number of kinks, the number of times the particle makes or breaks bonds, in order to arrive in the assembled state. We aim to use the measurements to quantify a system's reversibility over the assembly process and investigate how reversibility at optimal assembly relates to the properties of the assembling particle.

### 3.1.1 Making product reversibly: Two steps forward, One step back

In Fig.3-1 traffic and flux measurements are plotted for the lattice gas ($\phi \approx 0.1$) for the range of temperatures considered for the yield measurements, optimal assembly $T \approx 0.35$ is indicated. (In this plot, and in general throughout, where we make comparisons across a range of temperatures we use a spread of colours from red, for the hottest temperature, through purples to blue, for the coldest.) The traffic is monotonic in temperature with the greatest activity taking place at high temperature. Further at high temperature the traffic is approximately linear, as expected of a system close to equilibrium. As the temperature is reduced the traffic is seen to follow a series of plateaus associated with the activation times $t \approx \exp(\Delta n \epsilon_{\rm b}/T)$ for moves breaking $\Delta n$ bonds. At $t = 10^5$ the traffic ranges across almost four orders of magnitude for the range of temperatures considered.

In contrast the behaviour of the flux is very different in time and temperature.

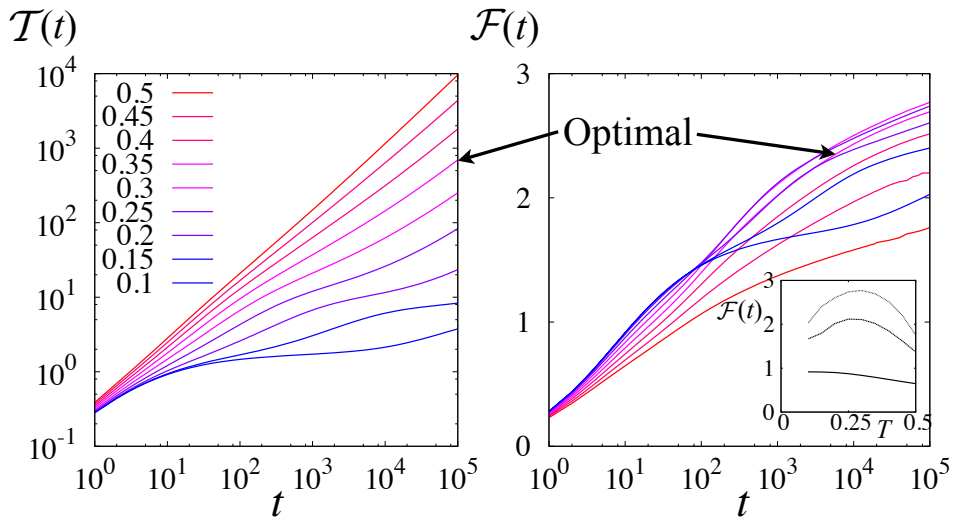


**Figure 3-1:** *Integrated traffic and flux in the Ising Lattice Gas. The traffic is monotonic in temperature at all times and is approximately linear at high temperature, while at lowest temperature a plateau associated with activation is observed. The flux is limited by the number of neighbours and shows a peak coinciding approximately with optimal assembly. Inset, flux plotted as a function of temperature at* $t = 10, 10^3, 10^5$.

Since the flux is limited to the number of bonds a particle can form the variation with temperature is far smaller than with the traffic. In the inset we plot flux against temperature for $t = 10, 10^3, 10^5$ which shows that apart from at very early times the flux is non-monotonic in temperature peaking near to optimal assembly. In practice the peak in flux is at lower temperature than optimal assembly since only those particles having 4 neighbours contribute to the yield. At low temperatures bonds initially form giving a high flux but kinetic trapping prevents further flux, delaying it reaching its equilibrium state.

The traffic divided by the flux as the system approaches the assembled state gives an indication of the reversibility of the assembly process. For the density considered at $t = 10^5$ the traffic is a few hundred at optimal assembly meaning that the number of kinks per net bond making event is typically of the order 100. This value may be a little surprising, in terms of the amount of making and breaking of bonds to obtain each bond. One might expect a few mistakes to be made before a particles joins a cluster in a correct position, but the large value is consistent with the idea of reversibility playing an important role in self-assembly. This of course is just one system at a single density and even here the broad assembly peak seen in Fig.2-3 means that a value in the range $10 - 1000$ (corresponding to $0.35 \leq T \leq 0.4$) covers two orders of magnitude a feature that

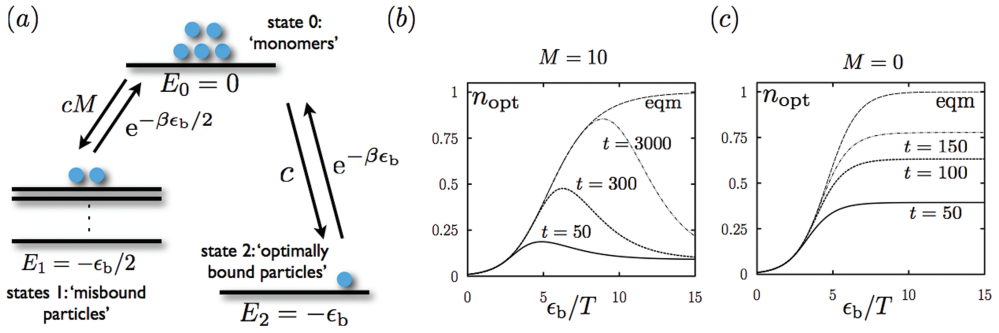


**Figure 3-2:** *a) Schematic for the toy model of kinetic trapping showing the three states and possible moves between the monomer state and either of $M$ misbound states, or a single optimal state. b) Yield plot of the toy model with $M = 10$ and c) $M = 0$.[28].*

would be useful to relate to the particles and structure formed.

### 3.1.2 A simple toy model

In order to compare and interpret the results in the different systems, it is useful to consider a toy-model of assembly which captures some of the behaviour. The model is illustrated in Fig. 3-2 having a disordered state of energy, $E = 0$, in which each particle is initiated, $M$ poorly, or misbound states of energy $E = -1$ and a single optimally bound state with $E = -2$[28]. Particles make random moves with a Metropolis algorithm ensuring that downhill energy moves are always accepted while those exiting bound states are activated. Moves between misbound and optimally bound states are forbidden. Although the model makes no pretence of capturing spatial behaviour of more physical models it does capture the principle effects of kinetic trapping.

Denoting the unbound, misbound and optimally bound states by $0, 1, 2$ respectively, the model is described by a master equation

$$\frac{\mathrm{d}}{\mathrm{d}t}\boldsymbol{P}(t) = W\boldsymbol{P}(t), \tag{3.3}$$

where $\boldsymbol{P}(t) \equiv (P_0(t), P_1(t), P_2(t))$; the variable $P_i(t)$ is the probability that a particle resides in state $i$ at time $t$; and the matrix $W$ is

$$W = \begin{pmatrix} -c(M+1) & \zeta & \zeta^2 \\ cM & -\zeta & 0 \\ c & 0 & -\zeta^2 \end{pmatrix}. \tag{3.4}$$

We have defined $\zeta \equiv \mathrm{e}^{-\epsilon_\mathrm{b}/2T}$ for compactness of notation and $c = 0.01$ is a concentration like parameter measuring the availability of optimally bound sites. The yield in this model is $n_\mathrm{opt} \equiv P_2$.

All particles start in the monomer state, so that Eq. 3.3 is to be solved with the initial condition $\boldsymbol{P}(0) = (1, 0, 0)$ and the solution obtained by matrix diagonalisation. In the long-time limit, $\boldsymbol{P}(t)$ converges to the equilibrium distribution $\boldsymbol{s} = \frac{1}{Z}(\zeta^2, cM\zeta, c)$ where $Z = c + cM\zeta + \zeta^2$ is the partition function. Thus the equilibrium (long-time) yield is $n_\mathrm{eq} = c/(c + cM\zeta + \zeta^2)$.

Figures 3-2b) and c) show the evolution of the system for $M = 10$ and $M = 0$, the former being indicative of the typical behaviour observed in 2D crystallisation while the latter may be thought of as a illustrative of a 1D filament former. With no misbound states the yield is monotonic, there is no possibility of becoming trapped, in the same way, when growing filaments there is no way in which a particle can be added in a way that prevents further assembly. As soon as there are misbound states however the non-monotonic yield seen in the Lattice Gas and patchy particle model is observed.

Flux and traffic measurements can be calculated for the model and, taking flux to be moves into the optimally bound state, total traffic is typically observed to be $\approx 2(M+1)$ (see Fig. 3-4a)) when the model approaches equilibrium. This is consistent with the idea of visiting each of the misbound states before finding the optimally bound configuration. Applying this idea directly to the results of the previous section gives the idea that if each particle makes $\approx 100$ bond making and breaking moves for each net bond, before arriving in its final destination there are of the order of 50 misbound states. It important to identify whether this is a realistic interpretation of the values of flux and traffic values observed.

The toy model presents a simple interpretation of the possibilities of misbinding. For instance in real spacial systems the accessibility of sites, whether bonding at a location will increase the number of optimal or misbound sites available, will all affect the observed behaviour. As a result the idea of forgivingness of the system has been introduced to aid interpretation of results[28]. A forgiving system will allow assembly more readily, corresponding to a low effective value of $M$ in the toy model. A system which is not forgiving will 'punish' a misbinding of particle and require particles to search out correct bonding sites enduring a lot of traffic to locate the optimally bound state.

### 3.1.3 Flux-Traffic Rates and Ratio

An alternative application of kinks is to consider rates of bonding and unbonding. If we record the number of events in an interval $\Delta t$ then we can define rates of traffic

$$\tau(t, \Delta t) = \frac{\langle K^+(t, t+\Delta t)\rangle + \langle K^-(t, t+\Delta t)\rangle}{\Delta t N} \tag{3.5}$$

and flux

$$f(t, \Delta t) = \frac{\langle K^+(t, t+\Delta t)\rangle - \langle K^-(t, t+\Delta t)\rangle}{\Delta t N} \tag{3.6}$$

in the limit $\Delta t \to 0$ the measurements converge on the true rates $\tau(t)$ and $f(t)$ but in practice we must approximate these by integrating over a finite interval. This is accurate as long as the change in rates over the period is negligible.

We define the flux-traffic ratio

$$Q(t) = \frac{f(t)}{\tau(t)} \tag{3.7}$$

which provides a dimensionless measure of the instantaneous reversibility of the system. While it is more difficult to obtain good statistics for rates than the integrated quantities described above, $Q(t)$ is closer to the qualitative description of (an instantaneous measurement of) reversibility and allows changes in the behaviour to be observed as the system evolves. This is because while the integrated quantity effectively averages over greatly varying stages of assembly, the rates allow comparison with the typical states of the system during its evolution.

As with the integrated measurements one can consider limiting values of the ratio $Q(t)$: if all moves are coagulative then we have $f(t) = \tau(t)$ and $Q(t) = 1$; a system at equilibrium will have $Q(t) = f(t) = 0$. Additionally since the integrated flux is limited to at most the number of bonds a particle can form we know that at long times $f(t) \leq t^{-1}$ and since $\tau(t)$ tends to a constant at long times and equilibrium, the same limiting behaviour also applies to $Q(t)$.

### 3.1.4 Flux and traffic rates in the lattice gas

Rate data for the traffic, flux and the flux-traffic ratio in the lattice gas is presented in Fig.3-3. This is consistent with the findings of the integrated measurements, the traffic varies least with time at high temperature, and at fixed time reduces rapidly with temperature. The flux however shows little temperature dependence, and may be approximated by $t^{-1}$ as required by the limitation of

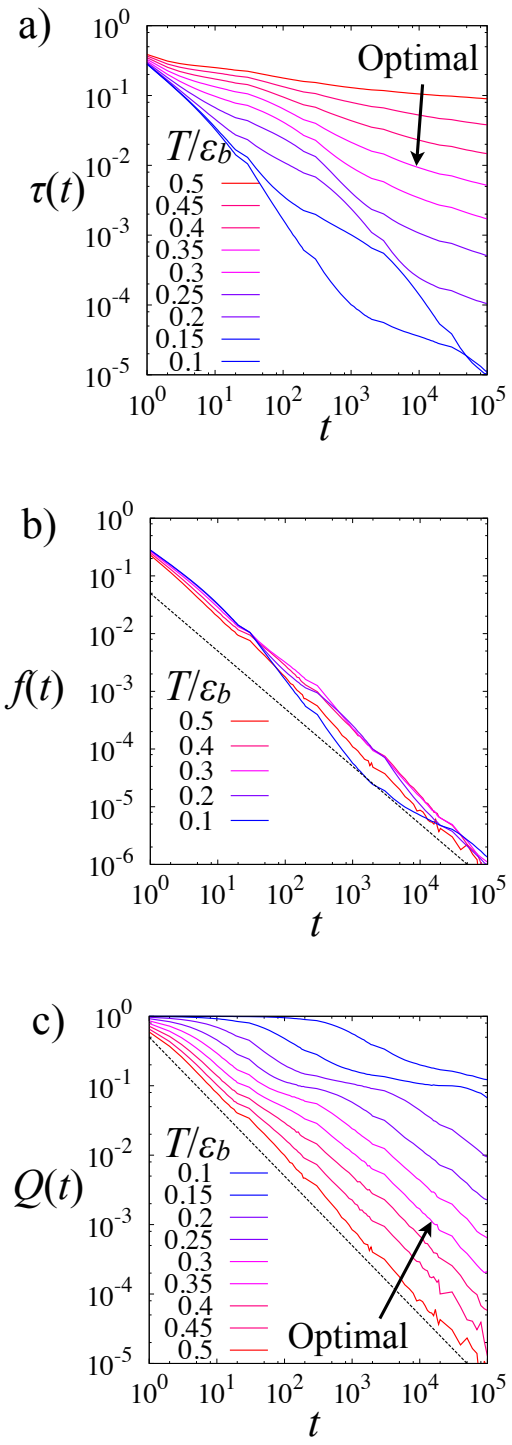


**Figure 3-3:** *Rates of traffic and flux in the Ising Lattice Gas. By later times the traffic varies over 4 orders of magnitude across the temperature range considered. In contrast the flux, constrained by the maximum number of neighbours, shows little variation across the temperature range. Dashed lines indicate $t^{-1}$ in plots of flux and the ratio. The ratio of flux and traffic is dominated by the traffic, with assembly occurring at a range of ratios, relaxing approximately as $t^{-1}$ [28].*

the integrated flux. Intriguingly the flux-traffic ratio shows that rather than a certain level of reversibility corresponding to optimal assembly in a particular system there is great variation in time. For example for times $t \leq 10^6$ optimal assembly is stable at $T^* = 0.35$ but the ratio lies in the range $1 < Q(t) < 10^{-4}$, but all other $T/\epsilon_b$ have $Q(t)$ in this range during the times considered.

While there is no clear separation between temperatures representative of different regimes allowing the prediction of the different regimes of behaviour there are features that may contribute to understanding of the processes. At high temperature $Q \approx t^{-1}$ and as the temperature is reduced a shoulder begins to develop as optimal assembly is passed. This continues to grow into a plateau when kinetic trapping occurs revealing the activation associated with kinetic trapping. Further investigation may reveal more detailed information relating to the decrease in $Q(t)$ which will allow us to make predictions based upon the measurement.

The flux-traffic ratio is an instantaneous measure of reversibility, it is the number of kinks required to make a net bond per particle at a given time. In dilute systems initial random configurations consist primarily of monomers. This means that at early times all temperatures will have values of $Q(t)$ close to one since no bond breaking moves will be possible until some bonds have begun to form. Understanding the decrease in $Q(t)$ across the range of temperatures and how its behaviour at optimal assembly relates to the assembling particle, the final product and the system's $M$ value (if one is appropriate) are the key challenges addressed in the remainder of this chapter.

## 3.2 Flux and Traffic measurements

### 3.2.1 Integrated Measurements

The use of kinks to measure reversibility in assembling systems was first reported in Grant *et al*[28], where we presented integrated flux and traffic measurements in the chaperonin model and the lattice gas at density $\rho = 0.002$. Parametric plots of the flux against traffic are reproduced in Fig.3-4, isochrones, shown as dashed lines, for the lattice gas are at $10^4, 10^5$ and $10^6$. Certain features of these plots are common to all system: At low temperature systems have significant flux at low traffic as bonding events dominate dynamics while at high temperatures flux remains low until high values of traffic. At optimal assembly, near to where the highest flux is observed we can estimate the reversibility of the process by

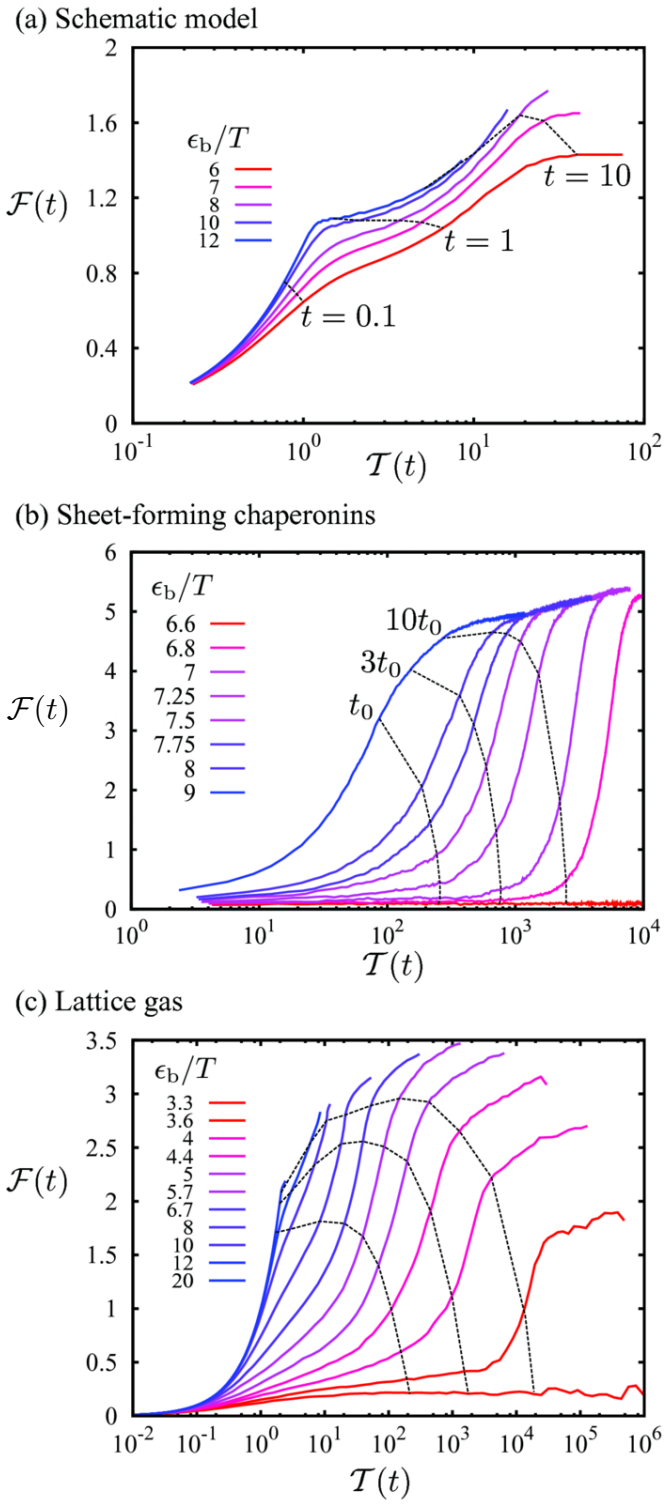


**Figure 3-4:** *Plots of integrated flux against traffic for a) toy model with M=10, b) chaperonin sheet former and c) lattice gas at density $\rho = 0.002$. The dashed lines represent isochrones which are plotted at $t = 10^4, 10^5$ and $10^6$ for the lattice gas. The schematic model gives an intuitive result of $\approx 20$ kinks for each net bond. In each of the other systems this value rises to $\approx 1000$[28].*

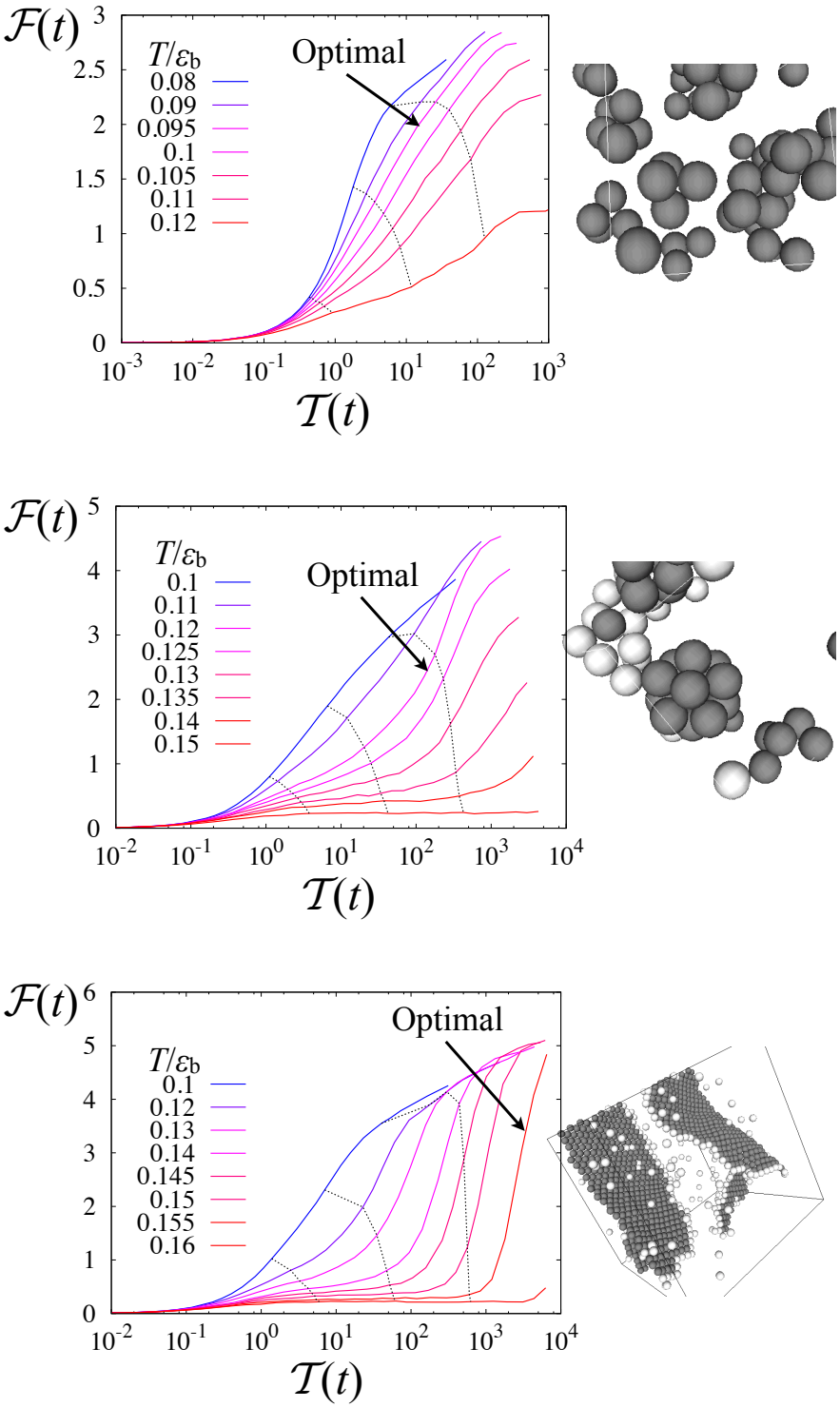


**Figure 3-5:** *Plots of integrated flux against traffic for patchy particles forming a) tetrahedra, b) icosahedra and c) close packed hexagonal sheets at volume fraction of* $\phi = 0.076$. *Isochrones (dashed lines) are plotted at* $t = 10^4, 10^5$ *and* $10^6$ *MCS.*

comparing the total flux and traffic. For the toy model it is found that typically $2M + 1$ events are required for each net bonding event into the optimal state. As suggested earlier, with $M = 0$ optimal assembly occurs when $T = 0$ since no kinetic trapping is possible and yield is maximised by never breaking bonds.

In the previous section we showed that in the lattice gas with a volume fraction of $\phi = 0.1$ roughly 100 bonding and unbonding events were required to make each bond at optimal assembly. In the chaperonin and more dilute lattice gas $\phi = 0.002$ models this rises to $\approx 1000$, suggesting that the system is highly reversible over the course of the assembly process. That the two models happen to have similar values is interesting and suggests that the forgvingness of the systems at the densities simulated may be similar. However any general explanation for their similarity must also account for the difference observed with change of volume fractions. Before attempting an explanation we will first consider three instances of the patchy particle model, which show distinct variation that may be interpreted more easily.

In the chaperonin and lattice gas models the equilibrium structures are extended crystals. In contrast the tetrahedral and icosahedral systems form closed structures. Furthermore since the patches are located at specific locations the possibility of forming misbound structures is reduced. For instance the particles forming tetrahedra can form two low energy three particle structures, illustrated schematically in Fig.3-6. The three particles form a stable triangular structure in which each is bonded to the others, bonds are shown in red. The free, unbonded patches of the particles are free to point 'up' or 'down' with the patches aligned as in Fig.3-6a), or with one misaligned, Fig.3-6b) (we borrow the magnetic notation for the free patches directed into and out of the page). Simple considerations suggest that the correct structure will be achieved in one quarter of occurrences. A fourth particle is likely to attach, forming a tetrahedron, whenever these structures form. This leads us to expect the tetrahedra system to be able to tolerate a far lower value of $M$ than seen in extended systems, and the icosahedra should lie somewhere in between.

This is indeed the case and for tetrahedra we see in Fig.3-5, where optimal assembly occurs at $T^* = 0.095$ at $t = 10^7$, that a final $\mathcal{T}(t) = 200$ corresponding to an effective $M \approx 30$. For the icosahedra formers optimal assembly occurs at $T^* = 0.12$ for which the traffic gives a value of forgivingness $M \approx 100$. In contrast the close-packed sheet former gives a value of $M \approx 500$. These results are consistent with the interpretation of forgivingness and how it relates to the

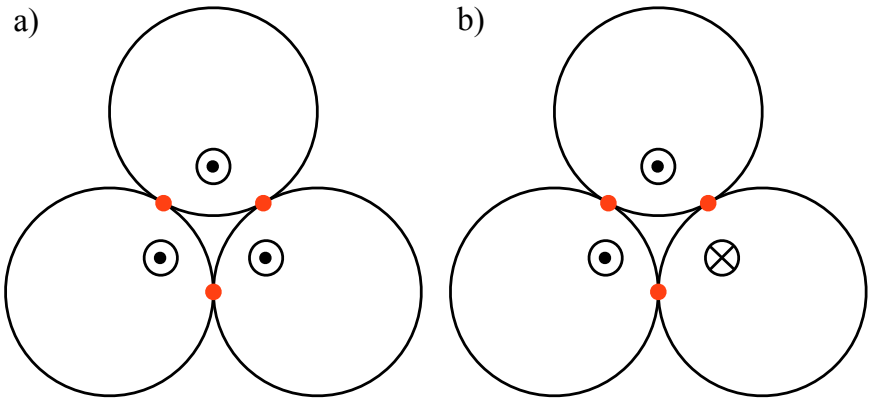


**Figure 3-6:** *Schematics of stable trimers of tetrahedron forming particles. Bonds between the three particles are shown in red and magnetic notation of up and down fields is borrowed for the orientation of the free patch. In a) the free patches are aligned and assembly can proceed easily with the addition of a forth particle. In b) the free patches are not aligned and the trimer must break at least one bond and reorient before assembly can occur.*

particle and target structure. The tetrahedra system, being the simplest structure has the lowest $M$ indicating that it is the most forgiving of the three systems. The extended close-packed sheet is the most complex final structure and is the least forgiving, its high $M$ revealing the highly reversible dynamics required for assembly, and the icosahedral system lies in between. The useful feature of the patchy particle systems is that it allows the comparison of measurements in closed and extended model systems; although the particles and target structures differ, the dynamic scheme and inter-particle interactions are the same.

Additionally the measurements can also help to identify the mechanism by which assembly takes place. In the sheet forming patchy particles, chaperonins and at high temperature lattice gas there are characteristic signals of nucleation prior to phase separation and in the first two systems optimal assembly lies in the nucleation regime. This is identified in parametric plots of flux against traffic by increasing $\mathcal{T}$ initially at constant $\mathcal{F}$. At a certain point the flux rises indicating the formation of a stable nucleus from which phase separation can then proceed readily. In contrast at lower temperatures in extended systems and in closed systems, structures appear to form more by aggregation and annealing. The dynamic properties of the different mechanism will be found to be of importance as we seek to use measurements to predict long term assembly from measurements early in the process.

There are however caveats that need to be considered. The time at which we stop simulations is to a certain extent arbitrary: for each system simulations have been run until a significant yield has been achieved, but this varies from 70-90% across the systems considered. This has a significant effect on the value of $\mathcal{T}(t)$ when the simulation is stopped and so on the value $M$ that is extracted. However, considering just patchy particle systems the achieved yield is highest in the tetrahedral system and lowest in the close-packed sheet. Thus as yield increases in each of the systems we would expect the trend in value of $M$ to be preserved or increased in line with our analyses.

More relevant with regard to the aims of the present work is that $M$ is only obtained once a system has assembled. In this respect the measurement has limited potential for predicting assembly. It does however offer a way of demonstrating and quantifying the need for reversibility in assembling systems. We now turn to measurements of rates of flux and traffic which being instantaneous indicators of reversibility may allow the prediction of the long-term behaviour of systems in addition to confirming the validity of the forgivingness interpretation of flux and traffic measurements.

### 3.2.2 Rate Measurements

In Fig.3-3 measurement of the rates of flux and traffic and their ratio $Q(t)$ in the lattice gas were presented. These measurements at volume fraction $\phi = 0.1$ show at that optimal assembly the flux traffic ratio decreases approximately as $t^{-1}$. As the temperature is lowered there is a shoulder which extends to longer times, signalling the excess of bond-making that results in kinetic trapping. An initial period of bond formation at all temperatures leads to $Q > 0.1$ at early times, as monomers aggregate. At the stage of dimer formation it is not possible to form a kinetically trapped state, all dimers are equivalent. Trapping and the need for its prevention through more reversible behaviour only becomes significant as larger clusters begin to form in the system.

Fig.3-7 presents measurements of $Q(t)$ in patchy particle systems for times up to $t = 10^5$, two orders of magnitude shorter than is required for significant yield to be achieved. As with the integrated measurements we expect the systems to require more reversible dynamics in order to assemble as we consider the closed tetrahedra, icosahedra and extended close-packed sheets. For a large range of temperatures in the tetrahedral formers $Q(t) > 0.1$ and only at the highest tem-

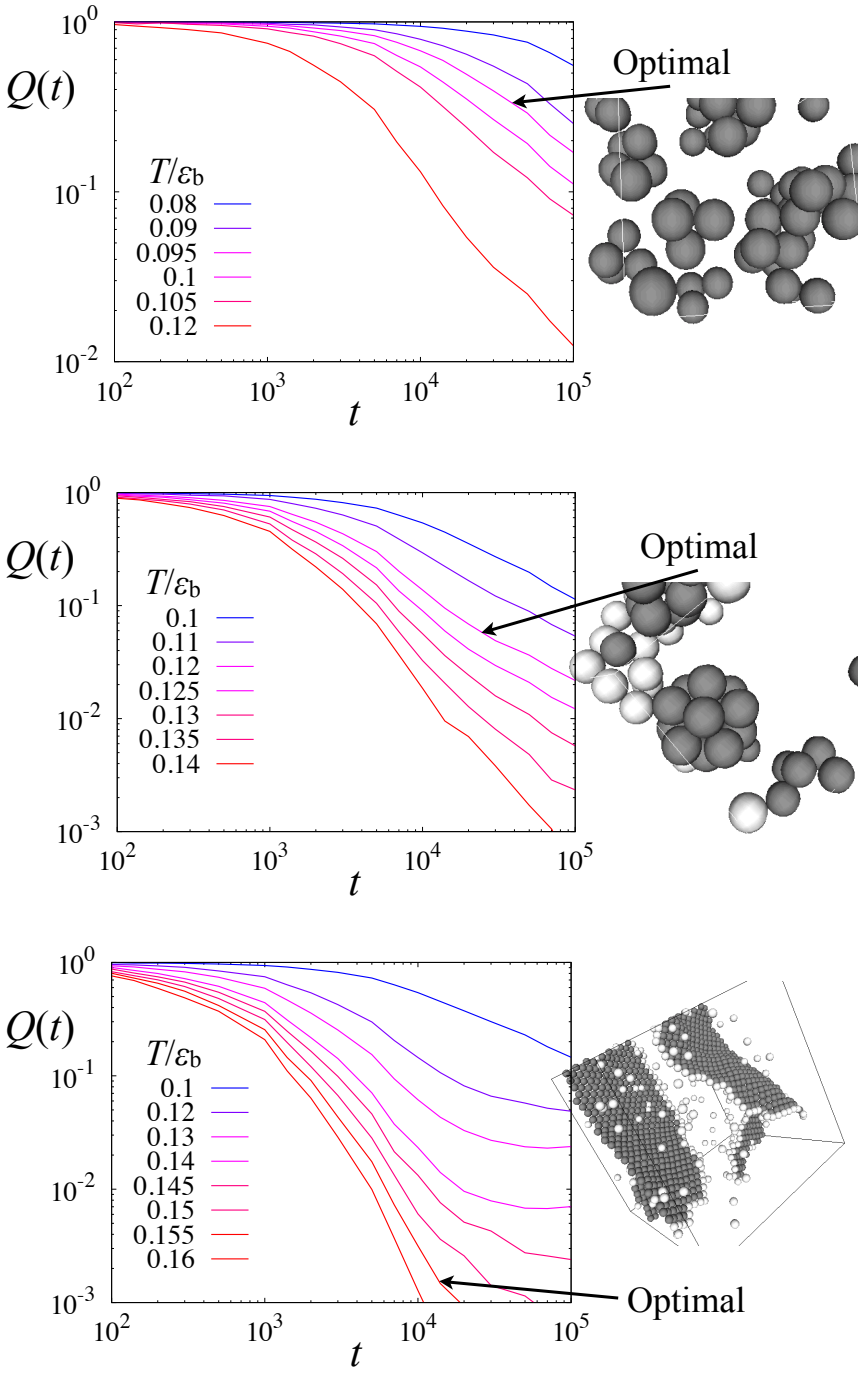


**Figure 3-7:** *Plots of flux-traffic ratio for patchy particles forming a) tetrahedra, b) icosahedra and c) close packed hexagonal sheets at volume fraction of* $\phi = 0.076$.

perature considered is the limiting decrease approaching $t^{-1}$ observed. At optimal assembly the ratio decreases from 1 to $\approx 0.2$ by $t = 10^5$. In the icosahedral formers values of the flux-traffic ratio are typically smaller than for the tetrahedral system, with optimal assembling showing a value $Q(t) \approx 0.02$ at $t = 10^5$ an order of magnitude smaller than in the tetrahedral system.

In the sheet formers values are in general lower still (values of $Q(t)$ less than $10^{-3}$ are not shown due to poor statistics). In the sheet forming patchy particles we have already noted that optimal assembly is located in the nucleation regime. Here we find that the flux traffic ratio has fallen rapidly in the times considered and there is little indication in dynamic measurements up to $t = 10^5$ whether the system quenched to $T/\epsilon_{\mathrm{b}} = 0.155$ will assemble. We would expect the flux to rise at optimal assembly once nucleation occurs, but as with integrated measurements we would have to wait until assembly has occurred before we can identify the location of optimal assembly with any confidence. As such we cannot expect the flux-traffic ratio alone to serve as a predictor of optimal assembly in systems which may undergo nucleation near to the location of optimal assembly.

## 3.3 Discussion

We have described the use of kinks in simulation which provide intuitive measurements of reversibility. The integrated flux and traffic allow the reversibility of the assembly process as a whole to be quantified and serve to verify the qualitative argument originally put forward by Whitesides[76]. A naive 'two steps forward, one step back' approach might lead to the idea that a particle needs to make and break bonds a handful of times in order to assemble. Where the equilibrium state is an extended crystalline structure however, instead we find that bonds may need to be made and broken thousands of times before a bond is formed that remains present in the final structure.

By analogy with a simple toy model this value can be associated with a 'forgivingness' of the assembly process which can be thought of as a measure of the ratio of misbound sites to optimal sites. In a more forgiving system, with a lower value of $M$, a particle is less likely to bond incorrectly or at the wrong site than it is to bond optimally, allowing closed structures to form or crystals to grow. This interpretation is borne out by the study of the patchy particle system, for which tetrahedral formers have only a limited possibility of forming trapped states and a correspondingly low value of $M$ is recorded. Icosahedral formers have an

intermediate forgivingness, while patchy particles forming extended close-packed sheets returns to the values typically seen in lattice gas and chaperonin systems.

Although the idea and measurement of forgivingness as it stands may be appropriate for systems forming closed structures such as the tetrahedra its applicability to the self-assembly of crystal structures is not as clearly defined. We have already seen the dependence upon the density of the lattice gas, the variation in measured $M$ is at least an order of magnitude. Furthermore the measurements of the flux-traffic ratio, $Q(t)$ shows that the 'instantaneous forgivingness' of systems can vary enormously over the course of the assembly process. While work is still needed to clarify how the particular values observed relate to the particles, their dynamics and assembled structure, we briefly discuss possible approaches before turning to a second measurement of reversibility.

The high values of $Q(t)$ observed at short times in all systems measured have been put down to the aggregation of monomers. From an assembly perspective however it is useful to note that with the particles considered there is no way in which a dimer can be malformed (this is not necessarily the case as particles could have different 'patches' with differing interactions meaning that not all bonds are equivalent). In the systems we have considered kinetically trapped arrangements of particles can only form once at least three particles have formed a cluster. In this case at very early times the system is very forgiving, like filament forming chaperonins. As soon as the cluster begins to grow further however the possibility of developing kinetic traps increases, requiring increasingly forgiving dynamics in order to continue assembling. By this same argument it is possible to envisage a situation where the measured $Q(t)$ is too forgiving, bonds are being broken more often than they need to be, and assembly might be accelerated by reducing the temperature such that $Q(t)$ is more appropriate for the structures present.

## 3.4 Summary

So have we been able to answer the questions with which we started the chapter? How reversible are assembling systems and how does the measurement relate to the particles and structures? We can provide an intuitive measurement of the reversibility of systems, quantifying the requirement for reversibility in self-assembly[76]. In measurements over the entire assembly process we find that in models of particles forming tetrahedral and icosahedral structures at optimal assembly a typical particle will make and break each bond 60 and 200 times

respectively. These correspond to a forgivingness, the ratio of bad bonding sites to optimal sites, of $M = 30$ and 100. Simulation of crystals give a value of $M = 100$ to 1000 depending upon the density of the system and the particular crystal model.

The case of tetrahedra provide a persuasive argument as to how the measured reversibility depends upon the particles and target structure. The tetrahedral is the most irreversible of the systems measured. Through geometric considerations we have explained how this is likely due to the relative paucity of 'wrong' structures at a key stage in the assembly pathway. The increasing complexity of structure formed is further argued as the cause of larger reversibility of icosahedral and crystal formers.

We have answered one question and the second has resulted in more. By considering the forgivingness of a system as a function of time we have provided evidence that the rate of bonding and unbonding may vary considerably during assembly and we will investigate this further in the following chapter. This has already led to the idea of 'specificity' of interaction resulting in the observed forgivingness. Were it possible a perfect novel assembling system is suggested: ensure that interparticle interactions only allow correct bonds to form and as with chaperonins assembling into 1D filaments the possibility of kinetic trapping is avoided.

# Chapter 4

# Correlations, Responses and the Flux Relation

The work presented in this chapter includes material reproduced from Grant and Jack[27].

In the previous chapter we focussed on quantifying reversibility over the whole assembly process and how it changed as the system developed. We discussed how the measured reversibility relates to the particles while measuring an instantaneous rate of reversibility begins work towards predicting when self-assembly is likely to occur. In the present chapter we will investigate whether it is possible to identify reversibility giving way to irreversibility as we move from microscopic to macroscopic timescales using correlation and response functions. A brief introduction will introduce these potentially confusing objects and the relationship between them.

We then ask whether the crossover from reversible to irreversible behaviour is measurable. This is an important feature of assembling systems, they need to be reversible to avoid kinetic traps but assemble as quickly as possible to attain the highest yield. If the change happens on short enough timescales it could be used as a predictor of where self-assembly will occur. As before it would be useful to relate measurements to the particles and final structure. Further, correlation and response functions are more readily measurable in experiment[35, 29] than the measurements of flux and traffic so it would be useful to relate the two approaches. This would allow the complex behaviour of the functions to be related to the intuitive idea of breaking and making bonds potentially aiding the interpretation of reversibility and its role in self-assembly.

## 4.1 Fluctuation Dissipation Theory

### 4.1.1 Onsager's Regression Principle

Fluctuation dissipation theory(FDT) is a result of statistical mechanics that relates two-time correlation and response functions in a system at equilibrium[20]. In experimental systems at equilibrium this is useful since it is often easier to measure one to obtain the other. Historically FDT goes back to the Einstein relation between the diffusive macroscopic Brownian motion of particles and the underlying fluid. It finds a clear description in Onsager's Regression Principle relating linear responses to fluctuations in a system.

The regression principle rests upon the idea that a system at equilibrium is macroscopically and statistically stationary but at the microscopic level is in constant motion, fluctuating about its mean behaviour. This is represented schematically in Fig.4-1a) by a Gaussian probability distribution as a function of energy. If a small perturbation is switched on, a configuration, initially at the equilibrium energy, is now displaced from the new equilibrium energy, as in Fig.4-1b) and will relax to a new distribution having a different mean energy as shown in Fig.4-1c).

Alternatively imagine the perturbation was already applied and the system now at equilibrium about $E_2$ had undergone a spontaneous fluctuation to a configuration close to $E_1$ as in Fig.4-1c). The system disturbed from its mean expectation will relax as the effects of the fluctuation dissipate. But if the systems are previously at equilibrium, are in the same or similar configurations and are at the same conditions, there can be no historical dependence on the subsequent behaviour of each. There is nothing different in the two cases described. Provided we stay in the linear regime the relaxation of the correlation relevant to the fluctuation in the second case is equal to the response to the perturbation in the first[20]. (Alternative formulations of the regression principle may consider a system initially perturbed which is subsequently allowed to relax. The argument is equivalent.)

Since Onsager, FDT has developed into a study in its own right and various mathematical formulations have been developed which demonstrate the equivalence of the two functions. In non-equilibrium systems comparisons of correlation and response functions with the equilibrium expectation of FDT have been used extensively in the study of glasses. The idea has been that if a system is *close* to equilibrium it will behave similarly to one *at* equilibrium and the prediction

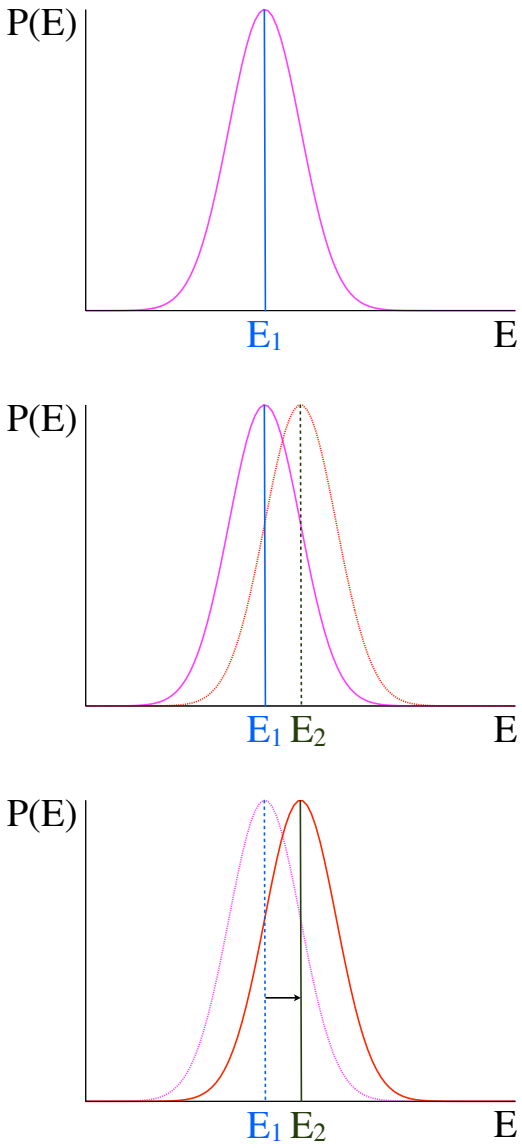


**Figure 4-1:** *Top: The system is prepared at equilibrium in state 1 where we represent the probability of a configuration with a given energy by a simple Gaussian. Middle: A perturbing field is applied such that it doesn't alter the energy of the current configuration but shifts the equilibrium energy and associated distribution of configurations of the new state, 2. Bottom: The energy of the system relaxes from its original configuration to its new equilibrium expectation value.*

of FDT will be closely followed. If a system is far from equilibrium then the opposite will be true and it will be very different from the prediction.

## 4.2 Correlations and Responses

We have already seen the response function $R(t, w)$ expressed as a correlation function in Eq.2.10 as part of the derivation of its 'no-field' measurement. Here the measurements are explored in detail in order to introduce the plots required to compare the two functions and the proximity of the system to equilibrium behaviour. Correlation functions can be of many forms taking a single or several properties of the system, such as the energy or number of bonds of a particle or the occupation of a cell or lattice site, and can be over time or space. For our purposes the appropriate choices are two-time correlation functions. As will be explained in the following sections the measurement of interest is the relaxation of fluctuations in the system, how strongly the properties of the system correlate as the system ages. These can be written generally as

$$\begin{aligned} C(t, w) &= \langle A(t)B(w)\rangle - \langle A(t)\rangle\langle B(w)\rangle \\ &= \langle \delta A(t)\delta B(w)\rangle \end{aligned} \tag{4.1}$$

where $\delta A(t) = A(t) - \langle A(t)\rangle$ is introduced for compactness of notation. This is the form of the connected correlation function where the product of the average values of the observables at the two times is subtracted (in the unconnected correlation function this term is not included). The result of subtracting the average terms is that the function relaxes to zero when there is no correlation between the system at the two times.

The relevant correlation functions, which are the focus of the present work, take particle energies as the observable of interest. In this instance the correlation function is obtained by setting the observables to the particle energy, $A = B = E_p$ and averaging over particles and trajectories. The energy correlation function measures the relaxation of fluctuations in particle energies averaged over the ensemble. If all particles energies are the same, $E_p = \langle E_p\rangle \forall p$, at either time then from Eq.4.1 the correlation function evaluates to zero.

More typically, particles will not have identical environments and the correlation function will have a finite value. If we concentrate on the first term of the correlation function we may re-write it as a sum over particles, $p$, initial, $\mu$, and

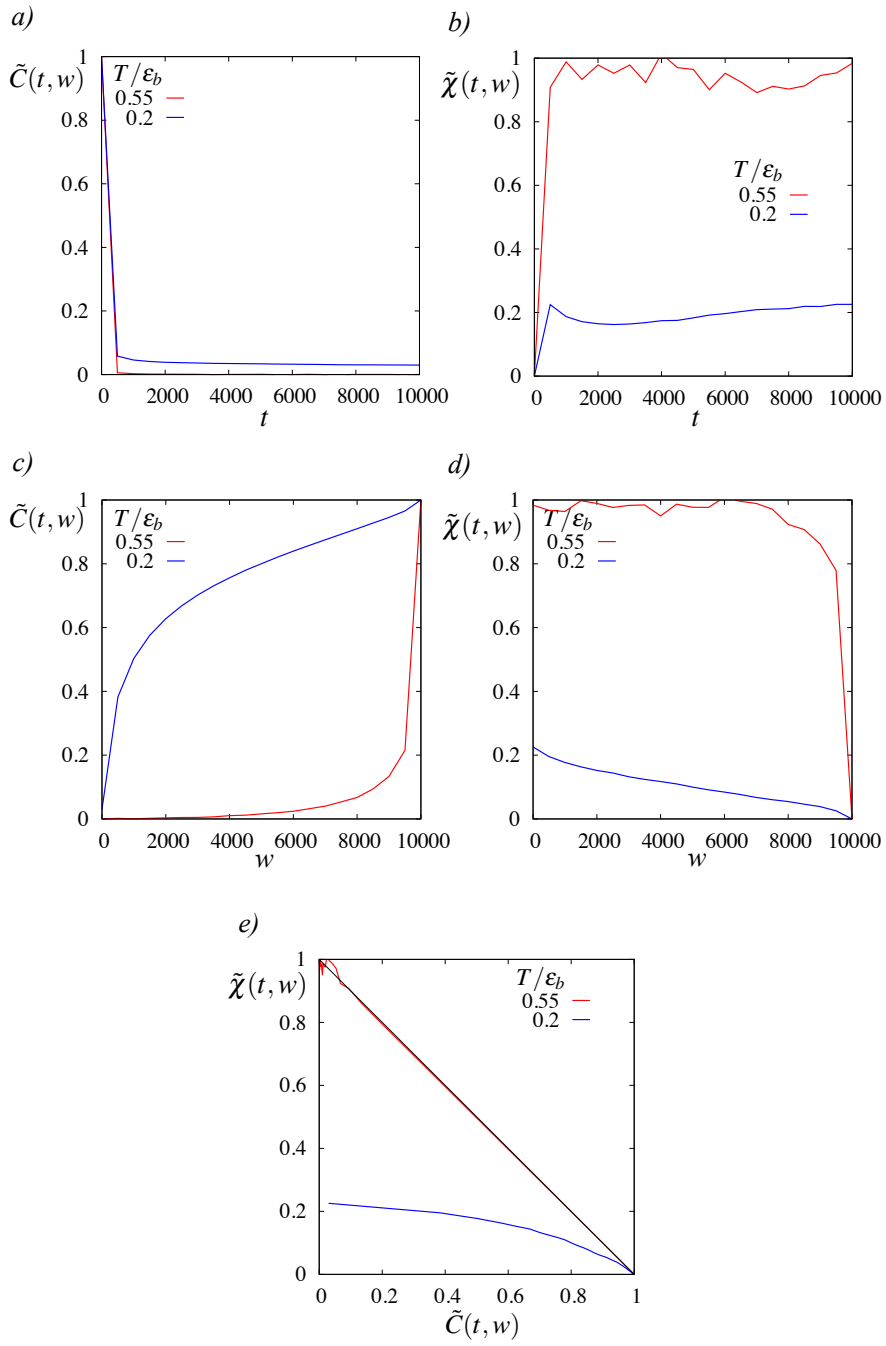


**Figure 4-2:** *Example hot and cold behaviour of a) correlation functions, b) response functions and c) the Fluctuation Dissipation (FD) plot. At high temperature, even though the system is not at equilibrium the prediction of FDT is closely followed. In contrast at low temperature the response is much lower than predicted.*

final, $\gamma$, configurations

$$\langle E_p(t)E_p(w)\rangle = \sum_{p,\mu} \mathcal{P}_u^A(\nu)E_p(\mu)\rho_w(\mu), \tag{4.2}$$

where we have defined a general propensity $\mathcal{P}_u^A(\mu) = \sum_\gamma A(\gamma)G_u(\gamma \leftarrow \mu)$ and if we set $A(\gamma) = E_p(\gamma)$ we obtain the expectation of the energy of particle $p$ a time $u = t - w$ after being in configuration $\mu$. When $u$ is small, initial and final configurations will be similar meaning that there will be a strong correlation between particle energies at the two times. As $u$ increases however the system will explore configuration space such that $\mathcal{P}_u^A(\mu) \to \langle E_p(t)\rangle$ the energies are independent. The result is that as the separation increases beyond the relaxation time for the system it remembers less of its initial state and the correlation between each particle's energy at the two times decreases to zero. If the correlation function is normalised by the one time correlator $\tilde{C}(t,w) = C(t,w)/C(t,t)$ then the correlation function relaxes from one to zero as the separation between $t$ and $w$ increases.

Recall that the impulse response is defined, generally, as the change in an observable at the time of measurement $t$ due to the application of a perturbation at time $w$. In the specific case of the response of particles' energy to a perturbation the response is

$$R(t,w) = \frac{1}{\delta t}\frac{\partial}{\beta \partial h_w}\langle E_p(t)\rangle. \tag{4.3}$$

FDT says that for a system at equilibrium this is equal to the waiting time ($w$) derivative of the correlation function. Since we will be studying non-equilibrium systems we define the equilibrium expectation,

$$S(t,w) = \frac{\partial}{\partial w}C(t,w), \tag{4.4}$$

so that at equilibrium $R(t,w) = S(t,w)$. For integrated measurements we have seen that the integrated response is defined by

$$\chi(t,w) = \int_w^t R(t,t')dt', \tag{4.5}$$

and at equilibrium this is equal to $C(t,t) - C(t,w)$.

The functions $S(t,w)$ and $R(t,w)$ and their integrated counterparts $C(t,w)$ and $\chi(t,w)$ are two time quantities. This can make them appear obscure and in particular the plot that is used commonly to compare integrated measurements in fluctuation dissipation studies is not immediately intuitive. As a result it is useful to consider the latter two functions in detail and illustrate typical behaviour with some representative data before introducing the 'FD plot' and its interpretation.

Fig.4-2 shows example behaviour of correlation and integrated response functions for, illustrative, high and low temperatures obtained in the lattice gas. The first two figures, a) correlation and b) response functions are at fixed $w = 0$ varying $t \leq 10^4$. The correlation function is at a maximum when $t = w$ and at both temperatures relaxes quickly, quicker at higher temperature. Conversely the response is initially zero at $t = w$, and as the field is applied for longer the response increases. At high temperature the response quickly saturates, the plots show that the statistical noise in measuring response is typically much greater than for correlation functions (only those particles which acquired a contribution to their Chatelain field contribute to the response whereas all particles contribute to the correlation).

The second line of plots c) and d) are made for fixed $t = 10^4$ for $0 \leq w \leq t$ so that the function approaches 1 for both temperatures when $w \to t$. The choice of whether to fix $t$ or $w$ does not affect the correlation function as it is symmetric if the times are interchanged, $C(t,w) = C(w,t)$, however the choice is significant in non-equilibrium systems when correlation and response functions are compared[72]. Because $t$ needs to be fixed to extract relevant information about the system, it means that it is useful to read the plots from right to left, so that the relaxation occurs with increasing separation between $t$ and $w$. At high temperature, bonds are broken more readily allowing the correlation function to relax more quickly. At lower temperatures the relaxation is slower because bonds persist longer and may result in multistage relaxation corresponding to breaking single, double etc. bonds.

Fig.4-2d) shows integrated response functions for the same system and times as the correlation functions. This is the response to a field that is turned on at $w$ until the measurement at $t$. Again reading from right to left, we see that if $w$ is close to $t$, the field has not been on long, the system has not had the chance to respond and the measurement is close to zero. As the separation increases the system responds increasingly due to the increasing duration of the field so that the response increases. For a system close to equilibrium, which has relaxed, as

is the case for the high temperature system, the response saturates at 1, as would have been predicted by FDT. In the low temperature case when the system is far from equilibrium, even when $w \to 0$ the response remains relatively small, $R(t,0) < 1 - C(t,0)$.

Information relating the response and correlation functions can be intuitively seen by making a parametric, fluctuation dissipation (FD) plot, of the response against the correlation, as a function of $w$ again keeping $t$ fixed. This is done for the correlation and response data in Fig.4-2e) which also has a line marked FDT. The FDT line is what the plot would look like for equilibrium systems. The hot system closely follows the equilibrium expectation for all $w$, indicating that the system may be regarded as behaving in a manner close to equilibrium. The cold system however departs immediately from the FDT line indicating that is is far from equilibrium.

The plots are read in decreasing $w$, from the bottom right to the left. As a result the plots are read with increasing length of trajectories, $u$, or application of the field, as the correlation relaxes and the response grows. The high temperature plot closely follows the FDT prediction at all times. Fluctuations at earliest $w$ are just due to the statistical noise seen in the response Fig.4-2d). At low temperatures the behaviour falls away from the equilibrium behaviour immediately indicating that even over short histories the dynamics are not equilibrium-like. At earliest $w$ in the cold system the FD plot reveals that the system moves further from the FDT expectation, behaving less reversibly as the length of the trajectory increases.

If reversibility is equated with equilibrium-like systems and irreversibility with far from equilibrium behaviour then FD plots may be used to discriminate between different assembly regimes. The remainder of the chapters focusses on whether and how correlation and response functions and these plots may be interpreted and quantified to identify the (ir)reversible nature of the assembly process. In particular we are interested to know whether this information may be obtained at times two or three orders of magnitude earlier in the assembly process than it takes for a system giving optimal assembly to produce significant yield.

### 4.2.1 Departure from equilibrium

When correlation and response measurements are made in non-equilibrium systems the Fluctuation Dissipation Theory no longer necessarily applies. Several relationships have been derived between the response and correlation functions. Typically these introduce the fluctuation dissipation ratio(FDR) or relation $X(t, w)$[72],

$$X(t, w) = \frac{R(t, w)}{S(t, w)} \tag{4.6}$$

and describe limits to its value. In particular, when combined with the definition of the response one may obtain the effective temperature[72]

$$T_{\text{eff}} = \frac{T}{X(t, w)}. \tag{4.7}$$

This interpretation of the departure from equilibrium is attractive because it is intuitive to say that the effective temperature arises because the non-equilibrium system behaves similarly to an equilibrium system at a higher temperature, $T_{\text{eff}}$ recovering FDT. Under specific conditions it can be shown that there are certain limits under which $T_{\text{eff}}$ has a well defined value. While these reinforce the idea that the effective temperature is a real property of the dynamics of the system it is interesting to ask when $T_{\text{eff}}$ applies.

$T_{\text{eff}}$ is derived from correlation and response functions of times $t$ and $w$. In particular it relates the measurement at $t$ to a perturbation at $w$. In our measurements $T_{\text{eff}}$ taken as a function of one of the times, with the other fixed, changes continuously. It is not simply a case of saying $T_{\text{eff}}$ is the effective temperature of the system at $w$. In our measurements, of assembling and in general, rapidly changing systems, $T_{\text{eff}}$ is not a simple function of the two times but depends upon the two times and the trajectories between them.

Our studies[27] have taken the difference between the correlation and response functions, $\Delta(t, w)$[27], as the object of interest, for example we define a deviation

$$\Delta(t, w) = S(t, w) - R(t, w), \tag{4.8}$$

which is related to the FDR as $X(t, w) = 1 - \Delta(t, w)/S(t, w)$. This does not have the same intuitive interpretation as the effective temperature but we will show that it allows us to clearly identify irreversibility as the origin of departure

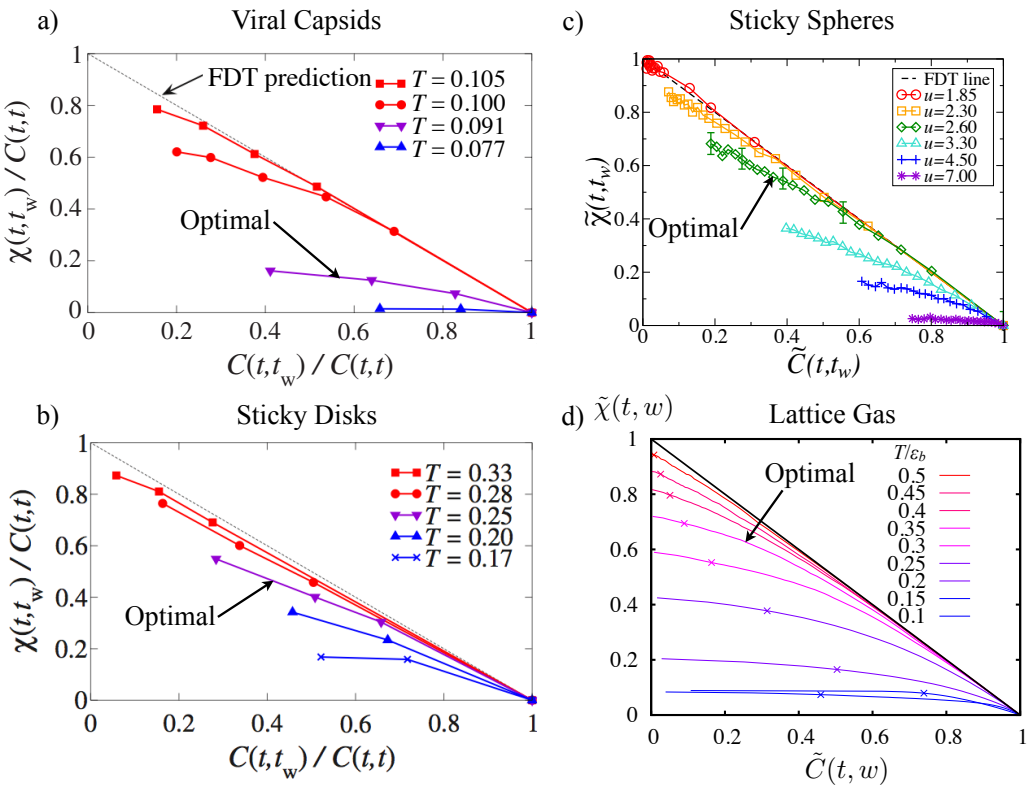


**Figure 4-3:** *FD plots for the a) viral capsid model[36], b) a 2D system of sticky disks[36], c) a sticky sphere model[43] and d) the lattice gas in 2D[27].*

from equilibrium. Additionally our analysis arrives at a formulation for the deviation which provides an explanation of the continuous variation of the effective temperature approach.

Other studies have not explicitly derived forms for $\Delta(t, w)$ but have related expressions for the response to the expected correlation in attempts to identify how the departure from equilibrium arises mathematically[50, 5]. The important feature of all approaches is that one can make comparisons of response and correlation functions in order to quantify the departure from equilibrium of a non-equilibrium system's dynamics.

### 4.2.2 Integrated Measurements

Having described the basic features and methodology of the FD plots and general behaviour of the correlation and response functions we are now in position to compare the measurements in different systems, in order to identify the signature

of assembly. In Fig.4-3 we reproduce a selection of FD plots taken from recent papers for the viral capsid model and sticky disks[36], spheres with a short range attractive square well[43] and the 2D lattice gas[27]. These show a range of behaviour from FDT-like to far from equilibrium, as temperature is decreased which at first inspection appears qualitatively similar in spite of the very different underlying nature of the systems and particles. In each plot optimal assembly is indicated.

Recall that the plots are read from right to left, in decreasing $w$, which increases the length of trajectories $u$ over which perturbations are measured. At high temperature all four systems closely follow the expectation of FDT in spite of the systems remaining far from equilibrium at the latest measurement time $t$. At the highest temperatures any slight departure from the FDT prediction arises only over long trajectories, when $u = t - w$ is large, which appear in the top left of plots. This largest departure from equilibrium therefore corresponds with when the system is changing most quickly during aggregation from the initial random configuration.

At very low temperatures the behaviour falls away from the equilibrium behaviour immediately indicating even at short times the irreversible dynamics of the systems. Over longer histories in cold systems the response is seen to plateau indicating at the time $t$ that the system does not respond to a field applied at much earlier times. (Later we will see cases where the response can fall at longer times.) In between the two limiting conditions of reversible or irreversible we observe optimal assembly and varying degrees of departure from FDT.

Setting aside briefly the viral capsid plots in the top left of Fig.4-3, the three crystal formers, whether 3D for spheres or 2D for the disks and lattice gas show consistent behaviour in spite of differences in dimension and being lattice or continuum models. Typically optimal assembly, indicated in each plot, shows strongly FDT like behaviour when $u = t - w$ is small (bottom right of plots), indicating that short timescale behaviour appears largely reversible. This gives way to progressively more irreversible dynamics as $u$ increases. This is reminiscent of the role of reversibility in self-assembly where we expect reversible short term behaviour giving way to irreversibility on macroscopic scales.

The situation with viral capsid formers is slightly different as here optimal assembly coincides with dynamic behaviour that is clearly irreversible even over short histories. The response almost plateaus over the duration of simulations, indicating that the continued application of the perturbation is not producing

further response. Since this is the only one of the four systems in the figure which forms closed equilibrium structures the more irreversible behaviour over short timescales may be related to the findings of the previous chapter. We will consider the patchy particle systems before looking at impulse measurements that allow more direct comparison with flux-traffic measurements.

As we have previously noted the benefit of considering closed and extended systems within the patchy particle scheme means that both bonding and dynamics are identical minimising the differences between the three systems and simplifying comparison. The FD plots in Fig.4-4 are for the three structures described in the previous chapter, tetrahedra, icosahedra and close-packed sheets with $t = 10^5$ when there is little yield at any temperature. Again a broad range of behaviour is seen in systems ranging from hot to cold. Optimal assembly in each of the systems is identified and shows a progression towards more reversible, FDT-like dynamics, as the size and complexity of making the target structure increases. In the two closed systems optimal assembly, as it is for the capsids, appears irreversible throughout its history.

The trend across the systems is consistent with the behaviour found in the previous chapters measurements of flux and traffic. As the complexity of the particle and target structure increases the systems are more reversible, having a higher value of $Q(t)$ at optimal assembly. In the case of close-packed sheets optimal assembly is FDT-like until the very longest time separations.

### 4.2.3 Impulse Measurements

The integrated measurements are made at fixed time of measurement $t$, plotted as a function of the time at which the field is switched on, $w$. This means that in the previous section when we considered trajectories of increasing length and noted their decreasing reversibility with increasing length of trajectory, there is the caveat that different initial times are being compared. In order to directly compare the changing reversibility from a single $w$ we turn to measurements of the impulse response. Since the response can only be calculated for finite trajectories, and in order to obtain reasonable statistics the response is calculated for an impulse lasting $\Delta t = 10$MCS.

Figure 4-5 shows plots of the normalised equilibrium expectation according to FDT, $\tilde{S}_{\Delta t}(t, w) = S_{\Delta t}(t, w)/S_{\Delta t}(w + \Delta t, w)$, normalised by the 'immediate' correlation (that is immediately following the period of the impulse) $S_{\Delta t}(w+\Delta t, w)$.

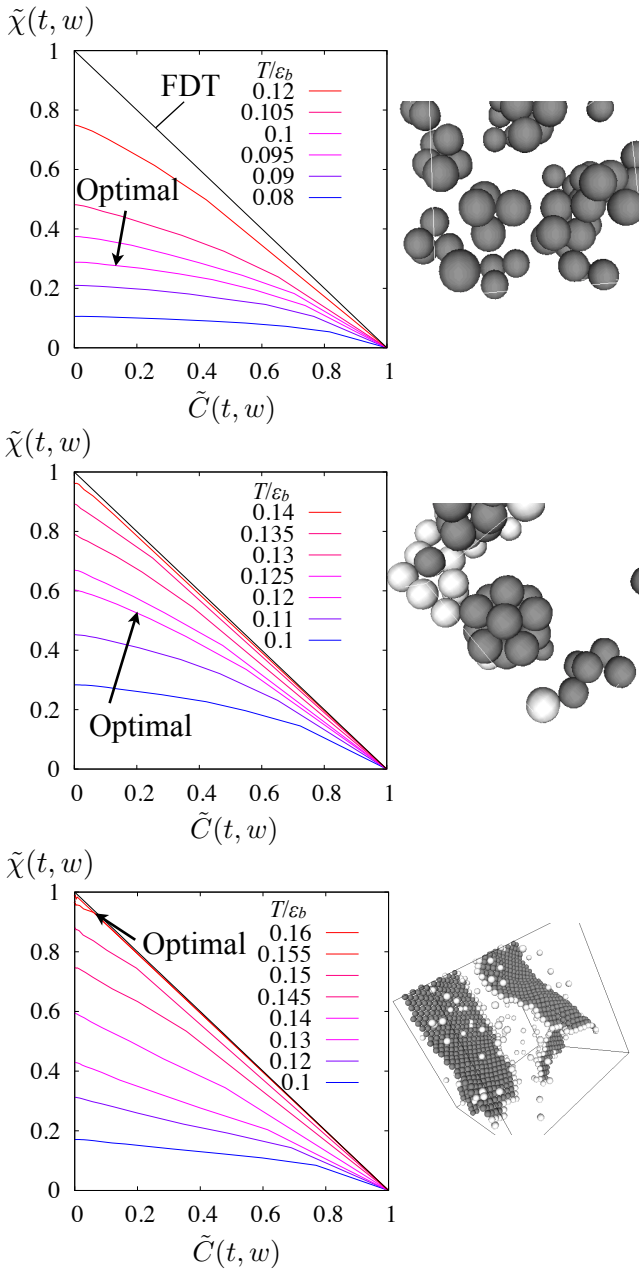


**Figure 4-4:** *FD plots for the patchy particles systems forming tetrahedra (top), icosahedra (middle), and closed packed hexagonal sheets (bottom) at $t = 10^5$. In the tetrahedra optimal assembly is located further from the FDT expectation than for icosahedra formers. In closed pack sheets optimal assembly is located on the FDT expectation, while it remains in pre-nucleation metastable regime.*

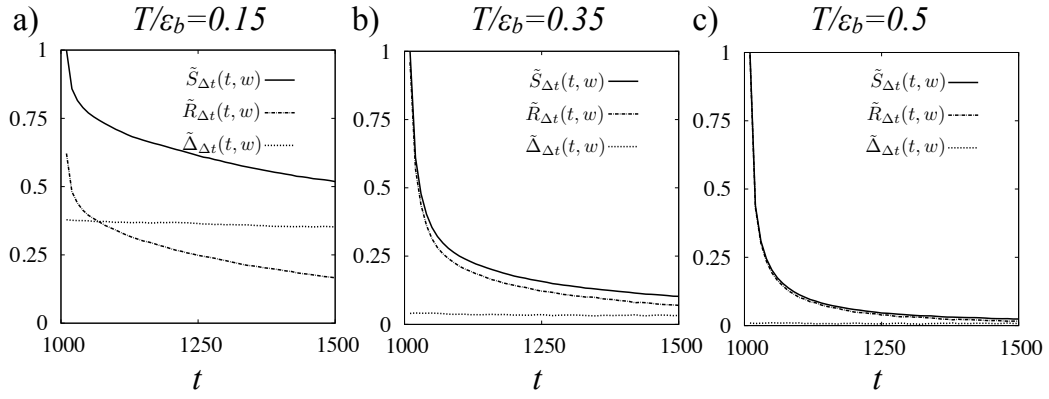


**Figure 4-5:** *Data for $\tilde{S}_{\Delta t}(t,w)$, $\tilde{R}_{\Delta t}(t,w)$ and $\tilde{\Delta}_{\Delta t}(t,w)$ at three representative temperatures. The data are obtained at fixed $w = 10^3$ MCS, while the time $t$ is varied. The deviation between correlation $S(t,w)$ and response $R(t,w)$ is small in both good assembly and poor assembly regimes, but significant in the kinetically frustrated regime.*

The normalised response $\tilde{R}_{\Delta t}(t,w) = R_{\Delta t}(t,w)/S_{\Delta t}(w+\Delta t,w)$ and deviation $\tilde{\Delta}_{\Delta t}(t,w) = \Delta_{\Delta t}(t,w)/S_{\Delta t}(w+\Delta t,w)$ are similarly defined. Measurements are in the lattice gas at 10% volume fraction. The plots are for the temperatures indicative of each regime of behaviour a) kinetic trapping, $T = 0.15$, b) optimal assembly, $T = 0.35$, and c) poor assembly $T = 0.5$ As the temperature is increased the deviation from the prediction of FDT, $\tilde{\Delta}_{\Delta t}(t,w)$ decreases, indicating that the system is becoming more irreversible, consistent with the findings of the integrated response and correlation functions and flux-traffic measurements.

In the measurements at $T = 0.15$ and 0.35 the FDT expectation $\tilde{S}(t,w)$ decreases to 0.5 and 0.1 respectively over the times considered. The response also decreases significantly, however in both cases the deviation from equilibrium expectation is approximately constant (it should be noted that this is for a trajectory of up to 500MCS, 50 times the duration of the impulse field). At optimal assembly the deviation is initially small in comparison with $S$ and $R$ but is comparable by the final times considered, again suggestive of the property of assembly appearing microscopically reversible but noticeably irreversible over longer trajectories. This difference in timescales for the relaxation of $R$ and $\Delta$ suggests that the contributions to the correlation which result in the deviation are in some way decoupled from those which are able to relax on shorter timescales. This phenomenon and its physical origins are examined in the remainder of the chapter.

## 4.3 The Flux Relation: A Proof of FDT

It has been seen that in quenched systems comparisons of response and correlation functions, whether integrated or impulse measurements, reveal information which correlates with the assembly of the system. It would be useful however to obtain an expression for the departure from equilibrium and see whether this can be related to other features, for example the flux and traffic measurements explored in Chapter 3. Several such expressions have been derived previously and will be discussed at the end of the section. Here we relate a form of the deviation that we published in a recent paper[27] that may prove to be useful in quantifying the idea of reversibility in self-assembly and aiding the design of assembling systems. Additionally this serves as a mathematical proof of FDT that has so far has only been presented qualitatively through Onsager's Regression Principle.

The derivation makes use of the notation introduced in the initial derivation of the no-field method for measuring the response. In this notation the general form of the correlation is written as

$$S(t,w) = \sum_{\nu\mu C} [\mathcal{P}_u^A(\nu) - \langle A(t)\rangle]\delta A(\nu,\mu) W^0(\nu \overset{C}{\leftarrow} \mu)\rho_w(\mu) \tag{4.9}$$

where we define $\mathcal{P}_u^A(\nu) = \sum_\gamma A(\gamma)G_u(\gamma \leftarrow \nu)$ as the *propensity*, which gives the expectation of the observable $A$ a time $u$ after being in configuration $\nu$. The correlation only picks up contributions when the observable $A$ changes at $w$, and the propensity $\mathcal{P}_u^A(\nu)$ differs from the total expectation.

Earlier it was seen that the no-field method for the response does not receive contributions from energy decreasing moves, because the perturbation does not change the probability of accepting the move. Additionally contributions from diffusive moves were shown to involve a factor of a half due to the Glauber type acceptance probability. To account for these factors we introduce the step function $\Theta(\Delta E(\nu,\mu))$ where $\Theta(0) = \frac{1}{2}$. Finally, in order to simplify the analysis we sum over fixed intermediate configurations $\nu$ so that the propensity terms from rejected and accepted moves are the same.

$$\begin{aligned} R(t,w) = \sum_{\nu\mu C} [\mathcal{P}_u^A(\nu) - \langle A(t)\rangle]\Big(&\Theta(\Delta E(\nu,\mu))\delta A(\nu,\mu) W(\nu \overset{C}{\leftarrow} \mu)\rho_w(\mu) \\ &- \Theta(\Delta E(\mu,\nu))\delta A(\mu,\nu) W(\mu \overset{C}{\leftarrow} \nu)\rho_w(\nu)\Big) \end{aligned} \tag{4.10}$$

The first term counts the contributions from accepted moves from $\mu$ into $\nu$, while

the second arises from the rejected moves, from $\nu$ to $\mu$. The contribution to the Chatelain field for rejected moves includes the ratio of the acceptance and rejection probabilities. This is why the acceptance rate $W(\mu \overset{C}{\leftarrow} \nu)$ appears in the second term even though no move takes place.

In the definition of the correlation form of the response the unconnected form is used $R(t,w) = \langle A(t)B(w)\rangle$. The expression for the response above however corresponds to the connected form $R(t,w) = \langle A(t)B(w)\rangle - \langle A(t)\rangle\langle B(w)\rangle$ since this simplifies the analysis when $S(t,w)$ and $R(t,w)$ are compared. This is possible because contributions to the 'Chatelain field' from accepted and rejected moves are equal and opposite. As a result under the average, $\langle B(w)\rangle = 0$, and so the connected part is zero and its inclusion leaves the response unchanged.

Introducing the $\Theta$ notation, making use of $1 \equiv \Theta(\Delta E(\mu,\nu)) + \Theta(\Delta E(\nu,\mu))$ into the expression for the correlation in Eq.4.9 gives

$$\begin{aligned} S(t,w) = \sum_{\nu\mu C} [\mathcal{P}_u^A(\nu) - \langle A(t)\rangle][\Theta(\Delta E(\mu,\nu)) + \Theta(\Delta E(\nu,\mu))] \\ \times \delta A(\nu,\mu) W^0(\nu \overset{C}{\leftarrow} \mu)\rho_w(\mu), \end{aligned} \tag{4.11}$$

allowing the deviation term $\Delta(t,w) = S(t,w) - R(t,w)$ to be evaluated

$$\begin{aligned} \Delta(t,w) = \sum_{\nu\mu C} [\mathcal{P}_u^A(\nu) - \langle A(t)\rangle]\Big(\Theta(\Delta E(\mu,\nu))\delta A(\nu,\mu) W(\nu \overset{C}{\leftarrow} \mu)\rho_w(\mu) \\ + \Theta(\Delta E(\mu,\nu))\delta A(\mu,\nu) W(\mu \overset{C}{\leftarrow} \nu)\rho_w(\nu)\Big) \end{aligned} \tag{4.12}$$

Noting that $\delta A(\nu,\mu) = -\delta A(\mu,\nu)$ and defining a current

$$J_w(\mu \overset{C}{\leftarrow} \nu) = W(\mu \overset{C}{\leftarrow} \nu)\rho_w(\nu) - W(\nu \overset{C}{\leftarrow} \mu)\rho_w(\mu) \tag{4.13}$$

the final form of the flux relation is obtained:

$$\Delta(t,w) = \sum_{\nu\mu C} [\mathcal{P}_u^A(\nu) - \langle A(t)\rangle]\Theta(\Delta E(\mu,\nu))\delta A(\nu,\mu) J_w(\nu \overset{C}{\leftarrow} \mu). \tag{4.14}$$

This is an interesting result for several reasons. The first point to notice is that in systems at equilibrium by definition there are no currents. These deviation terms vanish at equilibrium providing a further derivation of the fluctuation dissipation theory, $R = S$. For systems that are not at equilibrium the deviation

arises at the time at which the perturbation is applied. The way in which deviation propagates to later time, whether it dominates the behaviour or relaxes away depends upon the propensity of the configurations. In considering this it is worth spending a little time on the physical origin of the deviation.

### 4.3.1 Immediate responses and the flux traffic ratio

An interesting relation that can be demonstrated relates the flux traffic ratio of the previous chapter and the fluctuation dissipation ratio, $X(t,w) = 1 - \Delta(t,w)/S(t,w)$. We define flux as any property of the system that may be written in the form:

$$Z(w) = \sum_{\nu,\mu} z(\nu,\mu) J_w(\nu \leftarrow \mu), \tag{4.15}$$

where $z(\nu,\mu)$ is an observable or property related to an observable of interest. (We have dropped explicit dependence upon the particular cluster as the functions considered depend only upon configurations, but this will not be generally true.) When $z(\nu,\mu) = \delta E_p(\nu,\mu)$, the change in energy of particles then $Z(w)$ is similar the flux rate $f(t)$ described in the previous chapter, weighted by the energy change. We omit this in our definition of the flux but this has a minimal affect as the vast majority of kinks involve energy changes of $\pm\epsilon_{\rm b}$[27].

If however we set

$$z(\nu,\mu) = [\mathcal{P}_u^A(\nu) - \langle A(t)\rangle]\Theta(\Delta E(\mu,\nu))\delta A(\nu,\mu), \tag{4.16}$$

we see that the FDT deviation term may also be written in the general form of a flux, although much complicated behaviour has been absorbed into the propensity. In the limit of $t \to w$, i.e. turning on the perturbation and measuring the response as soon as it is switched off, the *instantaneous* response, the propensities depend only upon the initial configuration $\mathcal{P}_0^A(\nu) = E_p(\nu)$. In this case the function $z(\nu,\mu)$ takes a form similar to the case of the flux rate, $f(t)$, weighted by an additional factor of particle energies.

On the other hand when currents are small in comparison with the traffic the correlation is dominated by the activity from each accepted move weighted by propensity term and energy change so is similar to the traffic. Now although the particular weightings complicate the relationship this means that the flux traffic

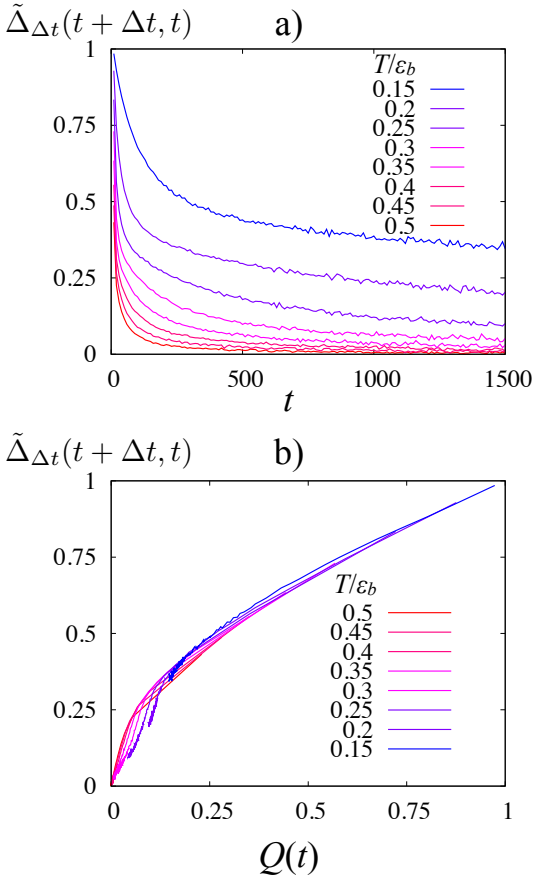


**Figure 4-6:** *Plots of flux traffic ratio against FDR in the lattice gas. (Top) Plot of the immediate FDR for* $t < 1500$ *and (bottom) parametric plot of FDR against flux traffic ratio.*

ratio, $Q(t)$ and instantaneous deviation term $\tilde{\Delta}(w+\delta t, w)$ both take the form of a flux divided by a traffic. This suggests that the instantaneous departure from FDT like behaviour may be related directly to the flux traffic ratio.

In Fig. 4-6 we test the relationship with a plot $\tilde{\Delta}_{\Delta t}(t+\delta t, t)$ against time and parametrically against $Q(t)$ for the lattice gas. As before the subscript $\Delta t$ recalls that we measure the response over a finite interval in order to obtain reasonable statistics. As a function of time the deviation term falls rapidly from early times where monomer aggregation into dimers dominates the dynamics. The behaviour soon settles down to a relatively stable value for the remainder of the times accessible. While the parametric plot of the deviation term against the flux traffic ratio is not linear there is clear correlation between measurements in spite of the differences in the weighting factors and complexity of the move algorithm. Of particular significance is the lack of temperature dependence of plots in spite of the vastly different dynamic regimes ranging from poor assembly at high temperature to kinetic trapping in cold systems.

In Fig.4-7 we present similar plots for the patchy particle models using just three sample temperatures. Only in tetrahedra formers is there large deviation from an approximately linear relationship, where this is believed to arise from the high values of $\tilde{\Delta}_{\Delta t}(w+\delta t, w)$. Since the approximation $\tilde{\Delta}_{\Delta t}(w+\delta t, w) \approx \tilde{\Delta}(w+\delta t, w)$ assumes particles undergo a single kink during the interval it is likely invalid when the rate of kinks is high at early times or rapidly aggregating systems. The remaining plots for icosahedra and close-packed sheets give similar results to the lattice gas with a clear relationship between the two measurements, independent of temperature and dynamic regime.

## 4.4 Coupling of the response

In the measurements of response presented so far the perturbation has been applied to the bonding strength of particles. This is relevant to the investigation of the dynamics of self-assembly because it measures the persistence of bonds which is vital to the study of reversibility as it measures whether or not bonds are being made and broken. It is not the only choice of perturbation however and it is interesting to examine the behaviour of the response when an alternative choice is made. The lattice gas is used for illustration.

A logical alternative to perturbing the bonding between particles comes straight from the original definition of the energy of the Ising model given in Eq. 2.1. In

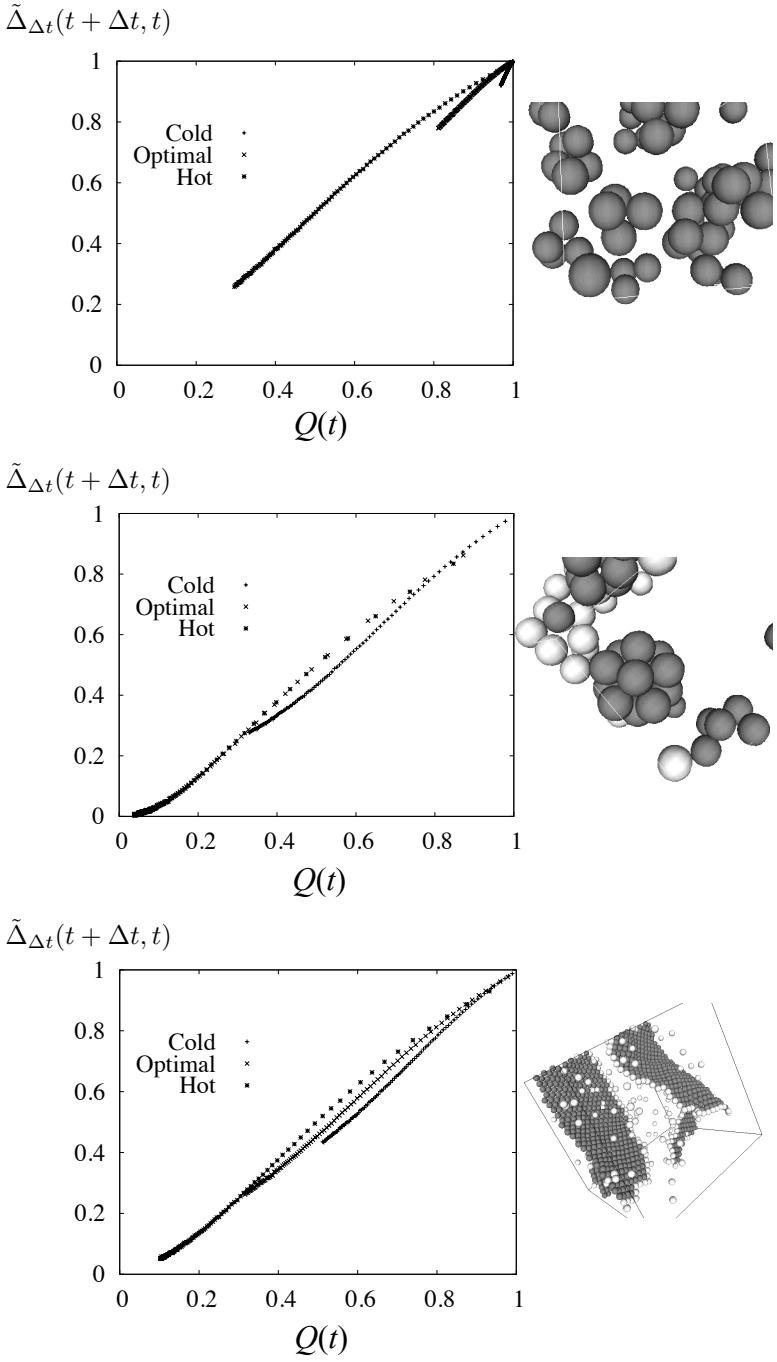


**Figure 4-7:** *Plots of flux traffic ratio against FDR for patchy particles systems forming tetrahedra (top), icosahedra (middle), and closed packed hexagonal sheets (bottom).*

addition to the energy due to bonding between particles (or spins) this allows for the application of a site dependent field $h_i$, where $i$ is the site index. The no-field method for measuring the response works in much the same way as the perturbation to a particle's bonding strength. The acceptance probability for moves would be modified if a site's occupancy changes while a perturbation is applied at that site.

In this case the response is the change in the occupancy of the site at which the field is applied

$$R_2(t,w) = \frac{1}{\delta t}\frac{\partial}{\beta \partial h_w}\langle n_i(t)\rangle, \tag{4.17}$$

where $\langle n_i(t)\rangle$ is the occupation of the $i$th site. The conjugate correlation function is the two-time site correlator

$$C_2(t,w) = \langle n_i(t)n_i(w)\rangle - \langle n_i(t)\rangle\langle n_i(w)\rangle. \tag{4.18}$$

As for the perturbation to a particle's bonding strength the impulse response $R_2(t,w)$ is equal to the waiting time derivative of the correlation at equilibrium. The integrated response and normalised quantities are defined in the same way. In order to demonstrate how the effect of site field differs from the perturbation to particle bonding strength, two cases are considered, which also allows the importance of the choice of dynamic scheme to be highlighted. Figure. 4-8 shows four fluctuation dissipation ratio plots: the upper panels are for energy perturbation, the lower panels, site fields; the left panels are for cluster cleaving dynamics, the right are for single particle moves. The comparison of the two move types helps to clarify the differences between the two perturbations.

At high temperature there is little difference between the systems with all showing equilibrium like behaviour. Additionally the energy perturbation shows little variation when the dynamics is changed. The site dependence is greatly affected by the choice of dynamics however. When single particle moves are implemented the energy and site perturbations behave similarly as the temperature is varied. This is because both perturbations rely upon the breaking of bonds to relax. If two particles form a bond, both responses relax through a thermally activated mechanism. We also note the apparent negative response in the bottom left panel in a low temperature simulation measuring the energy response with single particle moves. This pathological behaviour producing a negative

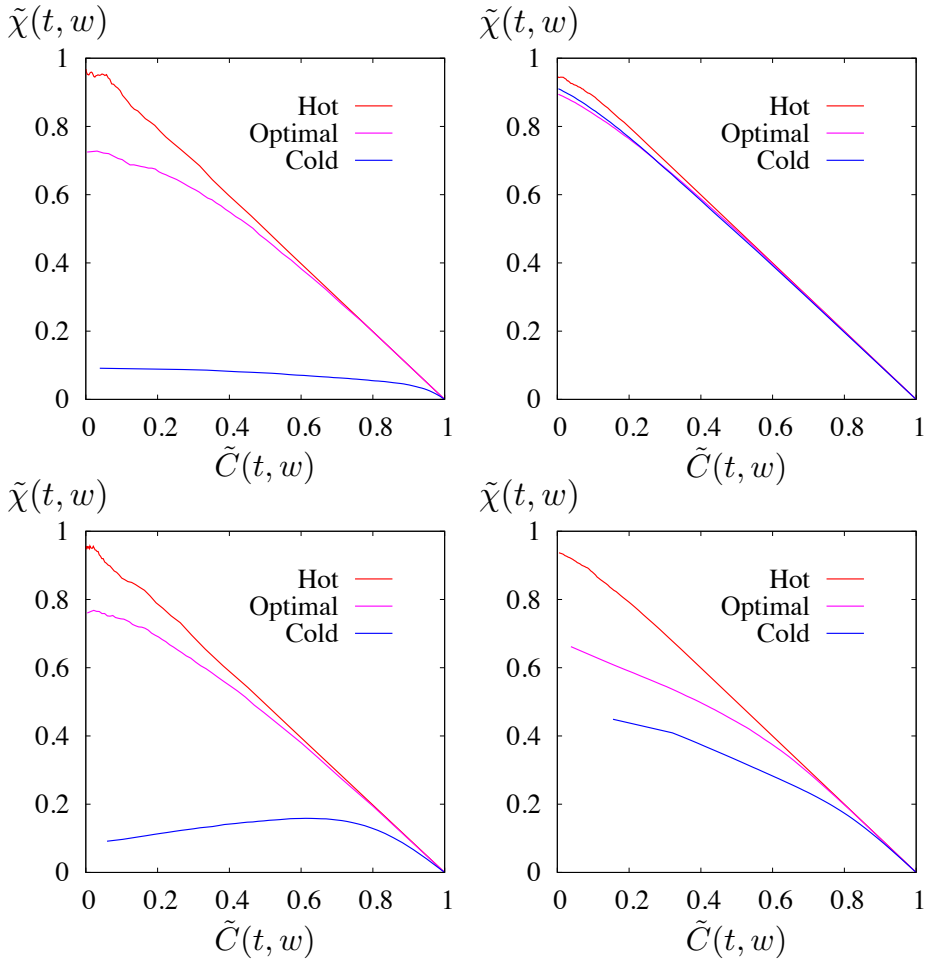


**Figure 4-8:** *FD plots for lattice gas. Top plots are for the cluster algorithm described above, the bottom plots are where only single particle moves are accepted. Left are for the response coupling to the bonding described above while the right are for the response to site dependent field and site correlation function.*

response has previously been observed and has been identified with activated ageing processes[52].

When cluster algorithms are used the two measurements are distinctly different reflecting the difference in the relaxation. The energy response is again, naturally, dependent upon the breaking of bonds. With the site response however the relaxation is no longer an activated process. Since clusters are able to diffuse away from the location where they formed the response relaxes once the cluster has moved. The relationship can be further clarified by considering the zero temperature limit where, in both dynamic schemes bonds once formed are unable to break. This means the energy response is never able to relax, and the same is true for site dependence when implementing single particle moves. However, as

discussed, in the cluster algorithm, clusters are able to diffuse from their initial position only the site dependence is able to relax.

The choice of perturbation and dynamics is therefore very important as if the response couples to the wrong relaxation mode then it will not be relevant to the properties of interest. It shows that when using a cluster algorithm the bonding perturbation is relevant justifying our choice. The cluster algorithm is implemented in order to obtain physically realistic diffusion. Were this unnecessary however and single particle moves appropriate, either perturbation would suffice as they reveal similar information.

## 4.5 Alternatives to the flux relation

Before concluding this chapter we will briefly review some other fluctuation dissipation relations that have been presented in the literature and compare them with our flux relation. The flux relation is based upon Chatelain's approach to measuring the response using a no-field method. At least two other forms fall into this general scheme[70] and one in particular has been used to derive a relationship for the departure from FDT. Where the no-field method we have used calculates the response for the trajectory followed, the alternative due to Lippiello *et al*[50] rather considers all possible moves that could happen at a certain time and evaluates contributions to $B(w)$ from these.

The expressions derived for the departure from FDT have a simple formulation in non-equilibrium steady states. Rather than considering the deviation from equilibrium directly, the response is written as a sum of symmetric and antisymmetric functions[50]. At equilibrium these are equal to each other and summed, equal to the correlation. In non-equilibrium systems such as we have in studies of self-assembly a third term must also be considered[27]. For the present purposes the benefit of the flux relation is that it gives an expression for the deviation directly, equating part of the correlation with the observed response leaving the remainder as a function of currents at the earlier time $w$ and the persistence of bonds formed at this time as measured by the propensity[27]. Furthermore the expression is valid for all non-equilibrium systems, not just those in steady states.

In Jack *et al*[36] a similar expression for the deviation is also considered. This however considered the time reversal symmetry of the trajectories considered, with the deviation term in integrated measurements depending upon (in our no-

tation) $G_u(\gamma \leftarrow \mu) - G_u(\mu \leftarrow \gamma)$. The flux relation applies directly to impulse measurements and separates the deviation into terms which can be more easily related to the qualitative ideas of reversibility and irreversibility that more intuitively describe what we expect and are beginning to observe in self-assembling systems.

## 4.6 Summary

As with previous studies of correlation and response functions in relation to self-assembly[36, 43] we find a range of behaviour that corresponds with the qualitative description of behaviour in different regimes of good and bad assembly. At high temperature where systems do not assemble, we typically observe equilibrium-like fluctuation dissipation plots throughout the majority of histories. Where deviation is observed at high temperature, it is usually in relation to the earliest times when systems undergo an initial aggregation from a random configuration. In contrast at low temperature far from equilibrium behaviour is seen at all timescales. This is the case for all systems, however when we consider optimal assembly the situation is not as clear-cut, and like the flux traffic measurements, depends sensitively upon the particular system studied.

In the majority of crystal formers we observe similar behaviour at optimal assembly, corroborating the idea of reversibility giving way to irreversibility as we consider longer timescales. Over short histories the measurements are consistent with those of the flux-traffic ratio appearing indistinguishable from equilibrium systems on short enough timescales. As the timescale is increased the measurements fall away from the prediction of fluctuation dissipation theory (FDT) indicating that the irreversible nature of trajectories is being revealed. The 'long' timescales at which we observe this crossover from reversibility to irreversibility are still very early in the assembly measurements generally two orders of magnitude earlier than the later yield measurements which we used to identify the location of optimal assembly. This means that as well as confirming qualitative ideas of the process of assembly, correlations and responses, which are measurable in experimental systems, provide the potential of predicting when self-assembly is likely to occur.

In the closed systems studied, tetrahedra, icosahedra and viral capsids, the situation is a little different. We do not see the equilibrium-like behaviour over short histories that is seen in crystal formers. Instead the systems show a depar-

ture from the prediction of FDT at all times, though the deviation does increase with the length of the trajectory. In the patchy particle system we have argued in the previous chapter that the tetrahedra assemble relatively irreversibly because there are only a few structures that can lead to kinetic trapping. This explains the relatively high flux traffic ratio measured and suggests why correlations and responses depart strongly from FDT measurements even at early times. In the viral capsid the departure from the FDT expectation is more pronounced and this may be related to the interaction between particles. Having an angular dependence the interaction tends to funnel particles into the orientation forming the strongest bond. A succession of downhill moves are likely to result in far from equilibrium behaviour. A similar result would however be expected if the times at which correlation and responses are measured is early in the assembly process when we have observed systems aggregate quickest and are most irreversible.

The flux relation provides a useful way of interpreting departure from equilibrium. Relating the flux-traffic ratio and instantaneous deviation from FDT supports the reversibility interpretation of FDT-like behaviour at early times. Furthermore the flux relation allows us to clearly identify how the relaxation of events can lead to the variation in reversibility of events. In self-assembling systems some events will lead to the target structure, some will not. Those events that do not aid progress toward equilibrium need to relax 'quickly', while those that do, need to persist. This results in a similar decrease in both response and correlation functions, which in turn increases relative contribution of the deviation term resulting in the varying fluctuation dissipation ratio (FDR) as systems assemble. In contrast in cold systems becoming kinetically trapped, events do not relax on the timescales measured, and are consistently far from equilibrium.

In order to be useful for prediction we need a clear distinction between different regimes. This means we must be able to distinguish between optimal assembly and poor assembly at high temperature and between optimal assembly and kinetic trapping. The clearer the distinction and the more specifically we can identify optimal assembly the better our prediction will be. At present we have provided further evidence of reversibility on short timescales giving way to irreversible behaviour over longer histories is a general feature of many assembling systems.

There are many caveats in these measurements. Establishing the timescales and values of the deviation term or FDR that reveal information currently have to be developed on a system by system basis, however the apparent generality across

the different systems presented suggests that correlation and response functions provide a robust means of classifying the dynamics of assembling systems and predicting where assembly will occur. It is important that correct measurements are made, coupling to modes that are appropriate to the information required. Also plots and data should be in the correct form, but provided this is done our observations provide further evidence that in some cases comparisons with FDT provide a promising means of identifying and potentially controlling assembly[44].

The patchy particle system forming close-packed sheets was the exception to this rule, with the system appearing FDT-like throughout the times considered. This however was not due to any failure of the flux relation or inability to make measurements but because of the nature of the system and its dynamics. Unlike the other systems we have studied in this section in the close-packed sheets self-assembly occurs in the nucleation regime, where the system needs to undergo a spontaneous fluctuation in order to develop a critical nucleus upon which the crystal can grow. Until this nucleus exists the system is in a quasi-equilibrium state so we should not be surprised to see equilibrium like behaviour of the correlation and response functions. If there is no sign of assembly in dynamic measurements we will not be able to locate it. In the following chapter we will look at a different type of measurement which considers instead the structures present in systems to see whether this can supplement the dynamic measurements or replace them in the case of nucleation driven assembly.

# Chapter 5

# Local Equilibrium

At the end of the last chapter we found that under certain conditions, particularly when optimal assembly is located in the nucleation regime in crystal systems dynamic measurements may not contain information about where assembly is likely to occur. Here we ask whether alternative approaches can complement the measurements of the previous two chapters to provide additional information that can help us predict the behaviour of assembling systems.

## 5.1 The Idea

In the study of glasses and other non-equilibrium processes there has been some discussion as to whether dynamics or structure plays the principal controlling factor in the changes to the system[42]. The two approaches to measuring reversibility considered in the previous chapters were dynamic approaches. We now turn to an alternative method which looks at structure, examining the properties of growing product as the system evolves towards equilibrium. Here the aim is to show that where limited information may be obtained from measurements of the dynamics, our understanding of a system's evolution may be improved by additional measurements of the structures present.

The principle of this idea is that in order for a system to self-assemble two features are required: Firstly large clusters must grow on experimental timescales; secondly these must either assemble directly or quickly anneal into locally equilibrated structures before undergoing further aggregation. If annealing occurs at faster rate than aggregation, clusters will look like they would at equilibrium, while if aggregation is faster it will 'freeze-in' existing defects leading to kinetic trapping. By comparing the properties of growing clusters with those in a system

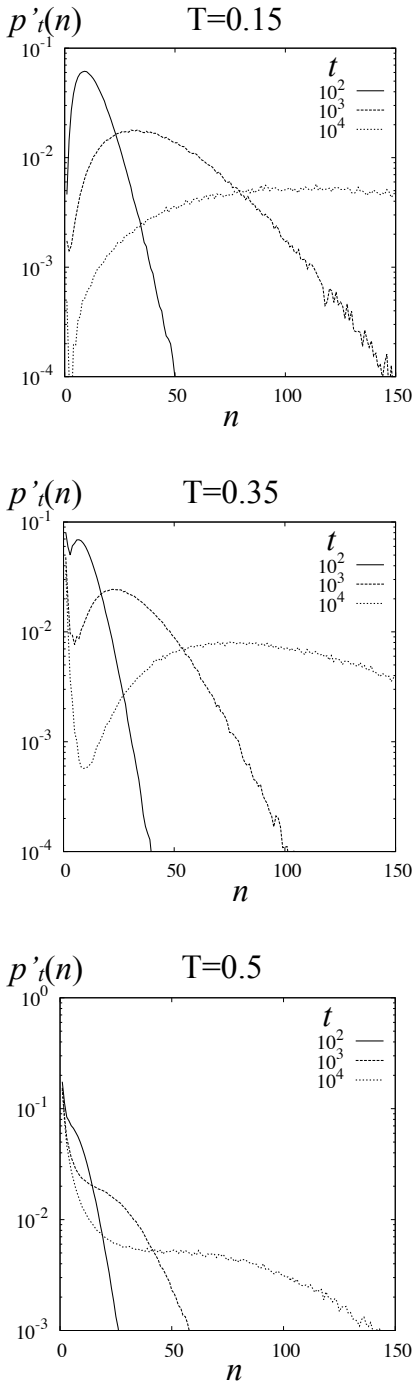


**Figure 5-1:** *Plots of cluster distributions by cluster size showing the development of a high density (large cluster) phase as the systems evolve. The peak at large cluster size develops quickest at low temperature a) where a lack of unbonding results in very few monomers and small clusters, b) at optimal assembly two peaks remain clearly defined while in c) close to the binodal the emergence of a high density phase is marked by a shoulder which moves steadily to larger cluster sizes as regular bond breaking limits their growth.*

at equilibrium we can examine whether individual clusters are equilibrium-like. We will use the term local equilibrium for these measurements, though cluster equilibration and quasi-equilibrium have also been used.

In the lattice gas below the binodal clusters grow as the system undergoes phase separation. Plotting the evolution of the distribution of cluster sizes we typically see two peaks at small and large cluster size representative of the low and high density phases. In Fig.5-1 we plot the probability of a particle being in a cluster of size $n$, $p'_t(n)$ for three temperatures. In all cases clusters grow larger as the systems evolve, though distinctions can be identified that are indicative of the three assembly regimes represented. At $T/\epsilon_{\rm b} = 0.15$ we see a rapid growth of clusters as particles and smaller clusters aggregate, while weak thermal interactions rarely break any bonds and few particles remain as monomers or in small clusters by $t = 10^4$. At $T/\epsilon_{\rm b} = 0.35$ the second peak moves rapidly to larger cluster sizes but the continued presence of monomers and small clusters in the system indicates that regular bond breaking events are taking place. Close to the binodal $T/\epsilon_{\rm b} = 0.5$ we see slow growth of clusters as bonds are more easily broken and a shoulder marks the steady emergence of the high density phase.

In theories of phase separation and nucleation cluster size, $n$, is taken as a reaction co-ordinate to quantify the progression to equilibrium. This assumes that the detail of structures is unimportant, that clusters are locally equilibrated. Krzakala [46] notes in a study using single particle moves, Kawasaki dynamics, that while the predicted growth rate $t^{\frac{1}{3}}$[9] does occur at long timescales there are significant deviations at early times. It is these early times which are relevant to self-assembly and predicting optimal assembly.

Krzakala identifies two timescales associated with breaking single bonds with a timescale $t_1 \propto e^{\beta}$ (for the lattice gas) at which the system breaks away from the 'zero temperature plateau'. In the limit of $T = 0$ no bonds can be broken since energy increasing moves are never accepted and all systems behave similarly. Theoretical behaviour is delayed further however until times greater than $t_2 \propto e^{2\beta}$. This is the timescale associated with breaking 2 bonds simultaneously or consecutively, necessary to evaporate larger clusters. Between the limits $t_1$ and $t_2$ current theories are not adequate to describe behaviour in the simplest systems. We will argue that one component in the failure of theories is due to the cluster size $n$ alone being an inadequate as a sole reaction coordinate.

If we consider 2 clusters of size $n$ having morphologies denoted by ★ and ♦ then we expect the probabilities of each cluster at equilibrium, $\rho_0(n, \iota)$, to be

related as[32]

$$\frac{\rho_0(n,\bigstar)}{\rho_0(n,\blacklozenge)} = \exp(\beta(E(n,\blacklozenge) - E(n,\bigstar))) \tag{5.1}$$

where $E(n,\bigstar)$ is the energy of morphology $\bigstar$. The star and diamond, might represent fractal like, and compact clusters. In evolving systems we expect this criterion to determine whether or not theoretic behaviour is observed. If the distribution of clusters of size $n$ satisfies Eq. 5.1 then they are locally equilibrated and $n$ should be a good reaction coordinate.

Probabilities of individual cluster morphologies are not easily measured making it difficult to test test Eq.5.1 directly. The average yield (or energy) of clusters of a given size is accessible however and comparison with equilibrium yields by size of cluster allows us to consider relative quality of clusters, indirectly probing of the condition for local equilibrium. The cluster distribution serves as a measure of the quantity of product but must be complemented by measurements of the quality of clusters of a given size relative to the equilibrium expectation. In comparing these measurements we measure the local-equilibration of clusters and provide a breakdown of yield by cluster size.

The work described here complements that of Hagan *et al*[32] where steady state measurements of assembling systems (viral capsid and lattice gas) were made by periodically removing clusters of a certain size and replacing them with randomly dispersed monomers. Measurements of clusters in the steady state were then compared with equilibrium properties in order to determine the degree of local equilibration at different temperatures as the systems evolved. In addition to the presentation of measurements the protocol here is different in that we consider trajectories and their properties at different times during assembly.

One particularly interesting idea presented by Hagan is that of breaking the yield into two components

$$Yield = Quantity \times Quality, \tag{5.2}$$

although they use rate rather than quantity[32]. As we have already seen it is not sufficient to grow large clusters if at low temperature they are poor quality fractal-like, or at high temperature where they typically have a high density of vacancies in the structure. By definition self-assembly occurs at the peak in yield due to the play off between rapid and quality production. We compare measurements of the time dependent and equilibrium yield as a function of cluster size to identify

(if and) when particular systems fall out of equilibrium and whether there is a correlation with self-assembly.

## 5.2 Measuring Local Equilibrium

We can establish the equilibrium properties of clusters by performing umbrella sampling where we reject moves which would produce clusters larger than a cut off size $n_{\mathrm{umb}}$. In doing so we restrict transition probabilities so that the probability of a move from configuration $\mu$ to $\nu$, the latter having a largest cluster of size $n_{\max}(\nu)$ is given by

$$P(\nu \overset{C}{\leftarrow} \mu, n_{\max}) = \begin{cases} P(\nu \overset{C}{\leftarrow} \mu) & n_{\max}(\nu) \leq n_{\mathrm{umb}} \\ 0 & n_{\max}(\nu) > n_{\mathrm{umb}} \end{cases} \tag{5.3}$$

where $P(\nu \overset{C}{\leftarrow} \mu)$ is just the move probability in the unrestricted ensemble. This ensures that allowed configurations are sampled in accordance with detailed balance and relax to an equilibrated state. By allowing the systems to equilibrate in the reduced ensemble and performing simulations with a range of $n_{\mathrm{umb}}$ we obtain properties across the range of cluster sizes.

In Fig.5-2 we plot equilibrium yield distributions $y_0(n)$ for the lattice gas as a function of cluster size for $n < 150$ at a range of temperatures. The equilibrium yield increases with decreasing temperature but at low temperature accurate umbrella sampling, like phase separation is hindered by kinetic trapping. As an estimate of yield distribution at low $T/\epsilon_{\mathrm{b}}$ we also plot the energy-minimised maximal yield which serves as a limit to the yield distribution. This is obtained by forming the lowest energy arrangement of $n$ particles, with the highest yield. At $T/\epsilon_{\mathrm{b}} = 0.3$, just below optimal assembly, we see that this limit is already being approached for the range of cluster sizes presented, justifying its use when $T/\epsilon_{\mathrm{b}} < 0.3$.

The sawtooth nature of the energy-minimised maximal yield distribution arises because of 'magic numbers' in cluster morphologies. If we consider a square cluster of 9 particles, the energy minimised structure, it has only one optimally bound particle and a yield of 1/9. Adding a tenth particle to the middle of one side gives a maximal yield of 2/10, almost doubling the value. The requirement of energy minimisation means that adding two more particles next to the tenth leaves the number of optimally bound particles unchanged while the yield reduces

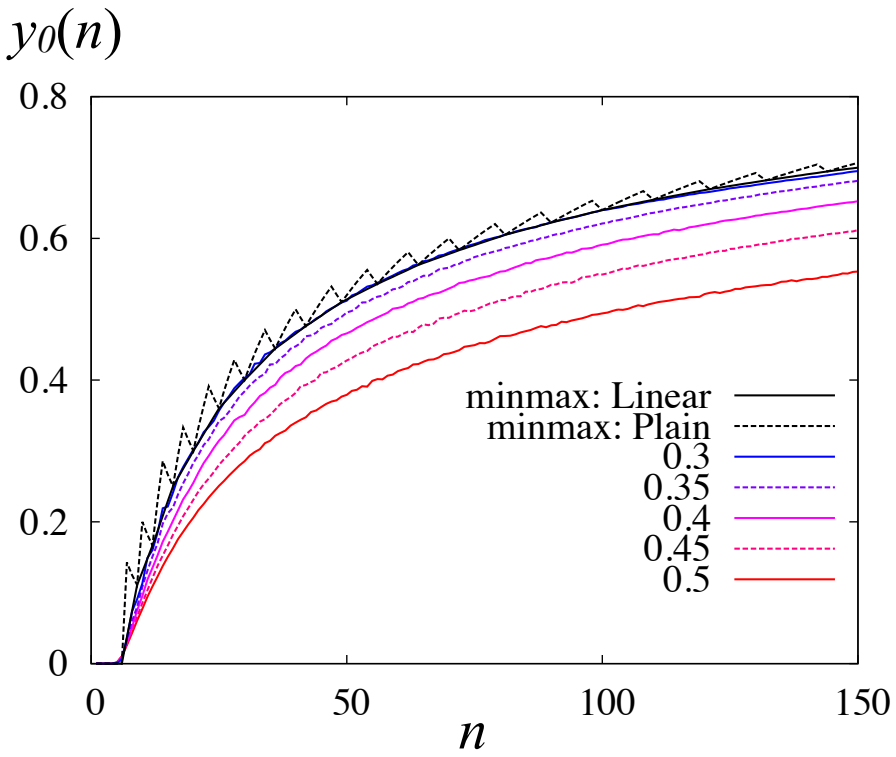


**Figure 5-2:** *Plots of equilibrium sampled yield for* $n < 150$ *for accessible temperatures. Also plotted are the energy-minimised maximum yield and a linear interpolation which removes the saw tooth effect of the 'magic numbers' which is not observed in simulation data.*

with increasing cluster size. Since the saw tooth is not present in measured distributions we perform a linear interpolation between the minima when comparing low temperature systems with equilibrium expectation.

Although we do not present equilibrium yield measurements for the patchy particle system umbrella sampling could be used to obtain similar information. As will become apparent however, the time-dependent measurements converge to the equilibrium yield so if measurements remain constant we have an indication that they are at or close to the equilibrium value (provided that activation is not significant).

## 5.3 Cluster Quality and Self-assembly

### 5.3.1 Lattice gas

We do not observe the lattice gas assembling directly to assembled structures by monomer addition to a growing equilibrated cluster. Rather small clusters aggregate into larger imperfect ones, before annealing to the equilibrium structure. If clusters anneal at a faster rate than they grow then typically they will have properties close to the equilibrium expectation. When this is not the case we expect defects to become frozen-in to the structure leading to kinetic trapping. We will examine whether comparison with locally equilibrated structures can be used to predict the system's behaviour and discriminate between different assembly regimes.

In Fig.5-3 we plot integrated cluster distribution and yield, $y_t(n)$, for the lattice gas at temperatures and times considered previously in Fig.5-1. The use of the integrated cluster size distribution allows a quick comparison between quality and probability of clusters sizes. In contrast with the probability plots seen previously, integrated plots are monotonic having a growing plateau between small and large cluster sizes, over cluster sizes unrepresentative of the high and low density phases. By comparing the yield plots with the integrated size distribution we can identify the proportion of particles in 'good' and 'bad' clusters.

There are several general features of the yield plots which provide clear information about the nature of the process of cluster growth and assembly which we discuss before considering the particular properties of the different regimes. Yield of a given cluster size increases monotonically in time as clusters anneal approaching their equilibrium properties. As the system evolves to equilibrium

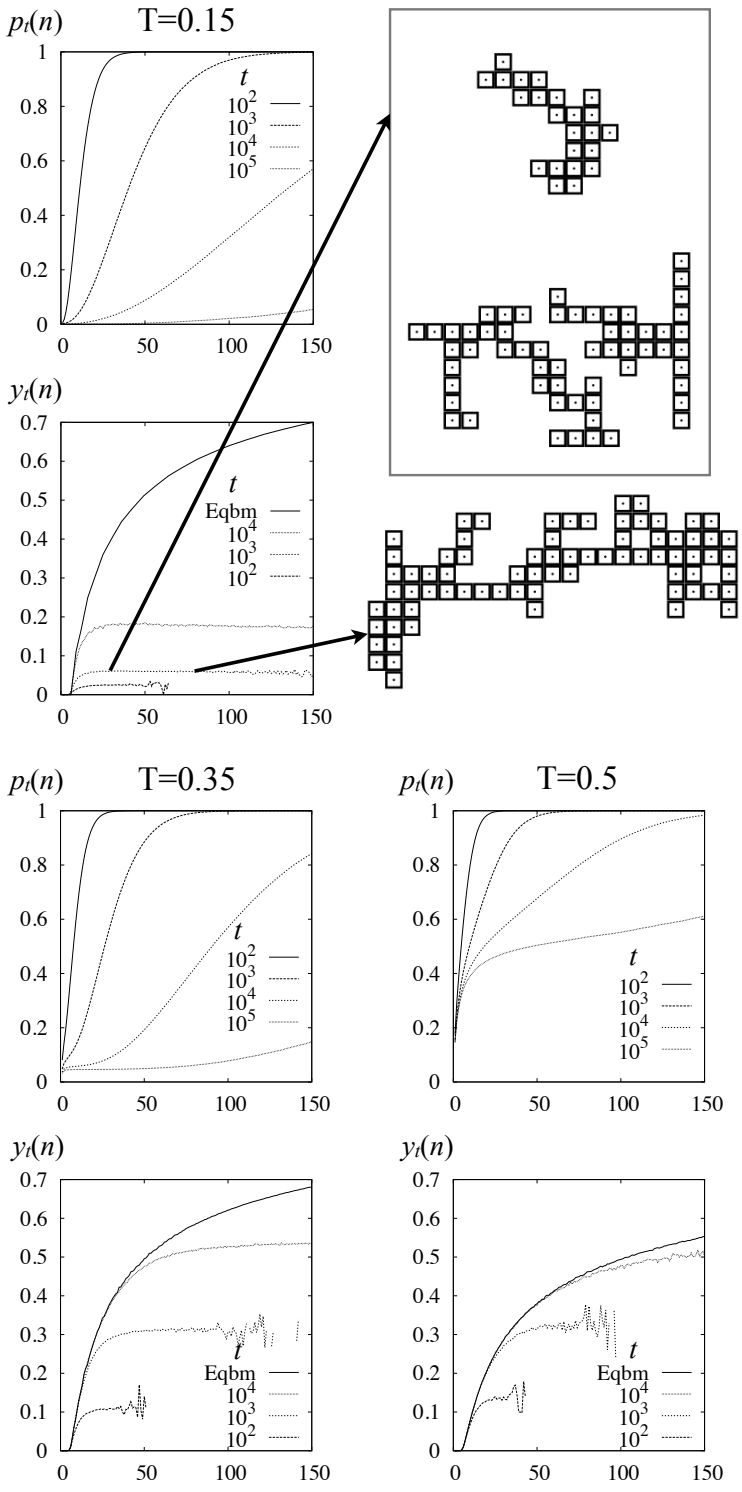


**Figure 5-3:** *Plots of integrated yield evolution in comparison with equilibrium expectation. At the latter two temperatures the evolving yield is initially close to the equilibrium expectation before falling away at large cluster size, indicating that the smaller cluster are in local equilibrium but that the larger have not yet annealed. Only at the lowest temperature is significant departure from the equilibrium expectation seen at all cluster sizes.*

the clusters must also move towards their expectation value, since clusters with more bonds are more stable on average the yield will increase.

At small cluster size we typically observe a yield $y_t(n)$ close to the equilibrium expectation. For small clusters there are few morphologies, for instance monomers and dimers have only one state, having zero and one bond respectively and energy minimised structures have zero yield until clusters of size $n \geq 7$. Thus the very smallest clusters have a limited range of yield and the equilibrium like yield is essentially a trivial matter, nothing else is possible. For clusters greater than this however the equilibrium yield is significant and suggests that clusters up to a certain size are locally equilibrated. As time passes local equilibration extends to larger cluster sizes although the maximum equilibrated cluster size has a strong temperature dependence.

As larger clusters are considered the yield falls away from the equilibrium expectation and soon after falling away from equilibrium value the yield reaches a plateau at $n_{\text{plat}}$. The interpretation of this is that larger clusters, $n > n_{\text{plat}}$ can be viewed as simple aggregations of smaller clusters. Having similar properties the clusters will anneal at similar rates meaning that the plateau continues to have the same yield as $n_{\text{plat}}$ even as $n_{\text{plat}}$ moves to larger cluster sizes with higher yield as the systems develop. As an indication of this we include three snapshots from cold configurations at $T = 10^3$ in the top right of Fig.5-3. In the box are typical clusters of the size $n$ at which the yield plateaus. The lower two of these are close together in the simulation and likely to aggregate. Also shown is a cluster approximately three times the size of the smaller, showing similar appearance as expected from the yield plot.

These general features appear across temperature ranges and systems however the specific details vary considerably as we will identify beginning with the lattice gas. In the hot system we see that at high $T/\epsilon_{\text{b}}$ the yield, $y_t(n)$, remains close to the equilibrium expectation as cluster size increases with typically $\sim 80\%$ of particles in clusters which are locally equilibrated. At low $T/\epsilon_{\text{b}}$ $y_t(n)$ falls away from the maximum yield almost immediately and the proportion of particles in equilibrated clusters is $\sim 0\%$. We also draw attention to the plateauing of the yield above $n_{\text{plat}}$, easily identified at low $T/\epsilon_{\text{b}}$, though present at all $T/\epsilon_{\text{b}}$ considered, which suggests that clusters where $n > n_{\text{plat}}$ are essentially non-annealed aggregates of the smaller clusters. As would be expected the clusters are least equilibrated$\leftrightarrow$most kinetically trapped in cold systems.

As we have shown, few particles at high $T/\epsilon_{\text{b}}$ are in clusters larger than $n_{\text{plat}}$

consistent with our idea of local equilibrium that newly formed clusters anneal before undergoing further aggregation, low production and the low quality of equilibrium product limit yield. In the low $T/\epsilon_{\mathrm{b}}$ case the majority of particles are in clusters where $n > n_{\mathrm{plat}}$ which is consistent with the idea that systems far from local equilibrium evolve via kinetically trapped states, in this case it is the poor quality of clusters that dominates yield.

We now compare the proportion of particles in equilibrated clusters and above $n_{\mathrm{plat}}$ during optimal assembly with the high and low $T/\epsilon_{\mathrm{b}}$ limits. In contrast to the measurements at high and low temperature the proportion of particles, at optimal assembly in the lattice gas in equilibrated clusters falls significantly during the times considered. The plots at $T = 0.35$ in Fig.5-3 show that the probability of finding particles in equilibrated clusters drops from $\sim 50\%$ at $10^2$ to $\sim 20\%$ at $10^3$ and $\sim 10\%$ by $10^4$. At the same times the proportion of particles in clusters where $n > n_{\mathrm{plat}}$ increases from $\sim 0\%$ to $\sim 20\%$ and $\sim 50\%$, though we note that determining an exact value $n_{\mathrm{plat}}$ is more difficult at optimal assembly. As a result we can clearly differentiate optimal assembly from the other regimes by considering its local equilibration, though the qualitative interpretation needs further study. It should also be borne in mind that the high and low temperatures have been chosen as illustrative of qualitative behaviour, rather than there being a clear transition between regimes.

Returning to our initial premise, 'in order to assemble, clusters in a system must anneal faster than they aggregate' we note that this does not completely describe the behaviour we observe at optimal assembly; rather when this happens the system is at high temperature in a poor assembly regime. During optimal assembly we instead find a significant departure from local equilibrium and one which at the times considered is increasing. This means that a significant proportion of particles are in clusters that are yet to completely anneal, i.e. that there have already been aggregation events that allow for increasing yield through annealing. In the initial premise the requirement that all clusters must be annealed before aggregation implies that aggregation is *much* slower than annealing whereas for optimal assembly there appears to be a balance between aggregation and annealing rates.

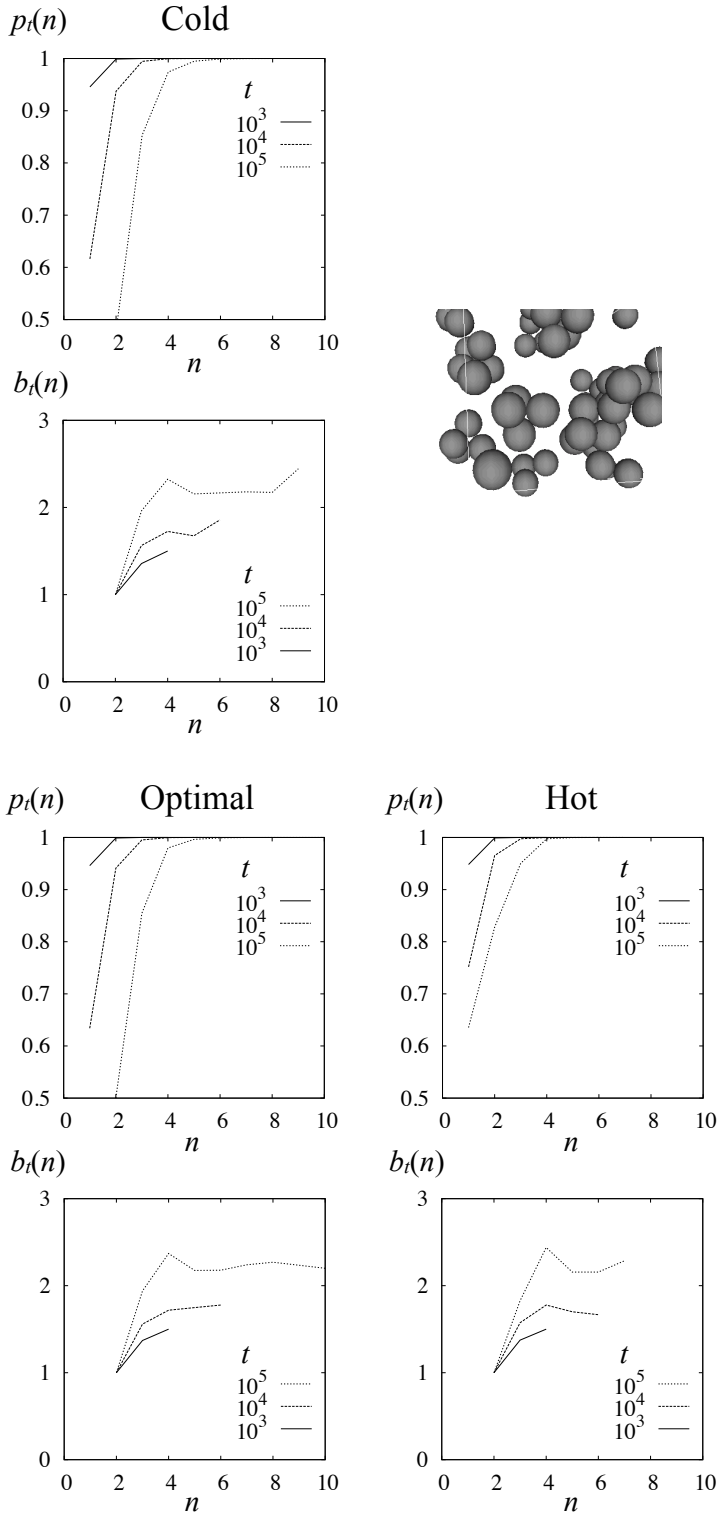


**Figure 5-4:** *Plots of cluster distribution and yield by cluster size in tetrahedra formers.*

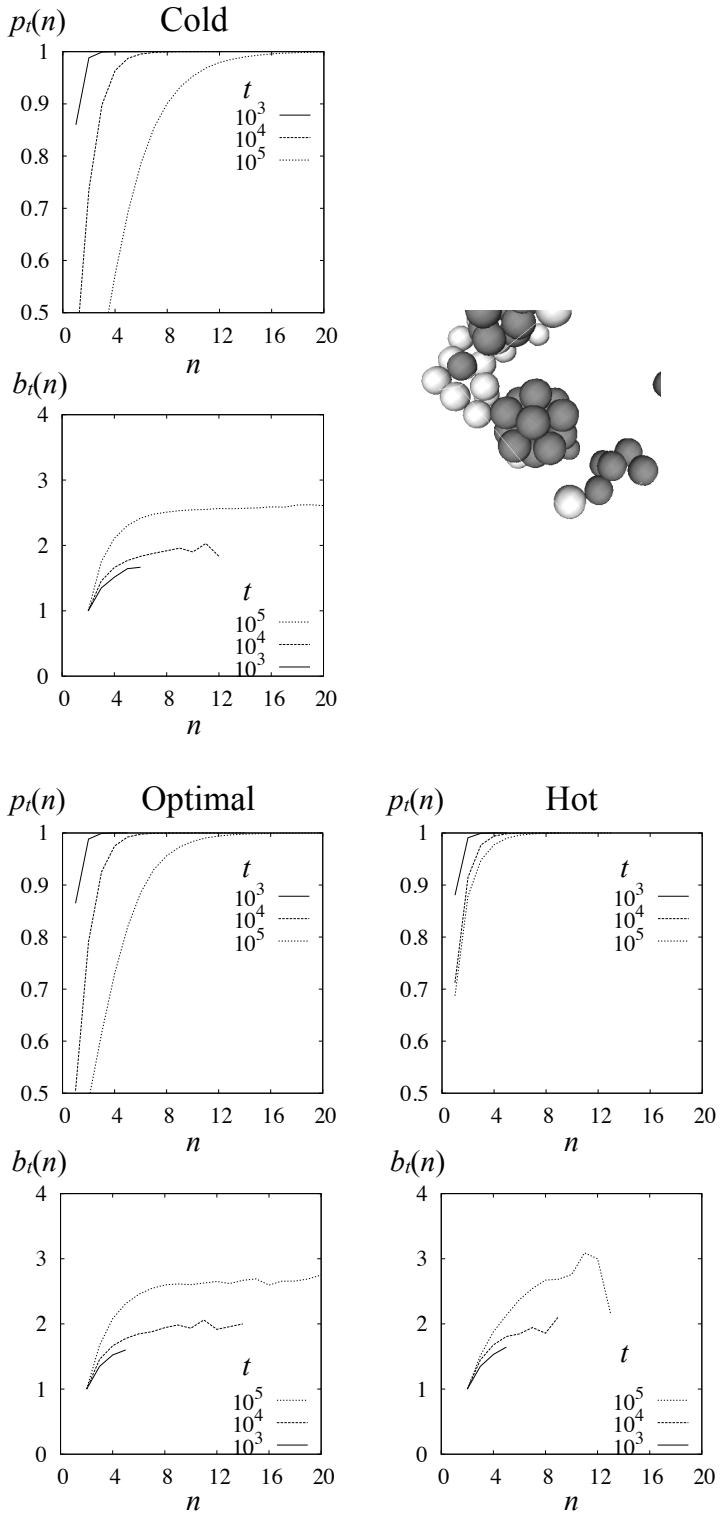


**Figure 5-5:** *Plots of cluster distribution and yield by cluster size in icosahedra formers.*

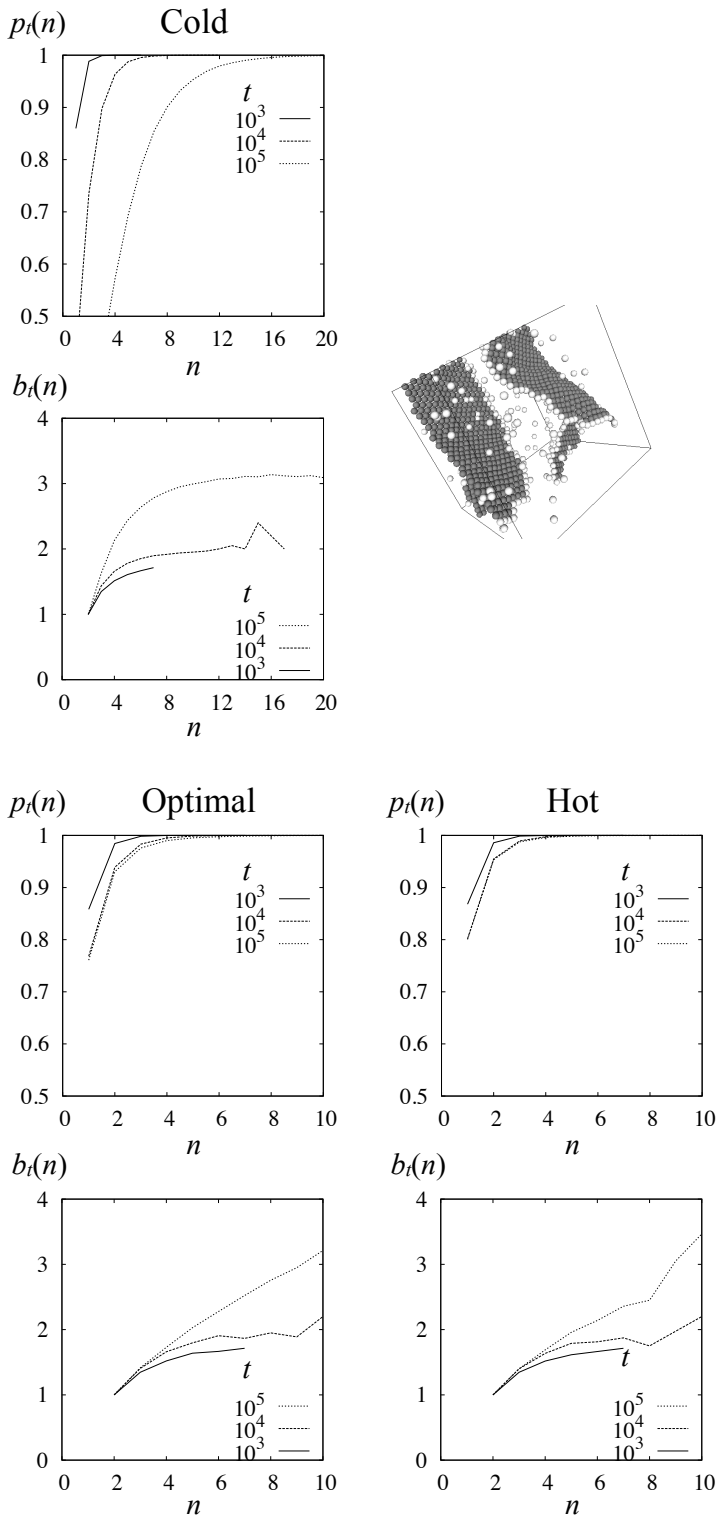


**Figure 5-6:** *Plots of cluster distribution and yield by cluster size in close packed sheet formers.*

### 5.3.2 Patchy Particles

We now present similar figures for the patchy particle models, with the only difference from the lattice gas measurements being the use of the average number of bonds of particles, $b_t(n)$ in clusters rather than the yield. This is used as an indicator of local equilibrium because even for the longest times considered here, $t = 10^5$, the yield is essentially zero for all patchy particle systems at all temperatures. Following the previous plot, for each of the patchy particle systems we present data made at temperatures representative of the hot, optimal and cold regimes and a snap shot of the systems as a reminder of the target structure. As in the previous chapters we consider the systems in order of increasing complexity of the particles and product.

The general behaviour seen in the lattice gas is broadly repeated with systems showing some equilibration of small clusters and a plateau in yield as function of cluster size. Fig.5-4 shows cluster distribution and yield plots for tetrahedra formers at low temperature ($T/\epsilon_{\rm b} = 0.8, 0.95$ and $0.12$). Because the equilibrium structure is finite there is only a narrow range of cluster sizes generally accessible at the temperatures of interest, the maximum number of bonds for tetrahedra forming particles is 3. Except for the trivial case of dimers none of the temperatures suggest that clusters are equilibrated at the times considered. In the cold and optimal systems both distributions and yield measurements are similar showing a small proportion of particles in clusters of size $n > n_{\rm plat}$ and larger than the target structure. At high temperature few particles are in clusters larger that the product.

In the icosahedral system the measurements presented in Fig.5-5 again reveals similar information. Temperatures are $T/\epsilon_{\rm b} = 0.1, 0.12$ and $0.15$ for the cold, optimal and hot systems respectively. In cold and optimal system only a few particles are in clusters greater than the product with twelve particles and there is little in the measurements to separate behaviour at the two state points. In both the closed product systems the limited size of the structures produced means that there is limited variation shown across the range of temperatures considered. In spite of this, the difference between optimal and hot regimes may prove to be useful in our understanding of the evolution of assembling systems.

For patchy particles undergoing crystallisation into close-packed sheets, the final structure is similar to the lattice gas, even if the assembly process, via nucleation is different. Data are presented for three temperatures representative of the three assembly regimes, $T/\epsilon_{\rm b} = 0.1, 0.155, 0.16$. Recall that in the yield for

the sheet forming patchy particle model assembly occurs via nucleation after $10^5$ the latest time shown in these plots. In contrast with the closed systems there is little difference between measurements in optimal and hot systems, however this is not surprising given the proximity of the state points. The main difference between these two systems is that there has been a slight change in the probability distribution between $t = 10^4$ and $10^5$ in the optimal system. However there is little to suggest the subsequent difference between the systems once nucleation has occurred in the optimal system.

## 5.4 Summary

Our measurement of local equilibration in evolving systems reveals interesting information that appears to correlate with a qualitative idea of cluster growth in assembling systems and extends previous work[32]. By looking at the evolution of cluster properties rather than concentrating on an assembling steady state we reveal dynamic information about the structural measurements. These reveal that at high temperature clusters grow (or particles aggregate) slowly and the properties of those containing the majority of particles are equilibrium like at all times.

As the temperature is dropped the quality of larger clusters relative to their equilibrium properties falls. At small cluster size we see some equilibration of clusters but eventually the yield plateaus suggesting that clusters larger than $n_{\text{plat}}$ can be thought as cluster aggregates of that size. At low temperature the majority of particles are found in clusters larger than $n_{\text{plat}}$ indicating that clusters are not annealing before undergoing further aggregation indicative of kinetic trapping. In contrast at optimal assembly the proportional of particles in equilibrated clusters reduces steadily indicating that although clusters are annealing there is a balance between the rates.

The fact that there is not a clear separation between annealing and growth rates at optimal assembly distinguishes the behaviour from that at hot and cold systems where in the former annealing dominates and in the latter aggregation. The initial premise that annealing must happen at a faster rate than aggregation proves to be too strong a statement but it is apparent from the observations that information may be extracted that moves to put our expectation on more qualitative ground.

In the plots presented particularly in the case of the the patchy particle system

the statistics could be improved with extended studies. In all cases this would allow us to consider the *rates* of growth and annealing directly and this may help to discriminate between the different regimes of poor and good assembly. In the final chapter we will consider the results of combining the measurements and how they have improved our understanding of the process of assembly and whether we are any closer to our goals of predicting, designing and controlling assembly.

# Chapter 6

# Outlook

## 6.1 Discussion

Our initial aims were connected with the measurement of reversibility, putting the idea of Whitesides[76] on quantitative foundations. This idea emphasised the need to both *make* and *break* bonds during assembly processes in order to avoid kinetic trapping. We set out to measure how reversible systems are during assembly and how measurements of reversibility relate to the particles and the structures they form. We conclude by assessing the progress towards this objective and how our findings suggest further lines of enquiry that may aid prediction, design and control in experiment to enable the process of self-assembly to be exploited.

We have seen several measurements which pursue two general approaches to quantifying reversibility in self-assembly: dynamic and structural. The first dynamic approach measured the number of *kinks*, which are particle energy changing moves, allowing us to generate a *flux* and *traffic*. From these we identify the average number of bonding and unbonding events (per bond) a particle undergoes as it assembles. This can be used to generate a forgivingness, $M_{\text{eff}}$, which measures the reversibility of the whole assembly process. Values of $100 - 1000$ in crystals give support to the importance of reversibility in assembling systems. Particles do not try to bond two or three times to make a lasting bond but have to make many attempts.

The toy model, which leads to the idea of the forgivingness of assembly processes, shows how the value of $M$ may be interpreted as a ratio of bad to good bonding sites. In closed systems, such as the tetrahedral and icosahedral systems, smaller values are observed and these can be related to the relative difficulty of

forming kinetically trapped structures, particularly in the tetrahedral formers. The 'specificity' of the interaction is responsible for limiting the formation of poor configurations. In tetrahedra, stable trimers form easily and on average a quarter of these will be able to assemble without any breaking of bonds. In the case of the capsid system the channelling of the interaction is believed to play an important role in the irreversible assembly observed. The specificity of structures or interactions between particles is therefore identified as an important parameter in determining the level of (ir)reversibility at which a system assembles.

By making rate measurements and introducing the flux traffic ratio $Q(t)$ we extend the use of kinks from identifying the reversibility of an (already) assembled system to something having the potential for prediction. The rate measurements show that over the course of assembling the reversibility may vary by several order of magnitudes. We have explained why the high values $Q(t) \approx 1$, in the systems studied, at the very earliest times arise from the fact that two particles cannot bond to form a structure that is kinetically trapped (this can only occur in larger clusters).

The second dynamic approach compared correlation and response functions with expectation of the fluctuation dissipation theory (FDT). Although these measurements are difficult both to make and interpret, they are experimentally realisable. We can use the instantaneous deviation from FDT to extract a value for the instantaneous reversibility of processes. The flux relation allows comparison of the instantaneous deviation and flux traffic ratio showing that the two reveal similar information.

The flux relation also allows us to identify the persistence of bonds required for assembly as a key feature in the use of longer time FDT measurements. While much of the reversible bond making and breaking is quickly forgotten those that remain are a key indicator of assembly, allowing us to discriminate, at least qualitatively, between assembly regimes. At high temperature, systems tend to follow the prediction of FDT as the length of trajectories is increased. At low temperature systems tend to deviate from equilibrium behaviour regardless of the length of the trajectories.

At optimal assembly we typically observe a crossover from equilibrium-like at short times to far from equilibrium behaviour over longer histories. Further both these timescales are far shorter, two orders of magnitude, earlier than when we identify optimal assembly. The problem of prediction is however not immediately resolved. The particular level of reversibility, irreversibility and the

timescales for each depend upon the particular system and the structure of the product. Quantifying the relationship between the properties and particular measurements remains an open problem though our findings should help to shape the understanding of these effects, particularly through the idea of forgivingness and the flux relation.

Our final approach was to consider structures within the systems through local equilibration, or cluster equilibrium. Rather than considering reversibility as a dynamic idea, measuring events that take place in the system, this considers the structures and how they develop during simulations. We made measurements of clusters and compared their properties as a function of the size of clusters with those of equilibrated clusters. The name comes from the idea that while clusters are not representative of a system at equilibrium which we expect to be phase separated, clusters of a given size may still have properties that they would have were they found in an equilibrated system; thus the clusters would be locally equilibrated.

As with the measurements of the dynamics, since the formation of dimers (in our systems) cannot happen incorrectly, small clusters are trivially equilibrated. As significant and non-trivial sized clusters are reached, interesting properties of the systems are revealed. Extending previous work[32] we considered the structure dynamically rather than in a steady state scenario. Clusters are seen to improve in quality with increasing size, having equilibrium properties until a certain size $n_{\text{plat}}$ at which the quality plateaus. Particularly noticeable in cold and self-assembling systems this suggests that large clusters can be viewed simply as aggregates of clusters of size $n_{\text{plat}}$. In the lattice gas this is consistent with illustrative snapshots of clusters drawn from systems.

As the system develops these clusters anneal at a similar rate so that the plateau is maintained but with $n_{\text{plat}}$ increasing as smaller clusters achieve their equilibrium properties. Although we argued that in order to assemble, particles should be in locally equilibrated clusters, annealing faster than they grow, we find at optimal assembly that the clusters fall away from locally equilibrated structures as the system ages. This suggests that there is more of a balance between the two rates. However further work would be required to extend the local equilibrium measurements to rate measurements as we have achieved with the two measurements of reversibility.

## 6.2 Future Work

An interesting possibility for enabling the prediction of where assembly will occur might be achieved through combining measurements. With FDT measurements we can identify the separation between high temperature, where the system remains equilibrium like throughout trajectories, and optimal assembly. Similarly at low temperature we observe systems deviating from the equilibrium expectation but not changing markedly as longer trajectories are considered. Although we don't know the exact degree of irreversibility required we can reduce the range of temperatures likely to result in optimal assembly. Local equilibrium measurements should also be able to aid prediction though may require the measurement and study of rates of growth and annealing of clusters. By combining the different measurements we will further restrict the range of temperatures where systems will assemble.

The exception in our systems were the close packed patchy particle sheets where optimal assembly is located in the nucleation regime, reducing the amount of information that is available either through dynamic or structural measurements: the changes that lead to assembly have not occurred on the timescales we have been simulating. As we move from considering prediction to design and control of assembling system we will try and avoid this problem altogether. Recall that by design we mean designing systems that assemble readily rather than simply having an ordered equilibrium state.

Ultimately, contributing to assembling useful functional systems has been the aim of this project. In designing systems that assemble, the recognition by Wilber[78] that triangular intermediate states found in their tetrahedral and icosahedral systems assemble more readily than for example the squares required for cubes is important. Avoiding kinetic trapping has been shown to be an important feature of assembling systems but flux and traffic measurements interpreted with the toy model of assembly have shown that the simplest approach would be to design systems that avoid kinetic trapping altogether. As an example, patterning of a number of patches could ensure that particles only bind in the correct orientation leading to assembly. These particles would be more complex than those currently envisioned however, complicating the manufacture and removing much of the elegance of the model systems. Additionally the idea would not help in the design of systems which piggyback on DNA or proteins where the interaction cannot be designed from scratch.

In order to think about design of assembling pathways in a more general sense we have to turn to the control of assembling systems. In the work we have described we have worked at fixed state points, temperature, density, no applied fields and this has in general been the case in similar studies[36, 77, 78, 59, 43, 28, 27]. This however need not be the case, indeed if we wish to aim for 100% yield changing the temperature is essential. We know that highest yield will be at low temperature, but optimal assembly is at higher temperature due to kinetic trapping effects. The very simplest scheme to improve yield would be to allow a system to assemble at optimal assembly $T^*$ and then reduce the temperature, increasing the equilibrium yield.

An idea for a more active control method[44] is to use fluctuation dissipation ratios(FDRs) to monitor the assembly process to gauge the system's reversibility. While thresholds would have to be devised for each system the general behaviour we have observed should help to determine appropriate levels. The feedback loop would involve measuring response and correlation functions for a period of time, over which the system relaxes into (the longer time) irreversible regime of behaviour. If the FDR is high, for example close to 1, the system is being too reversible and the feedback loop would reduce the temperature. Conversely an FDR of 0.2 over the duration of measurement might be too low and result in an increase to the temperature. This would maintain the temperature in the assembly regime throughout its application, automatically reducing the temperature as systems approach equilibrium, 'intelligently' mimicking the effects of the simple scheme suggested above.

A feature of using FDR measurements within a single simulation or experiments is that the system will respond to fluctuations in the dynamics. In measurements of integrated correlation and response functions we have typically obtained statistics over $10^3$ to $10^4$ simulations of $\approx 10^3$ particles. To obtain similar level of statistical accuracy in a single simulation or experiment would require a system of at least $10^6$ particles. Provided meaningful statistics are achieved however the natural fluctuations might be easily dealt with by the feedback system. A spontaneous fluctuation which resulted in more irreversible events which needs to be annealed would be overcome by the increase in temperature by the feedback. When the fluctuation resulted in more reversible behaviour, dropping the temperature would encourage net bond-making necessary for assembly.

An alternative approach might be to operate about a fixed temperature (or a slowly reducing one) and apply an alternating perturbation (via a real ap-

plied field or temperature sweep) to drive the system through periods of less and more reversible behaviour. Previous work has shown that an oscillating field in grand canonical implementations of the Ising model can reduce the critical temperature[45]. If similar behaviour could be demonstrated in the lattice gas model at fixed density then it might suggest dynamic schemes that would increase the rate at which systems can be pushed towards equilibrium. If a scheme could be described for systems in general, the result would be a big step towards controlling assembly and commercial viable implementations.

Although the measurements we have used, in simulations at fixed state points cannot tell us what will happen when we use schemes to design and control assembly, the approaches we have described will aid the interpretation of results. The ability to interpret results systematically through analysing the reversibility of dynamics and the properties of structures will remain key features of self-assembling systems. Indeed it may well be the case that identifying whether and how assembly protocols are working may help our understanding of measurements in systems at fixed state points.

# Bibliography


[1] B. Alberts et al. *Essential Cell Biology.* Garland, 1st edition, 1998.

[2] D.J. Ashton, L. Liu, E. Luijten, and N. B. Wilding. Monte carlo cluster algorithm for fluid phase transitions in highly size-asymmetrical binary mixtures. *J. Chem. Phys.*, 2010.

[3] D.J. Ashton, N. B.. Wilding, R. Roth, and R. Evans. Depletion potentials in highly size-asymmetric binary hard-sphere mixtures: Comparison of simulation results with theory. *Phys. Rev. E*, 84, 2011.

[4] D.J. Ashton, N.B. Wilding, and P. Sollich. Fluid phase coexistence and critical behavior from simulations in the restricted gibbs ensemble. *J. Chem. Phys.*, 2010.

[5] M. Baiesi, C. Maes, and B. Wynants. Fluctuations and response of nonequilibrium states. *Phys. Rev. Lett.*, 103, 2009.

[6] P. Bak. *How nature works: the science of self-organised criticality.* Oxford University Press, 1997.

[7] S. Bandyopadhyay. Self-assembled nanoelectronic quantum computer based on the rashba effect in quantum dots. *Phys. Rev. B*, 61, 2000.

[8] R.J. Baxter. *Exactly solved models in statistical mechanics.* Academic Press, 2002.

[9] A. J. Bray. Theory of phase-ordering kinetics. *Adv. Phys.*, 43, 1994.

[10] W. L. Brown, R. A. Mastico, M. Wu, K. G. Heal, C. J. Adams, J. B. Murray, J. C. Simpson, J. M. Lord, A. W. Taylor-Robinson, and P. G. Stockley. RNA bacteriophage capsid-mediated drug delivery and epitope presentation. *Intervirology*, 45, 2002.

[11] Stephen G. Brush. History of the Lenz-Ising model. *Rev. Mod. Phys.*, 39, 1967.

[12] Hilda Butler. *Poucher's Perfumes, Cosmetics and Soaps*. Springer - Verlag, 10th edition, 2000.

[13] Alan Cann. *Principles of Molecular Virology*. Elsevier, 4th edition, 2005.

[14] C Casagrande, P Fabre, E Raphael, and M Veyssie. Janus beads - realization and behaviour at water oil interfaces. *Europhysics Letters*, 9, 1989.

[15] David Chandler. *Introduction to Modern Statistical Mechanics*. Oxford University Press, 1987.

[16] C. Chatelain. On universality in ageing ferromagnets. *J. Stat. Mech.: Theory Exp.*, 06, 2004.

[17] N. E. Chayen, E. Saridakis, and R.i P. Sear. Experiment and theory for heterogeneous nucleation of protein crystals in a porous medium. *Proc. Natl. Acad. Sci. (USA)*, 103, 2006.

[18] S. Chung, S.H. Shin, C.R. Bertozzi, and J.J. De Yoreo. Self-catalyzed growth of s layers via an amorphous-to-crystalline transition limited by folding kinetics. *Proc. Natl. Acad. Sci. (USA)*, 107, 2010.

[19] F. Corberi, E. Lippiello, A. Sarracino, and M. Zannetti. Fluctuation-dissipation relations and field-free algorithms for the computation of response functions. *Phys. Rev. E*, 81, 2010.

[20] A Crisanti and F Ritort. Topical review violation of the fluctuation dissipation theorem in glassy systems: basic notions and the numerical evidence. *J. Phys. A*, 36, 2003.

[21] N. Dorsaz, G. M. Thurston, A. Stradner, P. Schurtenberger, and G. Foffi. Phase separation in binary eye lens protein mixtures. *Soft Matter*, 7, 2011.

[22] C Forastero, L I Zamora, D Guirado, and A M Lallena. A Monte Carlo tool to simulate breast cancer screening programmes. *Phys. Med. Biol.*, 55, 2010.

[23] J.M. Fox, G. Wang, J.A. Speir, N.H. Olson, J.E. Johnson, T.S. Baker, and M.J. Young. Comparison of the native CCMV virion with in vitro assembled CCMV virions by cryoelectron microscopy and image reconstruction. *Virology*, 244, 1998.

[24] M. Freitag and W. Benz. A new Monte Carlo code for star cluster simulations. *Astron. Astrophys.*, 375, 2001.

[25] S. C. Glotzer and M. J. Solomon. Anisotropy of building blocks and their assembly into complex structures. *Nat. Mater.*, 6, 2007.

[26] C. Godreche, F. Krzakala, and F. Ricci-Tersenghi. Non-equilibrium critical dynamics of the ferromagnetic Ising model with Kawasaki dynamics. *J. Stat. Mech.: Theory Exp.*, 04, 2004.

[27] J. Grant and R.L. Jack. Quantifying reversibility in a phase-separating lattice gas: An analogy with self-assembly. *Phys. Rev. E*, 85, 2012.

[28] J. Grant, R.L. Jack, and S. Whitelam. Analyzing mechanisms and microscopic reversibility of self-assembly. *J. Chem. Phys.*, 135, 2011.

[29] N. Greinert, T. Wood, and P. Bartlett. Measurement of effective temperatures in an aging colloidal glass. *Phys. Rev. Lett.*, 97, 2006.

[30] B.A. Grzybowski, C.E. Wilmer, J. Kim, K.P. Browne, and K. J. M. Bishop. Self-assembly: from crystals to cells. *Soft Matter*, 5, 2009.

[31] M.F. Hagan and D. Chandler. Dynamic pathways for viral capsid assembly. *Biophys. J.*, 91, 2006.

[32] M.F. Hagan, O.M. Elrad, and R.L. Jack. Mechanisms of kinetic trapping in self-assembly and phase transformation. *J. Chem. Phys.*, 135, 2011.

[33] J.D. Halley and D.A. Winkler. Consistent concepts of self-organization and self-assembly. *Complexity*, 14, 2008.

[34] E. Ising. Beitrag zur theorie des ferromagnetismus. *Zeitschrift für Physik A Hadrons and Nuclei*, 31, 1925.

[35] S. Jabbari-Farouji, D. Mizuno, D. Derks, G. H. Wegdam, F. C. MacKintosh, C. F. Schmidt, and D. Bonn. Effective temperatures from the fluctuation-dissipation measurements in soft glassy materials. *Europhys. Lett.*, 84(2):20006, 2008.

[36] R.L. Jack, M.F. Hagan, and D. Chandler. Fluctuation-dissipation ratios in the dynamics of self-assembly. *Phys. Rev. E*, 76, 2007.

[37] R.A.L. Jones. *Soft Condensed Matter*. Oxford University Press, 2002.

[38] K. Kawasaki. Diffusion constants near the critical point for time-dependent Ising models. i. *Phys. Rev.*, 145, 1966.

[39] K. Keren, R. S. Berman, E. Buchstab, U. Sivan, and E. Braun. DNA-templated carbon nanotube field-effect transistor. *Science*, 302, 2003.

[40] R. J. Kershner, L. D. Bozano, C. M. Micheel, A. M. Hung, A.R. Fornof, J. N. Cha, C. T. Rettner, M. Bersani, J. Frommer, P. W. K. Rothemund, and G. M. Wallraff. Placement and orientation of individual DNA shapes on lithographically patterned surfaces. *Nat. Nano.*, 4, 2009.

[41] R.W. Keyes. Physical limits of silicon transistors and circuits. *Rep. Prog. Phys.*, 68, 2005.

[42] C.L. Klix, C. P. Royall, and H. Tanaka. Structural and dynamical features of multiple metastable glassy states in a colloidal system with competing interactions. *Phys. Rev. Lett.*, 104, 2010.

[43] D. Klotsa and R. L. Jack. Predicting the self-assembly of a model colloidal crystal. *Soft Matter*, 7, 2011.

[44] D. Klotsa and R.L. Jack. Assembly feedback loops using fluctuation dissipation ratios. *in preparation*, 2012.

[45] G. Korniss, C. J. White, P. A. Rikvold, and M. A. Novotny. Dynamic phase transition, universality, and finite-size scaling in the two-dimensional kinetic Ising model in an oscillating field. *Phys. Rev. E*, 63, 2000.

[46] F. Krzakala. Glassy properties of the kawasaki dynamics of two-dimensional ferromagnets. *Phys. Rev. Lett.*, 94, 2005.

[47] J. Kubelka, J. Hofrichter, and W.A. Eaton. The protein folding 'speed limit'. *Cur. Opin. Struc. Biol.*, 14, 2004.

[48] H.N.W. Lekkerkerker and R. Tuinier. *Colloids and the Depletion Effect*. Springer, 2011.

[49] M.E. Leunissen, C.G. Christova, A.P. Hynninen, C.P. Royall, A.I. Campbell, A. Imhof, M. Dijkstra, R. van Roij, and A. van Blaaderen. Ionic colloidal crystals of oppositely charged particles. *Nature*, 437, 2005.

[50] E. Lippiello, F. Corberi, and M. Zannetti. Off-equilibrium generalization of the fluctuation dissipation theorem for Ising spins and measurement of the linear response function. *Phys. Rev. E*, 71, 2005.

[51] C. Maes, K. Netocny, and B. Wynants. Dynamical fluctuations for semi-markov processes. *J. Phys. A: Math. and Theor.*, 42, 2009.

[52] P. Mayer, S. Léonard, L. Berthier, J. P. Garrahan, and P. Sollich. Activated aging dynamics and negative fluctuation-dissipation ratios. *Phys. Rev. Lett.*, 96, 2006.

[53] P. Meakin. Formation of fractal clusters and networks by irreversible diffusion-limited aggregation. *Phys. Rev. Lett.*, 51, 1983.

[54] N. Metropolis, Rosenbluth A.W., M.N. Rosenbluth, A.H. Teller, and E. Teller. Equation of state calculations by fast computing machines. *J. Chem. Phys.*, 21, 1953.

[55] M. E. J. Newman and G. T. Barkema. *Monte Carlo Methods in Statistical Physics*. Oxford University Press, 2002.

[56] Z. Nie, W. Li, M. Seo, S. Xu, and E. Kumacheva. Janus and ternary particles generated by microfluidic synthesis:äâ design, synthesis, and self-assembly. *J. Am. Chem. Soc.*, 128, 2006. PMID: 16848476.

[57] L. Onsager. Crystal statistics. i. a two-dimensional model with an order-disorder transition. *Phys. Rev.*, 65, 1944.

[58] C. D. Paavola, S. L. Chan, Y. Li, K. M. Mazzarella, R. A. McMillan, and J. D. Trent. A versatile platform for nanotechnology based on circular permutation of a chaperonin protein. *Nanotechnology*, 17, 2006.

[59] D. C. Rapaport. Role of reversibility in viral capsid growth: A paradigm for self-assembly. *Phys. Rev. Lett.*, 101, 2008.

[60] D.C. Rapaport. *The Art of Molecular Dynamics Simulation*. Cambridge University Press, 2 edition, 2004.

[61] F. Ricci-Tersenghi. Measuring the fluctuation-dissipation ratio in glassy systems with no perturbing field. *Phys. Rev. E*, 68, 2003.

[62] F. Romano, E. Sanz, and F. Sciortino. Phase diagram of a tetrahedral patchy particle model for different interaction ranges. *J. Chem. Phys.*, 132, 2010.

[63] F. Romano and F. Sciortino. Two dimensional assembly of triblock janus particles into crystal phases in the two bond per patch limit. *Soft Matter*, 7, 2011.

[64] F. Romano and F. Sciortino. Patterning symmetry in the rational design of colloidal crystals. *Nat. Commun.*, 3, 2012.

[65] P. W. K. Rothemund. Folding DNA to create nanoscale shapes and patterns. *Nature*, 440, 2006.

[66] J. Russo and F. Sciortino. How do self-assembling polymers and gels age compared to glasses? *Phys. Rev. Lett.*, 104, 2010.

[67] S. Sacanna, W. T. M. Irvine, P. M. Chaikin, and D. J. Pine. Lock and key colloids. *Nature*, 464, 2010.

[68] E. Saeedi, S. Kim, and B. A. Parviz. Self-assembled crystalline semiconductor optoelectronics on glass and plastic. *J. Micromech. Microeng.*, 18, 2008.

[69] R. P. Sear. Nucleation of a liquid on aerosol nanoparticles. *Europhys. Lett.*, 83, 2008.

[70] U. Seifert and T. Speck. Fluctuation-dissipation theorem in nonequilibrium steady states. *Europhys. Lett.*, 89, 2010.

[71] D. J. Selkoe. Folding proteins in fatal ways. *Nature*, 426, 2003.

[72] P. Sollich, S. Fielding, and P. Mayer. Fluctuation-dissipation relations and effective temperatures in simple non-mean field systems. *J. Phys.: Condens. Matter*, 14, 2002.

[73] Z. K. Tang, G. K. L. Wong, P. Yu, M. Kawasaki, A. Ohtomo, H. Koinuma, and Y. Segawa. Room-temperature ultraviolet laser emission from self-assembled ZnO microcrystallite thin films. *Appl. Phys. Lett.*, 72, 1998.

[74] S. Whitelam and P.L. Geissler. Avoiding unphysical kinetic traps in monte carlo simulations of strongly attractive particles. *J. Chem. Phys.*, 127, 2007.

[75] S. Whitelam, C. Rogers, A. Pasqua, C. Paavola, J. Trent, and P. L. Geissler. The impact of conformational fluctuations on self-assembly: Cooperative aggregation of archaeal chaperonin proteins. *Nano Letters*, 9, 2009.

[76] G. M. Whitesides and M. Boncheva. Beyond molecules: Self-assembly of mesoscopic and macroscopic components. *Proc. Natl. Acad. Sci. (USA)*, 99, 2002.

[77] A. W. Wilber, J. P. K. Doye, A. A. Louis, E. G. Noya, M. A. Miller, and P. Wong. Reversible self-assembly of patchy particles into monodisperse icosahedral clusters. *J. Chem. Phys.*, 127, 2007.

[78] A.W. Wilber, J.P.K. Doye, and A.A. Louis. Self-assembly of monodisperse clusters: Dependence on target geometry. *J. Chem. Phys.*, 131, 2009.

[79] J.M. Yeomans. *Statistical Mechanics of Phase Transitions*. OUP, 1992.